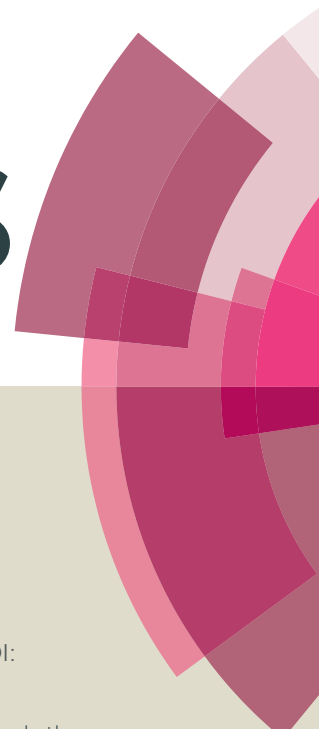


# RSC Advances



This article can be cited before page numbers have been issued, to do this please use: S. Salunke-Gawali, G. Agarwal, D. N. Lande, D. Chakravarty, S. P. Gejji, A. S. Patil and P. Gosavi, *RSC Adv.*, 2016, DOI: 10.1039/C6RA20970J.



This is an *Accepted Manuscript*, which has been through the Royal Society of Chemistry peer review process and has been accepted for publication.

*Accepted Manuscripts* are published online shortly after acceptance, before technical editing, formatting and proof reading. Using this free service, authors can make their results available to the community, in citable form, before we publish the edited article. This *Accepted Manuscript* will be replaced by the edited, formatted and paginated article as soon as this is available.

You can find more information about *Accepted Manuscripts* in the [Information for Authors](#).

Please note that technical editing may introduce minor changes to the text and/or graphics, which may alter content. The journal's standard [Terms & Conditions](#) and the [Ethical guidelines](#) still apply. In no event shall the Royal Society of Chemistry be held responsible for any errors or omissions in this *Accepted Manuscript* or any consequences arising from the use of any information it contains.



## Bromine substituted aminonaphthoquinones: Synthesis, Characterization, DFT and metal ion binding studies†

Gunjan Agarwal<sup>a</sup>, Dipali N. Lande<sup>a</sup>, Debamitra Chakrovarty<sup>b</sup>, Shridhar P. Gejji<sup>a</sup>, Prajakta Gosavi-Mirkute<sup>a</sup>, Amit Patil<sup>a</sup>, Sunita Salunke-Gawali<sup>\*a</sup>

Received 00th January 20xx,  
Accepted 00th January 20xx  
DOI: 10.1039/x0xx00000x  
[www.rsc.org/](http://www.rsc.org/)

Bromo substituted aminonaphthoquinone ligands viz. 2-(2'-aminomethylpyridyl)-3-bromo-naphthalene-1,4-dione; (2MPA), 2-(3'-aminomethylpyridyl)-3-bromo-naphthalene-1,4-dione; (3MPA), 2-(2'-aminoethylpyridyl)-3-bromo-naphthalene-1,4-dione; (2EPA) and 2-(2'-aminomethylthiophenyl)-3-bromo-naphthalene-1,4-dione (2AMT) and 2-(2'-aminoethylthiophenyl)-3-bromo-naphthalene-1,4-dione (2AET) have been synthesized and characterized by the single-crystal X-ray diffraction experiments in conjunction with the dispersion corrected density functional theory. The heterocyclic amines on the naphthoquinone ring render diverse crystal structures. It has been shown that bromine substitution influences the planarity and mutual orientation of naphthoquinone and heterocycles in aminonaphthoquinone ligands. The 2MPA, 3MPA, 2EPA, 2AET aminonaphthoquinone ligands crystallize in monoclinic space group whereas the 2AMT led to the triclinic space group *P-1*. Furthermore molecular packing of 2MPA and 2EPA revealed dimeric structures while 3MPA and 2AMT are rendered with 'stair-case' arrangements of molecules. The 2AET when viewed down c-axis showed a 'butterfly like' arrangement. A broad charge transfer band 400-600 nm was observed in the UV-Visible spectra of these ligands. Besides 2MPA and 2EPA exhibit remarkable selectivity toward Cu<sup>2+</sup> ions accompanied by color change from orange to blue in methanol and methanol-water mixture.

### Introduction

1,4-naphthoquinones comprised of an amino or a substituted amino group, have been focus of attention owing to their use as therapeutics<sup>1,2</sup> in a variety of medicinal and biological applications encompassing antituberculars<sup>3</sup>, antimalarials<sup>4,5</sup>, anticancer agents<sup>6</sup>, antitumor agents<sup>7-9</sup>, antifungal<sup>10</sup>, antiparasitic and phytotoxic activities.<sup>11,12</sup> The biological activity of quinones stem from their ability to accept one or two electrons to form the corresponding radical anion or dianion species and their acid base behaviour<sup>13,14</sup>. It has been

recognised that electron attracting or donating substituent's modulate the redox<sup>15</sup> properties of quinones. The molecular basis of quinone toxicity suggested that enzyme catalyzed reduction to semiquinone radicals is followed by reduction of oxygen to superoxide anion radicals<sup>16-18</sup> which regenerates the quinone. The electron donor effect of amine substituent on 1,4-naphthoquinones and the hydrogen bond between the -NH group and quinone carbonyl groups significantly influences the electron acceptor capability<sup>19</sup> of the quinone nucleus and subsequently electron transfer from the analyte to electroactive quinone nucleus. The presence of nitrogen atom modulates electronic properties of quinone which further induces structural modification of neutral molecules or reduction intermediate. Optical characteristics of quinone derivatives are governed by hydrogen bonding as well as other intermolecular interactions. The present work aims deriving the molecular insights accompanying the molecular interactions.

Aminonaphthoquinones owing to their biological importance serve as chemical sensors. The functionalisation of 1,4-naphthoquinone with amines facilitate a variety of interaction sites for metal ion binding. In this regard aminonaphthoquinones are known to bring about intramolecular charge transfer (ICT)<sup>20</sup> transitions; the intensity of which largely depends on the substituent<sup>21</sup> attached to amine moiety in particular, the charge density near nitrogen centre. The receptor molecules to be used as chemosensors should absorb and emit at longer wavelengths and show selective response to specific ions. It has been conjectured that the amine moiety being an electron donor group when present in the quinone ring at C(2) position facilitate a strong charge-transfer<sup>22,23</sup> (CT) from the electron donor amine substituent to the carbonyl group, attributed to intramolecular hydrogen bonding between carbonyl oxygen and the hydrogen of the substituent pin C(1) position, which reflects as  $\pi-\pi^*$  absorption band in the visible region of its absorption spectrum.

<sup>a</sup> Department of Chemistry, Savitribai Phule Pune University, Pune 411007, Maharashtra, India; Fax: +912025693981; Tel: +912025601397 -Ext-531; E-mail: [sunitas@chem.unipune.ac.in](mailto:sunitas@chem.unipune.ac.in)

<sup>b</sup> Central Instrumentation Facility, Savitribai Phule Pune University, Pune 411007, Maharashtra, India

† Electronic Supplementary Information (ESI) available: FT-IR, <sup>1</sup>H and <sup>13</sup>C NMR, 2D HSQC, UV-visible spectra are presented in Fig.S1 through Fig.S8. Crystallographic figures Fig.S9 through Fig.S13. UV-visible spectra of 2EPA in various solvents Fig.S14. Job plot Fig.S15, Fig.S16. Binding constant Fig.S17, Fig.S18. Competitive metal ion binding studies Fig.S19 through Fig.S21. FT-IR Table S1, NMR chemical shifts Table S2 and S3. Crystallographic Table S4-S23. DFT studies Table S24 through Table S28. CCDC 1446762 for 2MPA, 1446761 3MPA, 1446759 2AMT, 1446760 2EPA and 1446920 for 2AET

See DOI: 10.1039/x0xx00000x

Naphthoquinone and anthraquinone based sensing by functionalization of the quinone moiety using nitrogen containing receptors such as amines for cation sensing for example, 1,2 and 1,8-diaminoanthroquinones has been reported.<sup>24,25</sup> To this direction ureas<sup>26,27</sup>, thioureas<sup>28,29</sup> incorporated into anthraquinone as hydrogen bonding receptors have been employed for sensing inorganic and organic anions<sup>30,31</sup> those include halide, acetate, malate, fumarate, tartarate, aconitate and citrate to distinguish isomeric forms, since the urea forms strong hydrogen bonds. Urea anthraquinone assemblies where in the metal cation deprotonate the donor amine or amide have further been explored for metal ion detection<sup>32</sup>. Likewise imidazole moiety serves as excellent hydrogen bond donor in anion receptor systems<sup>33-35</sup> where the reactivity of the NH proton can be tuned by varying the electronic properties of the substituent at the ring. The presence of a donor pyridine like nitrogen atom within the ring capable of selectively binding cationic species converts imidazoles into excellent metal ion sensors<sup>36-38</sup>. The naphthoquinone based sensing has been focus of attraction for quite some time. The naphthoquinone molecules substituted with heterocyclic amines<sup>39-43</sup>, thiourea<sup>44</sup> and imidazole<sup>45</sup> receptors have been reported as sensors for metal cations such as Cu<sup>2+</sup> and the anions as well. It has further been demonstrated that Schiff base<sup>46</sup> of aminonaphthoquinone acts as a dual sensor for F<sup>-</sup> anion as well as Co<sup>2+</sup>, Ni<sup>2+</sup>, and Cu<sup>2+</sup> cations. Naphthoquinone based probes are also being used for sensing biomolecules<sup>44</sup> such as arylamine N-acetyltransferase (potential breast cancer biomarker). Bromine containing chemosensors were scarce in the literature. With our growing interest to develop naphthoquinone based redox active chemosensors, in the present work we carried out the syntheses of naphthoquinone based chemosensors, the thiophene and pyridyl ring bearing bromo derivatives of 1,4-naphthoquinone (Scheme 1). These ligands have further been characterized in terms of, molecular structure and their metal ion binding abilities combining experiment with the density functional theory.

### Scheme 1

## Results and discussion

The aminonaphthoquinone ligands were synthesized with high % yield via Michael addition of respective amines to the starting precursor 2,3-dibromo-1,4-naphthoquinone (DBrNQ) as shown in the Scheme S1 in ESI†. There was formation of side product observed in the synthesis of 2MPA and 3MPA and that of 2MPA has been isolated and characterized as 2-amino-3-methyl-1,4-naphthoquinone. All the aminonaphthoquinones were characterized by elemental analysis, FT-IR, <sup>1</sup>H, <sup>13</sup>C NMR, gDQCOSY, DEPT, gHSQCAD NMR and single crystal X-ray diffraction studies.

### FT-IR, NMR and UV-Visible studies

FT-IR spectra of aminonaphthoquinone ligands reveal characteristic -N-H stretching follows the order: 2EPA (3321 cm<sup>-1</sup>) > 2AMT (3284 cm<sup>-1</sup>) > 3MPA (3267 cm<sup>-1</sup>) > 2AET (3263 cm<sup>-1</sup>) > 2MPA (3242 cm<sup>-1</sup>) and sensitive to inter and intramolecular hydrogen bonding interactions (cf Fig.S1, Fig.S2 and Table S1 in ESI†). The carbonyl stretching frequency was observed at 1676 cm<sup>-1</sup> for the parent starting material DBrNQ, which exhibit a frequency up-shift from 2 to 9 cm<sup>-1</sup> respectively except for the 2-EPA in which a marginal shift of 4 cm<sup>-1</sup> in the opposite direction can be noticed. The characteristic paranaphthoquinone (p-NQ)

vibrations observed at 1292 cm<sup>-1</sup> and 1250 ± 9 cm<sup>-1</sup> in the aminonaphthoquinones ligands. The ν<sub>C-Br</sub> vibration reveals a largest blue-shift of 56 cm<sup>-1</sup> for 2AET which decreases steadily on traversing from 2EPA, 2MPA to 3MPA. The ligand 2AMT, on the other hand shows a marginal decrease of 4 cm<sup>-1</sup> in 2AMT compared to the 627 cm<sup>-1</sup> vibration in parent DBrNQ.

As shown in Scheme 2, <sup>1</sup>H and <sup>13</sup>C chemical shifts were assigned based on the <sup>1</sup>H, <sup>13</sup>C, DEPT, gHSQCAD gDQCOSY experiments (Fig.S3-Fig.S7, Table S2 and Table S3 in ESI†). The proton chemical shift of -N(1)-H(1) proton observed at δ = 6.2 ppm in 3MPA, 2AMT and 2AET, however it showed down field shift signal in 2EPA (δ = 7.12 ppm) as well as 2MPA (δ = 7.91 ppm). The <sup>13</sup>C chemical shifts in these ligands are affected significantly as evidenced from 2MPA, 3MPA and 3AMT emerge with the signals near 155.21, 134.11 and 148.99 ppm, respectively. Further 3MPA and 2MPA can be distinguished from the C(15) and C(16) signals in 3MPA emerge near δ = 148.99 and 149.18 ppm, respectively.

The UV-visible spectra of all compounds and the starting materials DBrNQ were recorded at 5 × 10<sup>-4</sup> M concentrations in DMSO (Fig.S8 in ESI†). The absorption in the visible region was observed in the starting materials viz. DBrNQ as well as in 2MPA, 3MPA, 2AMT, 2EPA, 2AET owing to a fully conjugated cyclic dione system<sup>47</sup>, where the π-π\* transitions are well pronounced in the UV region, sharp intense band near 336 nm of the starting material appears as a only as a hump in the ligands studied in this work. The nonbonding electrons of the amino group bring about n-π\* transition in the visible region. A low energy band centred ~440-477 nm has been observed in the visible, which is characteristic for the amino substituted quinones which stem from charge transfer (CT) band and weak n-π\* transitions of the carbonyl of the quinone.

### Scheme 2

### Single crystal X-ray diffraction studies

ORTEP plots of 2MPA, 3MPA, 2AMT, 2EPA and 2AET are shown in Fig.1 and the crystallography data has been summarized in Table 1. Except the 2AMT which crystallizes in triclinic space group *P*-1, the rest of aminonaphthoquinone ligands crystallize in monoclinic space group. The oxidation number of aminonaphthoquinones can be gauged from the bond distance parameters in quinonoid ring<sup>47-55</sup>. The carbonyl bond distances C(1)-O(1) and C(4)-O(2) are ~1.22 Å in all aminonaphthoquinone ligands except 3AMT the C(4)-O(2) distance is 1.24(2) Å. Thus, the ligands are in their oxidized form. The C(3)-N(1) and C(2)-Br distances respectively, were observed to be ~1.32-1.34 Å and ~1.88-1.90 Å.

Aminonaphthoquinones are comprised of C-H...O, N-H...O and others include C-H...N, N-H...N, C-H...Cl, C-H...π, π...π stacking interactions<sup>54,55</sup>. A charge transfer has also been observed subsequent to these noncovalent interactions. The chloro analogs containing pyridine functionalities studied in our laboratory serve as chemosensor, which bind to metal ions via bi- or tri -dentate coordination depending on the planarity of the ligand<sup>48-49</sup>. These chemosensors are known for specific detection of Cu<sup>2+</sup> ions in methanol-water mixture, also are explored to detect other metal ions under mild basic conditions in the presence of triethylamine. X-ray crystallography experiments further provide the coordination sites of the ligands. The present endeavour concerns with how the bromo substitution influences the planarity of naphthoquinone and the heteroatom rings in aminonaphthoquinones.

Intra as well as intermolecular hydrogen bonding interactions are observed in the aminonaphthoquinone ligands studied in this investigation. The hydrogen bond parameters including selected bond- distances and angles are given in Table 2. Except the 2MPA, the rest of ligands suggest the presence of the N(1)-H(1)···O(2) intramolecular hydrogen bonding. The N(1)-H(1)···N(2) along with intramolecular H(1)···Br(1) (2.515Å) interactions are inferred in 2MPA. The bond angle  $\angle$ N(1)-H(1)···O(2) was observed to be  $\sim 114^\circ$ , which shows a closure to  $\sim 105^\circ$  in 3AMT compared to that for the  $sp^2$  amino nitrogen.

The intermolecular interactions with similar neighbouring molecules, type of interaction and interplanar angles of naphthoquinone ring with pyridine/thiophene ring are represented in Table 3.

Fig.1

Table 1

Table 2

Table 3

### Molecular interactions in 2MPA, 3MPA, 2AMT and 2EPA, 2AET'

The usual N-H···O intramolecular hydrogen bonding interaction is absent in 2MPA, instead the orientation of pyridyl ring brings -NH proton vicinity of bromine facilitating N-H···N intramolecular hydrogen bonding interactions. The dimer is facilitated through head to tail orientation of 2MPA molecules via C(5)-H(5)···O(2) (-x,-y,1-z) interactions which subsequently brings about the C(14)-H(14)···O(1) intermolecular hydrogen bonding interaction (Fig.2) concomitant to Br··· $\pi$  interactions from neighbouring molecules specially by C(6) (3.517(8) Å,  $\frac{1}{2}$ -x,  $-\frac{1}{2}$ +y,  $\frac{1}{2}$ -z) and C(7) (3.297(7)Å).

Fig.2

The quinonoid oxygen O(1) of 3MPA further showed bifurcated hydrogen bonding (Fig.3a). Polymeric chain of 3MPA molecules is extended by C(8)-H(8)···O(2) and N(1)-H(1)···O(1) interactions, with the pyridine moiety being placed on same side of the chain (Fig.3a). The pyridyl rings of two neighbouring chains orient in opposite directions with the polymer chains stacked via C(1)···O(2) (3.161(4), x,-1+y,z) contacts (Fig.3a). The C···O stacked chains are further stabilized by the C(16)-H(16)···O(1)(x,-1+y,z) and C(14)-H(14)···Br(1)(1-x,-y,2-z) interaction (Fig.3b). Pyridyl ring distances were observed to be 4.047Å.

Fig.3

The C(3)-N(1)-C(11)-C(12) dihedral angle in 2AMT turns out to be  $73.3(4)^\circ$ , which suggests the thiophene ring is above the plane of naphthoquinone ring. The crystal network in the 2AMT extends via head-to-tail C(8)-H(8)···O(2) and N(1)-H(1)···O(1) interactions. A "stair-case like" polymeric chains with the thiophene rings separated by C(15)-(H15)···O(1)(-1+x,-1+y,z) interactions down the b-axis can further be noticed from Figs.4a and 4b. As shown the slipped  $\pi$ - $\pi$  stacking have also been inferred along polymeric chain down the a-axis (Fig.4a), in particular the benzenoid and quinonoid rings are stacked through C(9)···C(5) (3.66(1)Å) and C(7)···C(4) (3.69(1)Å) contacts.

Fig.4

The torsion angle C(3)-N(1)-C(11)-C(12) of 2EPA turns out to be  $-94.8^\circ$  whereas C(13)-C(12)-C(11)-N(1) show a deviation of  $\sim 10^\circ$  from planarity. Molecules of 2EPA formed a dimeric synthon via 'head to head' interactions through N(1)-H(1)···O(2) interactions portrayed in Fig.5. Furthermore the C(5)-H(5)···N(2)(-x,1-y,-z) interactions render stability to pyridyl rings of the dimer. Furthermore as shown in Fig.5 the polymer chain of dimers are formed through C-(15)-H(15)···O(1) interactions.

Fig.5

The torsion angle C(3)-N(1)-C(11)-C(12) in 2AET is  $83^\circ$  and C(13)-C(12)-C(11)-N(1) is  $175^\circ$ . Molecules of 2AET facilitate polymeric chain through N(1)-H(1)···O(1) interactions in addition to the C(14)-H(14)···Br(1) interactions. As shown in Fig.6a, the polymeric chains of 2AET molecule further reveal C-H··· $\pi$  interactions between benzenoid and thiophene rings, in particular C(7)-H(7)···C(15)(3.61(3),  $-1/2+x, 1/2-y, -1/2+z$ ) interactions. When viewed down c-axis (Fig.6b) the 'butterfly like' arrangement can be noticed (with bromines = eyes, ethyl thiophene = tentacles and naphthoquinone = wings of the butterfly).

Fig.6

### Overlay Structures of 2MPA, 3MPA, 2AMT and 2EPA, 2AET

Fig. 7 displays the orientation of pyridyl and thiophene rings with the naphthoquinone. In 2MPA (Fig.7a) pyridyl ring is nearly planar. The 2AMT and 3MPA reveal thiophene and pyridyl ring oriented respectively, above and below the plane of the naphthoquinone. A marginal variation in orientations of pyridyl and thiophene rings in the overlay structures of 2EPA and 2AET (Fig.7b) can be noticed. It should be remarked here that chemosensing ability to the metal ions and the biological activity can be correlated to the ring planarity. The aminonaphthoquinone ligands here facilitate either bidentate or tridentate coordination with the metal ion. The tridentate coordination sites through O(2), N(1) and N(2) is favored over the bidentate coordination in 2MPA. On the other hand for 2EPA, the structure with the additional -CH<sub>2</sub>, one of the nitrogen N(2) will be further away from O(2) and N(1) the bidentate coordination is preferred.

Fig.7

### Hirshfeld surfaces

To probe various molecular interactions, Hirshfeld surfaces and their associated 2D finger print plots were derived with the use of Crystal Explorer 3.1<sup>56</sup> employing the single crystal X-ray data. The function  $d_{\text{norm}}$  is a ratio encompassing the distances of any surface point to the nearest interior (di) and exterior (de) atom to the van der Waals radii of the atoms<sup>57-59</sup>. Figure 8a through 8d display surfaces those have been mapped with the  $d_{\text{norm}}$  shape index, curvedness and finger print plots of aminonaphthoquinone ligands. For the crystal structure of the hitherto ligands the Hirshfeld surface is unique and provide detail insights of the crystal structure. A direct visual comparison imparts intense red color around the N-H substituent of the ligands which contribute largely toward N-H···O interactions (cf. Figure 8a) except for the 2MPA. In addition to this C-H···O contacts are deciphered through the intense red spots within 2EPA, 2MPA and 2AMT. The characteristic packing modes and the ways in which the nearby molecules contact one another further gauged through shape index and curvedness parameters.

The shape index of all the molecules shows a red concave region on the surface around the oxygen atoms as well as  $\pi$  cloud of aromatic rings and a blue region around the hydrogen atoms. The presence of C-H $\cdots\pi$  and  $\pi$ - $\pi$  stacking interactions in aminonaphthoquinone derivatives further are evident from the pattern of adjacent red and blue triangles those appear on the shape index surfaces and relatively large and flat green region on the same side of the molecule on the corresponding curvedness surfaces (*cf.* Figure 8b and 8c). The breakdowns of finger-print plots for all such structures are illustrated in Figure 8d. From the FP plots, contributions from the N-H $\cdots$ O, C-H $\cdots$ O, C-H $\cdots\pi$ , C-H $\cdots$ N and  $\pi$ - $\pi$  stacking interactions can be segregated. Thus the volume ( $V_H$ ), area ( $S_H$ ), globularity ( $G$ ) and asphericity ( $\Omega$ ) parameters based on hirshfield surfaces have been calculated. The following inferences are drawn. The term, globularity<sup>60</sup> was observed at  $\sim 0.764$  for the aminonaphthoquinone derivatives which suggest that the molecular surface is more structured, and not a sphere. The asphericity<sup>61,62</sup> that provides measure of anisotropy follows order : 2EPA (0.385) > 2AET (0.357) > 2MPA (0.317) > 3MPA (0.163) > 2AMT (0.136).

Fig.8

### DFT Investigations

Optimized structures of aminonaphthoquinone derivatives from the wb97x based density functional theory are depicted in Fig.9. Selected bond- distances and angles are compared with X-ray crystal data in Table S24. Except for the NH bond bridging naphthoquinone and substituted pyridine moiety of 2MPA which is up to 0.22 Å longer the overall structural parameters agree well with those from the X-ray experiments. A comparison of 2MPA and 2AMT shows that carbonyl C(1)O(1) bond distances are shortened on substituting the thiophene instead of pyridine. It may readily be discernible that an increase of alkyl chain from methylene to ethylene engenders the reversal of the trend and accordingly longer C=O bond distances are predicted for 2AET compared to the 2EPA. These inferences are consistent with those observed from the X-ray crystal structure data. The bond angles show deviation maximally up to 2° compared to the X-ray crystal structures.

The structures of aminonaphthoquinone derivative anions are also obtained within the framework of  $\omega$ b97x/6-31+G(d,p) theory which are portrayed in Fig.10. Selected bond distances are given along with. As may readily be noticed the anions reveal longer C=O or C-Br bond distances compared to their neutral analogs with the elongation up to  $\sim 0.0238$  Å was predicted for 2MPA.

Structural ramifications in calculated vibration frequencies and accompanying molecular interactions can be probed through normal vibration analysis. Calculated frequencies of 2MPA, 2AMT, 3MPA, 2EPA and 2AMT with those measured in the experiment are compared in Table S25 and portrayed in Fig.11(a) and 11 (b). The N-H stretching assigned to 3242 cm<sup>-1</sup> of 2MPA engenders a large frequency up shift that amounts to  $\sim 73$  cm<sup>-1</sup> on substitution of the ethyl group instead of methyl as in 2EPA. The change of position of naphthoquinone to the 3 position of pyridine (in 3MPA) renders a blue-shift (up-shift) for the N-H stretching (3283 cm<sup>-1</sup>) vibration. A comparison of 2AMT and 2AET further led to similar inferences. The effect of pyridine or thiophene substitution on amino naphthoquinone derivative shows its signature in NH stretching vibration which shows the corresponding frequency shift in the opposite directions in the methyl and ethyl substituted derivatives (*cf.*

Table S25). The C(1)O(1) carbonyl stretching at 1651cm<sup>-1</sup> in 2AMT shifts to 1641cm<sup>-1</sup> in the calculated vibration spectra of 2AET. As opposed to this the carbonyl stretching at the 1640 cm<sup>-1</sup> in 2MPA shifts to higher wave number 1649 cm<sup>-1</sup> in the 3MPA isomer. The aromatic proton shows a band  $\sim 2988$  cm<sup>-1</sup>. The inferences borne out from the present DFT calculations are also in consonance with the experimentally measured spectra.

<sup>1</sup>H NMR chemical shifts ( $\delta_H$ ) in 2MPA, 2AMT, 3MPA, 2EPA and 2AET in DMSO (as solvent) were simulated through the SCRF-PCM theory. A comparison with the experiment is given in Table S26. The H(1) proton participating in N-H $\cdots$ Br interactions in 2MPA emerge with relatively large deshielding (8.3 ppm) in the spectra. The signals of the corresponding proton in the rest of aminonaphthoquinone derivatives facilitate the N-H $\cdots$ O interactions and appear at  $\sim 6.8$  ppm. The alkyl protons emerge with up-field  $\delta_H$  signals in the calculated <sup>1</sup>H NMR. These inferences on the calculated  $\delta_H$  values concur with the experiment.

Frontier orbitals HOMO and LUMO (isosurface of  $\pm 0.04$  au) in the aminonaphthoquinone ligands are portrayed in Fig.12, Fig.13. The complementarily in charge distributions between HOMO and LUMO is transparent for 3MPA, 2AMT and 2AET. Here the HOMO extends over the entire molecule. On the other hand, in 2MPA and 2EPA it has been largely localized near naphthoquinone framework. The electronic spectra in the presence of methanol were obtained using the TD-DFT theory. The wavelength maxima, oscillator strengths and orbital descriptors are summarized in Table S27. It is transparent that the absorption band arising from the HOMO to LUMO transition shows up near  $\sim 402$  nm. The HOMO-LUMO energies, global indices of reactivity viz., chemical potential ( $\mu$ ), hardness ( $\eta$ ), electrophilicity ( $\omega$ ) of amino naphthoquinone derivative and its anionic form are summarized in Table S28. A large separation of HOMO and LUMO energies ( $\Delta E$ ) in the molecule imply the reluctance toward the acceptance of electron in the LUMO while the removal of an electron from the HOMO renders electronic stability to the system. A large relative stability of 3MPA and 2AET is thus evident. The anionic forms of these emerge with the lower band gap energies relative to the corresponding neutral systems.

To delve further in metal coordination we derive the structure of the Cu<sup>2+</sup>-2MPA complex, as a test example. As pointed out earlier the HOMO (isosurfaces of  $\pm 0.04$  a.u.) of 2MPA largely resides on quinonoid ring of naphthoquinone moiety which on complexation extends over to the metal ion as shown in Fig. 14. The ligand to metal charge transfer, therefore can be inferred. These conclusions further may as well be extended to other metal complexes studied in the present work.

Fig.9

Fig.10

Fig.11

Fig.12

Fig.13

Fig.14

### Chemosensor evaluation Studies

The metal ion binding studies of all the ligands have been carried in methanol, methanol-water mixture and in

presence of triethylamine. It has been observed that only 2MPA and 2EPA showed colour change with specifically with few metal ions. The colour of the ligand solution changed usually due to the formation of metal complexes. Metal ions induced the deprotonation of -NH and create the legating sites. The extra stability of 3MPA and 2AET ligands do not favour the formation metal complexes at room temperature (26°C), thus there is no colour change was observed with the solvents used for this studies in present investigation.

Fig.15

Table 4

Fig.15 showed the UV-visible absorption spectra of chemosensors 2MPA and 2EPA in methanol, in 1:1(v/v) methanol-water in the absence and presence of a mild base triethylamine (TEA) while Fig.17 showed the UV-visible spectra of the chemosensor 2MPA in the presence of transition metal ions in different solvents (The UV-visible spectra of for 2EPA are shown in Fig.S14 in ESI†). Table 4 showed the respective maximum absorption wavelength which shows  $\lambda_{\max}$  at 455 nm in case of 2MPA and 468 nm for 2EPA in methanol which undergoes bathochromic shifts in other solvents (bathochromic shift in presence of water ~475 nm and hypsochromic shift in triethylamine. In UV region of the spectrum, the peak ~331 nm is observed only in triethylamine while for other mixture of solvents only a hump was observed, which was assigned to  $\pi$ - $\pi^*$  transition.

#### Metal ion binding studies

Metal ion binding studies were carried out in the following solvent systems, i) in methanol, ii) in 1:1(v/v) methanol-water, iii) in presence of a mild base triethylamine (TEA) in i) and ii) TEA was used to get the deprotonated form of the chemosensor ligands which can be used to detect other metal ions too. In typical experiments 2 ml of the chemosensor was mixed with 2 ml of metal ion solutions at room temperature (26 °C) and 1 ml of triethylamine was added in chemosensor solution in case of i) and ii) prior to the addition of metal ion solutions. UV-visible spectra of all solutions was measured using a typical concentration of  $10^{-4}$  M. Photographs (Fig.16 for 2MPA, Fig.17 for 2EPA) were obtained for  $10^{-3}$  M solutions of the chemosensor and metal ions ( $\text{Cu}^{2+}$ ,  $\text{Ni}^{2+}$ ,  $\text{Zn}^{2+}$ ,  $\text{Co}^{2+}$ ,  $\text{Fe}^{3+}$ ,  $\text{Mn}^{2+}$ ,  $\text{Cr}^{3+}$ ,  $\text{Hg}^{2+}$ ,  $\text{La}^{3+}$  and  $\text{Cd}^{2+}$ ).

Fig.16

Fig.17

Fig.18

#### Visual detection of metal ions in methanol

The orange color solutions of 2MPA and 2EPA showed colour changes on the addition of  $\text{Cu}^{2+}$ ,  $\text{Ni}^{2+}$  and ions in 2MPA (Fig.16a) while 2EPA could differentiate colour change in  $\text{Cu}^{2+}$  (blue) and  $\text{Cu}^{2+}$  (dark green) (Fig.17a). The solutions of  $\text{Mn}^{2+}$ ,  $\text{Co}^{2+}$  and  $\text{Zn}^{2+}$  of 2MPA and  $\text{Ni}^{2+}$  become dark, while there is no observable colour change was seen for the other metal ions. The colour change was observed due to formation of coordination complexes by deprotonation of N-H of the chemosensor ligand. A new band was noticed for respectively at  $\lambda_{\max}$  to 601 nm and 620 nm for  $\text{Cu}^{2+}$  solution.

#### Visual detection of metal ions in methanol-triethylamine

The deprotonation of N-H of chemosensor was achieved by addition of mild base such as triethylamine and thus several metal ions could bind to the anionic chemosensor and the detectable colour change could be visualized by naked eyes. In this experiment, triethylamine was added prior to the addition of the metal ion solution, wherein only  $\text{Cu}^{2+}$ ,  $\text{Ni}^{2+}$  and  $\text{Co}^{2+}$  caused a colour change in 2MPA (Fig.16b and Fig.17b). A new band appeared in 600-800 nm for  $\text{Cu}^{2+}$ ,  $\text{Ni}^{2+}$ ,  $\text{Zn}^{2+}$ ,  $\text{Co}^{2+}$  in methanol (Fig.18b), after addition of triethylamine. In addition the enhancement of peak at ~330 nm was observed for most of the metal ions in presence of triethylamine. For  $\text{Cu}^{2+}$  this peak was shifted to 372 nm and 375 nm.

#### Visual detection of metal ions in methanol-water

In 1:1 mixture of methanol: water, only  $\text{Cu}^{2+}$  showed colour change from orange to dark blue for 2MPA and dark green for 2EPA (Fig.16c and Fig.17c). The colour change observed for  $\text{Cu}^{2+}$  in pure organic solvent was (pale green) and it varied in presence of water. Thus Chemosensor 2MPA effectively differentiated the organic and aqueous media for  $\text{Cu}^{2+}$  ions. The visible absorption band of Chemosensor 2EPA appeared at  $\lambda_{\max}$  477 nm which on addition of  $\text{Cu}^{2+}$  (1:1) underwent an immediate visible colour change from orange to dark brown. Both chemosensors 2MPA and 2EPA did not undergo any colour change on addition of other metal ions like  $\text{Ni}^{2+}$ ,  $\text{Zn}^{2+}$ ,  $\text{Co}^{2+}$ ,  $\text{Fe}^{3+}$ ,  $\text{Mn}^{2+}$ ,  $\text{Cr}^{3+}$ ,  $\text{Hg}^{2+}$ ,  $\text{La}^{3+}$  and  $\text{Cd}^{2+}$  in 2EPA in methanol-water mixture.

#### Visual detection of metal ions methanol-water-triethylamine

With the introduction of triethylamine to the methanol-water mixture  $\text{Mn}^{2+}$  and  $\text{Co}^{2+}$  showed variable colour shades for the respective solutions (Fig.16d, Fig.17d). The UV-visible spectra (Fig.18d) showed complete absence of the band in the ranges 600-800 nm and an enhancement of intensity of  $\pi$ - $\pi^*$  transition band at ~362 nm in the methanol-water-triethylamine mixture.

#### Stoichiometry, affinity constant, competitive binding of metal ion of 2MPA and 2EPA

The binding stoichiometry of 2MPA and 2EPA (Fig.18) with  $\text{Cu}^{2+}$ ,  $\text{Ni}^{2+}$  was determined by Job plot method. With 2MPA it is found to be 1:1 for  $\text{Cu}^{2+}$  ions in methanol, methanol-water while it is 2:1 for  $\text{Ni}^{2+}$  in methanol (Fig.19) and for  $\text{Cu}^{2+}$  in methanol-water-trimethylamine mixture (Fig.S15). For 2EPA the stoichiometry was observed as 1:1 for  $\text{Cu}^{2+}$  in methanol, methanol-trimethylamine and methanol-water solvent mixture (Fig.S16).

The binding constant of  $\text{Cu}^{2+}$  ion has been determined (Fluorescence measurement) by Stern-Volmer plot (Fig.S17 and Fig.S18) in methanol. The concentration of 2MPA/2EPA and metal ion used for this experiment are respectively ( $5 \times 10^{-4}$ ) and ( $1 \times 10^{-3}$  M). The association constant ( $K_a$ ) value obtained for  $\text{Cu}^{2+}$  was found to be  $851 \text{ M}^{-1}$  for 2MPA and  $6079 \text{ M}^{-1}$  for 2EPA

In the competitive binding of metal ions, in a typical experiments 2MPA and 2EPA ( $5 \times 10^{-4}$  M) was mixed with equal volume of  $\text{Cu}^{2+}$ ,  $\text{Ni}^{2+}$  and  $\text{Co}^{2+}$  ( $5 \times 10^{-4}$  M). Noticeable colour changes occur in solution mixture of metal ions (Fig.S19) for 2MPA and 2EPA as well as in UV-visible and fluorescence spectra of selected metal ion (Fig.S20 for 2MPA and Fig.S21 for 2EPA).  $\text{Cu}^{2+}$  showed significant fluorescence quenching in both 2MPA and 2EPA while other metal ion only cause small changes

in fluorescence intensity. It was observed in competitive experiment, the  $\text{Ni}^{2+}$  and  $\text{Co}^{2+}$  competed to bind with 2MPA and 2EPA, however  $\text{Cu}^{2+}$  dominate all other metal ion because of higher binding constant.

Fig. 19

## Conclusions

The aminonaphthoquinones containing different heterocyclic amines were synthesized and characterized. Diverse crystal network patterns have been noticed for differently substituted heterocyclic rings. 2AMT and 3MPA reveal the thiophene and pyridyl rings near normal to naphthoquinone ring whereas the 2MPA shows pyridyl ring orients near planar facilitating tridentate coordination to metal ion(s). A bidentate coordination is preferred in case of 2EPA which can be attributed to an increased separation between N-H and pyridyl nitrogen. The separation being expected to be further increase in 2AET compared to 2EPA. The aminonaphthoquinone ligands possess a variety of hydrogen bonding in addition to those arising from C-H $\cdots$  $\pi$  and  $\pi$ - $\pi$  stacking interactions. The close proximity of pyridyl ring and -NH proton to Br atom in the 2MPA engenders the largely deshielded (8.3 ppm) signal in  $^1\text{H}$  NMR spectra compared to the rest of the ligands; the inference which has been corroborated by the DFT computations. 2MPA and 2EPA can be used for naked eye detection of  $\text{Cu}^{2+}$  from organic and aqueous media with the remarkable selectivity.

## Experimental Section

### General Materials and Methods

Chemicals and reagents viz. 2-3-dibromo-1,4-naphthoquinone (DBrNQ), 2-picolyamine, 3-picolyamine, 2-(2'-aminomethyl)thiophene, 2-(2'-aminoethyl)pyridine, 2-(2-aminomethyl)thiophene used were purchased from Sigma-Aldrich and used as received. The solvents used such as dichloromethane, toluene, methanol are of analytical grade were purchased from Merck Chemicals.  $\text{CuCl}_2 \cdot 2\text{H}_2\text{O}$ ,  $\text{NiCl}_2 \cdot 6\text{H}_2\text{O}$ ,  $\text{ZnCl}_2$ ,  $\text{CoCl}_2 \cdot 6\text{H}_2\text{O}$ ,  $\text{HgCl}_2$ , triethylamine, methanol and dichloromethane were obtained from Merck chemicals.  $\text{FeCl}_3 \cdot 6\text{H}_2\text{O}$  was obtained from Qualigens Chemicals.  $\text{CrCl}_3 \cdot 6\text{H}_2\text{O}$ ,  $\text{CdSO}_4$ ,  $\text{MnCl}_2 \cdot 4\text{H}_2\text{O}$  was obtained from Fluka.  $\text{LaCl}_3 \cdot 7\text{H}_2\text{O}$  was obtained from Thomas and Baker. Milli-Q water was used for preparation of aqueous solutions. Solvents were distilled by standard methods<sup>63</sup> and dried wherever necessary. Melting points of compounds was determined using melting point apparatus (Make-METTLER). The FT-IR spectra of all ligands was recorded between 4000-400  $\text{cm}^{-1}$  as KBr Fig.S1, Fig.S2 and Table S1 in ESI†) pellets on BRUKER Tensor 37 Spectrometer.  $^1\text{H}$ ,  $^{13}\text{C}$ , DEPT, HSQC, COSY NMR of all compounds were recorded (Fig.S3 and Fig.S7 Table S2 and Table S3 in ESI†) in  $\text{DMSO}-d_6$ , on Varian 500 MHz NMR instrument. TMS (tetramethylsilane) was used as the reference. UV-Visible spectra of all ligands in  $\text{CDCl}_3$  was recorded from 200 nm to 800 nm on Shimadzu UV 1800 spectrophotometer (Fig.S8 in ESI†). Elemental analysis was performed on Thermo Finnigan EA 1112 Flash series Elemental.

## Synthesis

1 mM of 2-3-dibromo-1,4-naphthoquinone (0.315 g) was dissolved in 15 ml of dichloromethane and the mixture stirred for

about 15 min. To this solution 1 mM, corresponding amines (1 mM = 0.104 ml of 2-picolyamine, 0.0103 ml 3-picolyamine, 0.126 ml of 2-aminoethylpyridine, 0.103 ml of 2-thiophenemethylamine, 0.120 ml of 2-thiopheneethylamine) were added drop wise. The reaction mixture was stirred for 24 hours at room temperature (26°C) with constant magnetic stirring till completion of the reaction monitored on TLC. The reaction mixture was evaporated under reduced pressure and the residue was column chromatographed over silica gel in methanol/toluene (1:9) system. The orange color solid products were obtained after evaporation of pure fraction from the column. In case of 2MPA a light orange color fraction was obtained other than the main product which was characterized as 2-bromo-3-methyl-1,4-naphthoquinone.

### Characterization

#### 2-(2'-aminomethyl)pyridyl-3-bromo-naphthalene-1,4-dione; 2MPA

Dark orange crystals. Yield: 0.222 g (65%). m.p.: 132-135°C. Anal. Data calcd. for  $\text{C}_{16}\text{H}_{11}\text{O}_2\text{N}_2\text{Br}$  (%): C, 55.99; H, 3.23; N, 8.16. Found(%): C, 55.83; H, 3.27; N, 7.95. FT-IR (KBr,  $\nu_{\text{max}}(\text{cm}^{-1})$ ): 3242, 3061, 1680, 1601, 1564, 1493, 1435, 1327, 1292, 1250, 1207, 1134, 1039, 1001, 895, 829, 787, 758, 723, 679, 638, 573, 542, 489, 449.  $^1\text{H}$  NMR ( $\text{CDCl}_3$ , 499.81 MHz,  $\delta(\text{ppm})$ ): 8.65 (d,  $J = 4.50$  Hz, 1H, Ar) 8.16 (d,  $J = 7.50$  Hz, 1H, Ar), 7.72 (m, 2H, Ar), 7.64 (t,  $J = 7.50$  Hz, 1H, Ar), 7.30 (d,  $J = 8.00$  Hz, 1H, Ar), 7.27 (t,  $J = 6.25$  Hz, 1H, Ar), 7.91 (s, 1H, -NH), 5.21 (d,  $J = 5.00$  Hz, 2H).  $^{13}\text{C}$  NMR ( $\text{CDCl}_3$ , 125.69 MHz,  $\delta(\text{ppm})$ ): 49.21, 121.97, 122.87, 127.02, 127.15, 130.00, 132.54, 132.59, 134.89, 137.11, 146.50, 149.18, 155.21, 176.50, 180.54. UV-Vis, ( $\lambda_{\text{max}}$ , DMSO (nm)): 467.

#### 2-(3'-aminomethyl)pyridyl-3-bromo-naphthalene-1,4-dione; 3MPA

Orange brown crystals. Yield: 0.301 g (88%). m.p.: 140.83°C. Anal. Data calcd. for  $\text{C}_{16}\text{H}_{11}\text{O}_2\text{N}_2\text{Br}$  (%): C, 55.99; H, 3.23; N, 8.16. Found(%): C, 56.46; H, 2.86; N, 8.37. FT-IR (KBr,  $\nu_{\text{max}}(\text{cm}^{-1})$ ): 3267, 3109, 3022, 2951, 2602, 2260, 1955, 1684, 1631, 1595, 1512, 1473, 1425, 1329, 1300, 1246, 1128, 1063, 1028, 964, 860, 717.54, 678, 634, 540, 499, 445.  $^1\text{H}$  NMR ( $\text{CDCl}_3$ , 499.81 MHz,  $\delta(\text{ppm})$ ): 8.62 (s, 1H, Ar), 8.57 (d,  $J = 4.50$  Hz, 1H, Ar), 8.12 (d,  $J = 7.50$  Hz, 1H, Ar), 8.01 (d,  $J = 8.00$  Hz, 1H, Ar), 7.70 (m, 2H, Ar), 7.64 (t,  $J = 8.00$  Hz, 1H, Ar), 7.33 (t,  $J = 6.50$  Hz, 1H, Ar) 6.28 (s, -NH), 5.11 (d,  $J = 6.50$  Hz, 2H, -CH<sub>2</sub>).  $^{13}\text{C}$  NMR ( $\text{CDCl}_3$ , 125.69 MHz,  $\delta(\text{ppm})$ ): 46.73, 124.06, 126.94, 127.21, 127.37, 129.98, 132.27, 132.91, 133.98, 135.12, 135.57, 146.36, 149.16, 149.435, 176.75, 180.08. UV-Vis, ( $\lambda_{\text{max}}$ , DMSO (nm)): 471.

#### 2-(2'-aminomethyl)thiophenyl-3-bromo-naphthalene-1,4-dione; 2AMT

Dark brown crystals. m. p.: 119.79°C. Yield: 0.337 g (97%). Anal. Data calcd. for  $\text{C}_{15}\text{H}_{10}\text{O}_2\text{NSBr}$ (%): C, 51.73; H, 2.89; N, 4.022, S, 9.21. Found C, 52.12; H, 2.87; N, 4.31; S, 8.67. FT-IR (KBr,  $\nu_{\text{max}}(\text{cm}^{-1})$ ): 3462, 3284, 3194, 3109, 3043, 3012, 2966, 2920, 2850, 2594, 2455, 2283, 2083, 1990, 1894, 1867, 1685, 1633, 1570, 1510, 1431, 1300, 1244, 1153, 1126, 1057, 1026, 860, 835, 781, 705, 623, 542, 447, 408.  $^1\text{H}$  NMR ( $\text{CDCl}_3$ , 499.81 MHz,  $\delta(\text{ppm})$ ): 8.14 (d,  $J = 7.50$  Hz, 1H, Ar), 8.03 (d,  $J = 7.00$  Hz, 1H, Ar), 7.72 (t,  $J = 7.74$  Hz, 1H, Ar), 7.64 (t,  $J = 7.50$  Hz, 1H, Ar), 7.29 (t,  $J = 5.00$  Hz, 1H, Ar), 7.07 (d,  $J = 3.00$  Hz, 1H,

Ar), 7.00 (t,  $J = 4.25$  Hz, 1H, Ar), 6.10 (s, -NH), 5.25 (s, 2H, -CH<sub>2</sub>). <sup>13</sup>C NMR (CDCl<sub>3</sub>, 125.69 MHz,  $\delta$ (ppm)): 44.06, 125.91, 126.59, 126.74, 126.97, 127.09, 127.20, 129.86, 132.16, 132.65, 134.86, 140.10, 146.00, 176.20, 180.00. UV-Vis, ( $\lambda_{\text{max}}$ , DMSO (nm)): 463.

### 2-(2'-aminoethyl)pyridyl-3-bromo-naphthalene-1,4-dione; 2EPA

Dark red crystals, Yield: 0.342 g (96%). m. p: 127.60°C. Anal. Data calcd. for C<sub>17</sub>H<sub>13</sub>O<sub>2</sub>N<sub>2</sub>Br(%): C, 57.16; H, 3.66; N, 7.84. Found(%): C, 57.21, H, 3.78, N, 7.47. FT-IR (KBr,  $\nu_{\text{max}}$ (cm<sup>-1</sup>): 3321, 3192, 3032, 3003, 2937, 2875, 1992, 1892, 1672, 1610, 1525, 1446, 1330, 1296, 1257, 1157, 1130, 1074, 1022, 993, 954, 786, 758, 727, 686, 653, 542, 497, 420. <sup>1</sup>H NMR (CDCl<sub>3</sub>, 300 MHz,  $\delta$ (ppm)): 8.59 (d,  $J = 5.00$  Hz, 1H, Ar), 8.13 (d,  $J = 7.00$  Hz, 1H, Ar), 8.00 (d,  $J = 7.00$  Hz, 1H, Ar), 7.58-7.70 (m, 3H, Ar), 7.21 (d,  $J = 8.49$  Hz, 1H, Ar), 7.18 (t,  $J = 3.75$  Hz, 1H, Ar), 7.12 (s, 1H, -NH), 4.32 (q,  $J = 6.33$  Hz, 2H, -CH<sub>2</sub>), 3.17 (t,  $J = 3.75$  Hz, 2H, -CH<sub>2</sub>). <sup>13</sup>C NMR (CDCl<sub>3</sub>, 125.69 MHz,  $\delta$ (ppm)): 38.05, 44.69, 122.09, 123.65, 126.97, 127.13, 130.20, 132.44, 132.58, 134.86, 137.04, 146.60, 158.65, 176.31, 176.10, 180.45. UV-Vis, ( $\lambda_{\text{max}}$ , DMSO (nm)): 477.

### 2-(2'-aminoethyl)thiophenyl-3-bromo-naphthalene-1,4-dione; 2AET

Dark brown crystals. m.p.: 115-116 °C. Yield: 0.347 g (96%), Anal. Data calcd. for C<sub>16</sub>H<sub>12</sub>O<sub>2</sub>NSBr(%): C, 53.05 ; H, 3.33; N, 3.86; S, 8.85. Found (%): C, 53.25; H, 3.47; N, 3.93; S, 8.58. FT-IR (KBr,  $\nu_{\text{max}}$ (cm<sup>-1</sup>): 3263, 3063, 2960, 1857, 1674, 1610, 1541, 1440, 1438, 1261, 1255, 1016, 603, 540, 495. <sup>1</sup>H NMR (CDCl<sub>3</sub>, 499.81 MHz,  $\delta$ (ppm)): 8.15 (d,  $J = 7.50$  Hz, 1H, Ar), 8.02 (d,  $J = 7.50$  Hz, 1H, Ar), 7.72 (t,  $J = 7.50$  Hz, 1H, Ar), 7.63 (t,  $J = 7.25$  Hz, 1H, Ar), 7.20 (d,  $J = 4.99$  Hz, 1H, Ar), 6.97 (t,  $J = 4.25$  Hz, 1H, Ar), 6.92 (d,  $J = 4.99$  Hz, 1H, Ar), 6.18 (s, 1H, -NH), 4.18 (q,  $J = 6.66$  Hz, 2H, -CH<sub>2</sub>), 3.23 (t,  $J = 6.25$  Hz, 2H, -CH<sub>2</sub>). <sup>13</sup>C NMR (CDCl<sub>3</sub>, 125.69 MHz,  $\delta$ (ppm)): 31.45, 46.50, 124.72, 126.19, 127.12, 127.31, 127.41, 130.01, 132.51, 132.67, 135.05, 140.03, 146.50, 176.60, 180.23. UV-Vis, ( $\lambda_{\text{max}}$ , DMSO (nm)): 472.

### X-Ray Crystallographic Data Collection and Refinement of the Structures

The X-ray quality red crystals of 2MPA, 3MPA, 2AMT, 2EPA and 2AET were obtained after evaporation of red pure fraction from the column. Crystals of appropriate size were chosen for data collection.

Data for all three compounds have been collected on D8 Venture PHOTON 100 CMOS diffractometer using graphite monochromatized Mo-K $\alpha$  radiation ( $\lambda = 0.7107$  Å) with exposure/frame = 10 secs for 2MPA and 3MPA, 15secs for 2AMT, 20secs for 2EPA respectively whereas Cu-K $\alpha$  radiation (1.5406 Å) with exposure/frame = 12 secs for 2AET respectively has been used. The X-ray generator was operated at 50 kV and 30 mA for Mo-K $\alpha$  radiation and at 50 kV and 1 mA for Cu-K $\alpha$ . An initial set of cell constants and an orientation matrix were calculated from total 24 frames and 60 frames for Mo and Cu source respectively. The optimized strategy used for data collection consisted different sets of  $\phi$  and  $\omega$  scans with 0.5° steps in  $\phi/\omega$ . Crystal to detector distance was 5.00 cm with 512 x 512 pixels / frame, Oscillation / frame -0.5°, maximum detector swing angle = -30.0°, beam centre = (260.2, 252.5), in plane spot width = 1.24. Data integration was carried out by Bruker SAINT program and

empirical absorption correction for intensity data were carried out by Bruker SADABS. The programs are integrated in APEX II package.<sup>64</sup> The data were corrected for Lorentz and polarization effect. The structure was solved by *Direct Method* using SHELX-97.<sup>65</sup> The final refinement of the structure was performed by full-matrix least-squares techniques with anisotropic thermal data for non-hydrogen atoms on F<sup>2</sup>. The non-hydrogen atoms were refined anisotropically whereas the hydrogen atoms were refined at calculated positions as riding atoms with isotropic displacement parameters. Molecular diagrams were generated using ORTEP-3<sup>66</sup> and Mercury programs.<sup>67</sup> Structural calculations were performed using SHELXTL<sup>65</sup> and PLATON<sup>68</sup>.

### DFT Studies

Optimized structures were derived using the wB97x<sup>69</sup> based density functional theory employing the Gaussian-09 program.<sup>70</sup> The internally stored 6-31G basis set with diffuse functions added to on all the heavy atoms (designated as 6-31+G(d,p) basis) have been used for optimizations.<sup>71</sup> The stationary point structures thus obtained were confirmed to be local minima on the potential energy surfaces through vibrational frequency calculations. Frontier orbitals were computed in the same framework of theory. Time dependent Density Functional Theory (TD-DFT) was employed to derive the electronic spectra. To understand a charge transfer accompanying the metal coordination we carried out computations on the Cu complex of 2MPA as a model example.

### Metal ion binding studies, Jobs Plot and Competitive binding experiment

Metal ion binding studies were evaluated by following methods, (i) in methanol solution of chemosensor and metal ions (1\*10<sup>-4</sup>) (ii) 1\*10<sup>-4</sup> M solution of (i) in presence of triethylamine, (iii) methanol (chemosensor (1\*10<sup>-4</sup> M) and water (metal ion, 1\*10<sup>-4</sup> M) mixture and (iv) 1\*10<sup>-4</sup> M solution of (iii) in presence of triethylamine. In all methods 2 ml of chemosensor was mixed with 2 ml of metal ion solution at room temperature (26 °C). 1 ml triethylamine was added in chemosensor solution in case of (ii) and (iv) prior to addition of metal ion solution. UV-visible and fluorescence spectra of all solution were measured.

Micro molar concentration (10-100  $\mu$ M) of chemosensor and metal ion were used for Jobs plot experiment. Solutions were prepared by varying concentration of chemosensor and metal ions. Binding constant of Cu<sup>2+</sup> ion was determined by Stern-Volmer plot. 5\*10<sup>-4</sup> M solution of chemosensor and 1\*10<sup>-3</sup> M metal ion solution in methanol were used to obtain the same.

For competitive binding of metal ions (5\*10<sup>-3</sup> M) with 2MPA and 2EPA (5\*10<sup>-3</sup> M) equal volume were mixed and UV-visible spectra of all solution were measured

### Acknowledgements

SSG grateful to RGYI scheme of Department of Biotechnology, New Delhi, India for Ref. No. (BT/PR6565/GBD/27/456/2012) and Mr. Rishikesh Patil for NMR spectra.

### References

- 1 C. C. Nawrat, L. I. Palmer, A. J. Blake, and C. J. Moody, *J. Org. Chem.*, 2013, **78**, 5587-5603.
- 2 C. A. Kuttruff, S. Geiger, M. Cakmak, P. Mayer and D. Trauner, *Org. Lett.*, 2012, **14**, 1070-1073.

- 3 B. D. Bala, S. Muthusarayanan, T. S. Choon, M. A. Ali and S. Perumal, *Eur. J. Med. Chem.*, 2014, **85**, 737-746.
- 4 B. Prescott, *J. Med. Chem.*, 1969, **12**, 181-182.
- 5 G. J. Kapadia, M. A. Azuine, V. Balasubramanian and R. Sridhar, *Pharmacol. Res.*, 2001, **43**, 363-367.
- 6 M. D. Sarma, R. Ghosh, A. Patra and B. Hazra, *Eur. J. Med. Chem.*, 2008, **43**, 1878-1888.
- 7 T. D. Suja, K. V. L. Divya, L. V. Naik, A. Ravi Kumar and A. Kamal, *Bioorg. Med. Chem. Lett.*, 2016, **26**, 2072-2076.
- 8 E. N. da Silva Jr., B. C. Cavalcanti, T. T. Guimarães, M. do C.F.R. Pinto, I. O. Cabral, C. Pessoa, L. V. Costa-Lotufu, M. O. de Moraes, C. K.Z. de Andrade, M. R. dos Santos, C. A. de Simone, M. O.F. Goulart, A. V. Pinto, *Eur. J. Med. Chem.*, 2011, **46**, 399-410.
- 9 S. L. de Castro, F. S. Emery, E. N. da Silva Júnior, *Eur. J. Med. Chem.*, 2013, **69**, 678-700.
- 10 O. Pawar, A. Patekar, A. Khan, L. Kathawate, S. Haram, G. Markad, V. Puranik and S. Salunke-Gawali, *J. Mol. Struct.*, 2014, **1059**, 68-74.
- 11 W. Wang, T. Li, R. Milburn, J. Yates, E. Hinnant, M. J. Luzzio, S. A. Noble and G. Attardo, *Bioorg. Med. Chem. Lett.*, 1998, **8**, 1579-1584.
- 12 E. Thines, H. Anke and O. Sterner, *J. Nat. Prod.*, 1998, **61**, 306-308.
- 13 E. A. Hillard, F. C. de Abreu, D. C. M. Ferreira, G. Jaouen, M. O. F. Goulart, C. Amatore, *Chem. Commun.*, 2008, **69**, 2612-2628.
- 14 M. O.F. Goularta, P. Falkowski, T. Ossowski, A. Liwo, *Bioelectrochemistry*, 2003, **59**, 85-87.
- 15 A. Illos, E. Harlev and S. Bittner, *Tetrahedron Lett.*, 2005, **46**, 8427-8430.
- 16 K. Boudalis, X. Policand, A. Sourmia-Saquet, B. Donnadiou and J. P. Tuchagues, *Inorg. Chim. Acta*, 2008, **361**, 1681-1688.
- 17 T. J. Monks, R. P. Hanzlik, G. M. Cohen, D. Ross, D. G. Graham, *Toxicol. Appl. Pharmacol.*, 1992, **112**, 2-16.
- 18 J. L. Bolton, M.A. Trush, T. M. Penning, G. Dryhurst, T. J. Monks, *Chem. Res. Toxicol.*, 2000, **13**, 135-160.
- 19 J. Benites, J.A. Valderrama, H. Taper and P. Buc. Calderon, *Chem. Pharm. Bull.*, 2009, **57**, 615-619.
- 20 Serrano-Andres, M. Merchan, B. O. Roos and R. Lindh *J. Am. Chem. Soc.*, 1995, **117**, 3189-3202.
- 21 Aguilar-Martinez, G. Cuevas, M. Jimenez-Estrada, I. Gonzalez, B. Lotina-Hennsen and N. Macias-Ruvalcaba, *J. Org. Chem.*, 1999, **64**, 3684-3694.
- 22 Fabian and M. Neprab, *Collect. Czech. Chem. Commun.*, 1980, **45**, 2605.
- 23 N. Diaz, *J. Photochem. Photobiol. A*, 1990, **53**, 141-273.
- 24 Miyaji and J. L. Sessler, *Angew. Chem., Int. Ed.*, 2001, **40**, 154.
- 25 Miyaji and W. Sato, J. L. Sessler, *Angew. Chem., Int. Ed.*, 2000, **39**, 1777-1780.
- 26 E. J. Cho, H.M. Yeo, B. J. Ryu, H. A. Jeong and K. C. Nam, *Bull. Korean Chem. Soc.*, 2006, **27**, 1967-1968.
- 27 D. Jimenez, R. M. Manez, F. Sancenon and J. Soto, *Tetrahedron Lett.*, 2002, **43**, 2823-2825.
- 28 Y.P. Tseng, G.M. Tu, C.H. Lin, C. T.Chang, C.Y. Lin and Y.P. Yen, *Org. Biomol. Chem.*, 2007, **5**, 3592-3598.
- 29 Z. H Liu, S. Devaraj, C. R.Yang and Y. P. Yen, *Sens. Actuators B: Chem.*, 2012, **174**, 555-562.
- 30 Y. S. Lin, G.M. Tu, C.Y. Lin, Y. T. Chang and Y. P. Yen, *New J. Chem.*, 2009, **33**, 860-867.
- 31 W. C. Lin, Y. P. Tseng, C.Y. Lin and Y. P. Yen, *Org. Biomol. Chem.*, 2011, **15**, 5547-5553.
- 32 H. Yang, Z.G. Zhou, J. Xu, F. Y li, T. Yi and C-H Huang, *Tetrahedron*, 2007, **63**, 6732-6736.
- 33 B. Wannalorse, T. Tuntulaniand B. Tomapatanaget, *Tetrahedron*, 2008, **64**, 10619-10624.
- 34 X. Peng, Y. Wu, J. fan, M. Tian and K. Han, *J. Org. Chem.*, 2005, **70**, 10524-10531.
- 35 N. Kumari, S. Jha and S. Bhattacharya, *J. Org. Chem.*, 2011, **76**, 8215-8222.
- 36 R. M. F. Batista, E. Oliveira, S. P. G. Costa, C. Lodeiro and M. M. M. Raposo, *Org. Lett.*, 2007, **9**, 3201-3204.
- 37 K. Yoshida, T. Mori, S. Watanabe, H. Kawai and T. Nagamura, *J. Chem. Soc. Perkin. Trans.*, 1999, **2**, 393-398.
- 38 S. P. Wu, K. J. Du and Y.M. Sung, *Dalton Trans.*, 2010, **39**, 4363-4368.
- 39 S.P. Wu, R.Y. Huang and K.J. Du, *Dalton Trans.*, 2009, **24**, 4735-4740.
- 40 S. Madhupriya and K.P. Elango, *Spectrochim. Acta A*, 2012, **97**, 100-104.
- 41 S. Madhupriya and K.P. Elango, *Spectrochim. Acta A*, 2012, **97**, 429-434.
- 42 B. R. Jali, K. Masud and J. B. Baruah, *Polyhedron*, 2013, **51**, 75-81.
- 43 S. Kumar, R. Saini and D. Kaur, *Sens. Actuators B*, 2011, **160**, 705-712.
- 44 A. Satheshkumar, R. Manivanan and K. P. Elango, *J. Organomet. Chem.*, 2014, **750**, 98-106.
- 45 S. Madhupriya and K. P. Elango, *Synth. React. Inorg. Met.-Org. Nano-Met. Chem.*, 2014, **44**, 1104-1114.
- 46 N. Laurieri, M. H. J. Crawford, A. Kawamura, I. M. Westwood, J. Robinson, A. M. Fletcher, S. G. Davies, E. Sim and A. J. Russell, *J. Am. Chem. Soc.*, 2010, **132**, 3238-3239.
- 47 S. Salunke-Gawali, O. Pawar, M. Nikalje, R. Patil, T. Weyhermüller, V. G. Puranik and V. B. Konkimalla, *J. Mol. Struct.*, 2014, **1056-1057**, 97-103.
- 48 D. Chadar, M. Camilles, R. Patil, A. Khan, T. Weyhermüller and S. Salunke-Gawali, *J. Mol. Struct.*, 2015, **1086**, 179-189.
- 49 R. Patil, D. Chadar, D. Chaudhari, J. Peter, M. Nikalje, T. Weyhermüller and S. Salunke-Gawali, *J. Mol. Struct.*, 2014, **1075**, 345-351.
- 50 L. Kathawate, P. V. Joshi, T. K. Dash, S. Pal, M. Nikalje, T. Weyhermüller, V. G. Puranik, V. B. Konkimalla and S. Salunke-Gawali, *J. Mol. Struct.*, 2014, **1075**, 397-405.
- 51 D. Chadar, S. S. Rao, A. Khan, S. P. Gejji, K. S. Bhat, T. Weyhermüller and S. Salunke-Gawali, *RSC Adv.*, 2015, **5**, 57917-57929.
- 52 D. Chadar, S. S. Rao, S. P. Gejji, B. Ugale, C.M. Nagaraja, M. Nikaljeand S. Salunke-Gawali, *RSC Adv.*, 2015, **5**, 76419-76426.
- 53 S. Pal, V. B. Konkimalla, L. Kathawate, S. S. Rao, S. P. Gejji, V. G. Puranik, T. Weyhermüller and S. Salunke-Gawali, *RSC Adv.*, 2015, **5**, 82549-82563.
- 54 A. Ware, A. Patil, S. Khomane, T. Weyhermüller, S. Pingale and S. Salunke-Gawali, *J. Mol. Struct.*, 2015, **1093**, 39-48.
- 55 A. Patil, A. P. Ware, S. Bhand, D. Chakrovarty, R. Gonnade, S. S. Pingale and S. Salunke-Gawali, *J. Mol. Struct.*, 2016, **1114**, 132-143.
- 56 S. Wolff, D. Grimwood, J. McKinnon, M. Turner, D. Jayatilaka, M. Spackman, *CrystalExplorer 3.1* (2013), University of Western Australia, Crawley, Western Australia, 2005-2013, <http://hirshfeldsurface.net/CrystalExplorer>.
- 57 F.L. Hirshfeld, *Theor. Chim. Acta.*, 1977, **44**, 129-138.
- 58 M.A. Spackman, D. Jayatilaka, *Cryst. Eng. Comm.*, 2009, **11**, 19-32.
- 59 M.A. Spackman, J. J. McKinnon, *Cryst. Eng. Comm.*, 2002, **4**, 378-392.
- 60 J. J. McKinnon, M. A. Spackman, A. S. Mitchell, *Acta Crystallogr.*, 2004, **B60**, 627-668.
- 61 J. Rudnick, G. Gaspari, *J. Phys. A: Math. Gen. Phys.*, 1986, **19**, L191-L193.
- 62 A. Baumgartner, *J. Chem. Phys.*, 1993, **99**, 7496-7501.
- 63 D. D. Perrin, W. L. Armarego and D. R. Perrin. 'Purification of Laboratory Chemicals', Pergamon Press, London, 1988, 260.
- 64 Bruker, 2007; APEX2, SAINT, and SADABS: Bruker AXS Inc., Madison, Wisconsin, USA.
- 65 G. M. Sheldrick, *Acta Cryst.*, 2008, **A64**, 112 - 122.
- 66 L. J. Farrugia, *J. Appl. Cryst.*, 2012, **45**, 849-854.
- 67 C. F. Macrae, I. J. Bruno, J. A. Chisholm, P. R. Edgington, P. McCabe, E. Pidcock, L. RodriguezMonge, R. Taylor, J. van de Streek and P. A. Wood, *J. Appl. Crystallogr.*, 2008, **41**, 466-470.
- 68 A. L. Spek, *Acta Cryst.*, 2009, **D65**, 148-155.

## Journal Name

## ARTICLE

- 69 J. D. Chai, M. Head-Gordon, *J. Chem. Phys.* 2008, **128**, 84-106.
- 70 M. J. Frisch G. W. Trucks H. B. Schlegel G. E. Scuseria, M. A. Robb J. R. Cheeseman J. A. Montgomery Jr, T. Vreven, K. N. Kudin, J. C. Burant, J. M. Millam, S. S. Iyengar, J. Tomasi, V. Barone, B. Mennucci, M. Cossi, G. Scalmani, N. Rega, G. A. Petersson, H. Nakatsuji, M. Hada, M. Ehara, K. Toyota, R. Fukuda, J. Hasegawa, M. Ishida, T. Akajima, Y. Honda, O. Kitao, H. Nakai, M. Klene, X. Li, J. E. Knox, H. P. Hratchian, J. B. Cross, V. Bakken, C. Adamo, J. Jaramillo, R. Gomperts, R. E. Stratmann, O. Yazyev, A. J. Austin, R. Cammi, C. Pomelli, J. W. Ochterski, P. Y. Ayala, K. Morokuma, G. A. Voth, P. Salvador, J. J. Dannenberg, V. G. Zakrzewski, S. Dapprich, A. D. Daniels, M. C. Strain, O. Farkas, D. K. Malick, A. D. Rabuck, K. Raghavachari, J. B. Foresman, J. V. Ortiz, Q. Cui, A. G. Baboul, S. Clifford, J. Cioslowski, B. B. Stefanov, G. Liu, A. Liashenko, P. Piskorz, I. Komaromi, R. L. Martin, D. J. Fox, T. Keith, M. A. Al-Laham, C. Y. Peng, A. Nanayakkara, M. Challacombe, P. M. W. Gill, B. Johnson, W. Chen, M. W. Wong, C. Gonzalez and J. A. Pople, Gaussian03, revision Gaussian, Inc., Pittsburgh, PA, 2003.
- 71 G. A. Petersson, T. G. Tensfeldt, and J. A. Montgomery Jr, *J. Chem. Phys.*, 1991, **94**, 6091-6101.

**Table 1** Single Crystal X-ray data for 2MPA, 3MPA, 3AMT, 2EPA and 2AET

Identification code	2MPA	3MPA	3AMT	2EPA	2AET
CCDC No	1446762	1446761	1446759	1446760	1446920
Empirical formula	C <sub>16</sub> H <sub>11</sub> BrN <sub>2</sub> O <sub>2</sub>	C <sub>16</sub> H <sub>11</sub> BrN <sub>2</sub> O <sub>2</sub>	C <sub>15</sub> H <sub>10</sub> BrNO <sub>2</sub> S	C <sub>17</sub> H <sub>13</sub> BrN <sub>2</sub> O <sub>2</sub>	C <sub>16</sub> H <sub>12</sub> BrNO <sub>2</sub> S
Formula weight	343.18	343.18	348.21	357.2	362.24
Temperature	296(2) K	296(2) K	296(2) K	296(2) K	296(2) K
Wavelength	1.54178 Å	0.71073 Å	0.71073 Å	0.71073 Å	1.54178 Å
Crystal system, space group	Monoclinic, <i>P2<sub>1</sub>/n</i>	Monoclinic, <i>P2<sub>1</sub>/c</i>	Triclinic, <i>P-1</i>	Monoclinic, <i>C2/c</i>	Monoclinic, <i>Cc</i>
Unit cell dimensions	a = 4.9001(3) Å, b = 14.5285(8) Å β = 96.875(2)° c = 19.5250(10)	a = 12.9287(2) Å, b = 7.70260(10) Å β = 109.1800(5)° c = 14.6188(2) Å	a = 7.3322(2) Å α = 91.4380(6)° b = 7.7451(2) Å β = 90.0420(7)° c = 12.5621(3) Å γ = 96.9860(7)°	a = 25.2419(4) Å, b = 4.46860(10) Å, β = 108.0900(8)° c = 27.7323(4) Å	a = 23.3217(11) Å, b = 4.4264(2) Å, β = 91.381(3)° c = 14.6193(7) Å
Volume	1380.01(13) Å <sup>3</sup>	1375.00(3) Å <sup>3</sup>	707.86(3) Å <sup>3</sup>	2973.47(9) Å <sup>3</sup>	1508.73(12) Å <sup>3</sup>
Z, Calculated density	4, 1.652 Mg/m <sup>3</sup>	4, 1.658 Mg/m <sup>3</sup>	2, 1.634 Mg/m <sup>3</sup>	8, 1.596 Mg/m <sup>3</sup>	4, 1.595 Mg/m <sup>3</sup>
Absorption coefficient	4.116 mm <sup>-1</sup>	2.995 mm <sup>-1</sup>	3.050 mm <sup>-1</sup>	2.773 mm <sup>-1</sup>	5.037 mm <sup>-1</sup>
F(000)	688	688	348	1440	728
Crystal size	0.46 × 0.11 × 0.063 mm	0.256 × 0.241 × 0.193 mm	0.268 × 0.143 × 0.122 mm	0.431 × 0.184 × 0.063 mm	0.180 × 0.119 × 0.103 mm
Theta range for data collection	3.802 to 68.386 °	2.873 to 28.535°	2.650 to 28.396°	3.029 to 28.277°	3.792 to 68.470°
Limiting indices	-5 ≤ h ≤ 5, -17 ≤ k ≤ 17, -23 ≤ l ≤ 23	-17 ≤ h ≤ 17, -10 ≤ k ≤ 10, -19 ≤ l ≤ 19	-9 ≤ h ≤ 9, -10 ≤ k ≤ 10, -16 ≤ l ≤ 16	-33 ≤ h ≤ 33, -5 ≤ k ≤ 5, -36 ≤ l ≤ 36	-28 ≤ h ≤ 28, -5 ≤ k ≤ 5, -17 ≤ l ≤ 17
Reflections collected / unique	19383 / 2515 [R(int) = 0.1625]	58520 / 3490 [R(int) = 0.0787]	25998 / 3546 [R(int) = 0.0688]	19705 / 3640 [R(int) = 0.0966]	7556 / 2600 [R(int) = 0.0646]
Completeness to theta = 25.242°	9960 %	99.90%	100.00%	99.90%	99.10%
Refinement method	Full-matrix least-squares on <i>F</i> <sup>2</sup>	Full-matrix least-squares on <i>F</i> <sup>2</sup>	Full-matrix least-squares on <i>F</i> <sup>2</sup>	Full-matrix least-squares on <i>F</i> <sup>2</sup>	Full-matrix least-squares on <i>F</i> <sup>2</sup>
Data / restraints / parameters	2515 / 0 / 190	3490 / 0 / 190	3546 / 0 / 181	3640 / 0 / 199	2600 / 2 / 190
Goodness-of-fit on <i>F</i> <sup>2</sup>	1.065	1.07	1.023	1.058	1.055
Final R indices [I > 2σ(I)]	R <sub>1</sub> = 0.0811, wR <sub>2</sub> = 0.2057	R <sub>1</sub> = 0.0501, wR <sub>2</sub> = 0.1206	R <sub>1</sub> = 0.0553, wR <sub>2</sub> = 0.1033	R <sub>1</sub> = 0.0625, wR <sub>2</sub> = 0.1064	R <sub>1</sub> = 0.0623, wR <sub>2</sub> = 0.1471
R indices (all data)	R <sub>1</sub> = 0.0978, wR <sub>2</sub> = 0.2260	R <sub>1</sub> = 0.0650, wR <sub>2</sub> = 0.1281	R <sub>1</sub> = 0.0977, wR <sub>2</sub> = 0.1181	R <sub>1</sub> = 0.1200, wR <sub>2</sub> = 0.1240	R <sub>1</sub> = 0.0861, wR <sub>2</sub> = 0.1642
Extinction coefficient	n/a	n/a	n/a	n/a	n/a
Largest diff. peak and hole	1.021 and -1.674 e.Å <sup>-3</sup>	0.581 and -0.959 e.Å <sup>-3</sup>	0.700 and -0.625 e.Å <sup>-3</sup>	0.780 and -0.809 e.Å <sup>-3</sup>	0.322 and -0.623 e.Å <sup>-3</sup>

Table 2 Hydrogen bonding geometries of compounds

Com	D-H...A	D-H(Å)	H...A(Å)	D...A(Å)	∠D-H...A(°)	
2MPA	C(5)-H(5)...O(2) <sup>(i)</sup>	0.929	2.511	3.42(1)	165.6	
	C(14)-H(14)...O(1) <sup>(ii)</sup>	0.930	2.647	3.43(1)	142.6	
	N(1)-H(1)...N(2) <sup>(intra)</sup>	0.859	2.129	2.601(9)	114.1	
	∠C(3)-N(1)-C(11)-C(12)				-177.2(7)	
3MPA	N(1)-H(1)...O(1) <sup>(iii)</sup>	0.860	2.290	3.036(4)	145.1	
	C(8)-H(8)...O(2) <sup>(iii)</sup>	0.930	2.298	3.214(5)	168.2	
	C(16)-H(16)...O(1) <sup>(iii)</sup>	0.930	2.536	3.347(4)	146	
	C(14)-H(14)...Br(1) <sup>(iv)</sup>	0.930	2.689	3.396(4)	133.3	
	N(1)-H(1)...O(2) <sup>(intra)</sup>	0.860	2.126	2.570(4)	111.6	
	∠C(3)-N(1)-C(11)-C(12)				-85.1(5)	
2AMT	N(1)-H(1)...O(1) <sup>(iii)</sup>	0.860	2.321	3.020(5)	138.6	
	C(8)-H(8)...O(2) <sup>(iii)</sup>	0.930	2.254	3.163(4)	165.7	
	C(15)-H(15)...O(1) <sup>(v)</sup>	0.930	2.662	3.508(4)	151.5	
	N(1)-H(1)...O(2) <sup>(intra)</sup>	0.860	2.208	2.577(3)	105.7	
		∠C(3)-N(1)-C(11)-C(12)				73.3(4)
2EPA	N(1)-H(1)...O(2) <sup>(vi)</sup>	0.861	2.230	2.987(3)	146.8	
	C(5)-H(5)...N(2) <sup>(vi)</sup>	0.929	2.570	3.406(5)	149.8	
	C(7)-H(7)...O(1) <sup>(vii)</sup>	0.929	2.621	3.403(4)	142.2	
	C(15)-H(15)...O(1) <sup>(viii)</sup>	0.930	2.707	3.542(6)	149.8	
	N(1)-H(1)...O(2) <sup>(intra)</sup>	0.861	2.099	2.575(4)	114.2	
		∠C(3)-N(1)-C(11)-C(12)				-94.8(4)
	∠C(13)-C(12)-C(11)-N(1)				-170.2(3)	
2AET	N(1)-H(1)...O(1) <sup>(ix)</sup>	0.86	2.13	2.79(2)	133.2	
	C(14)-H(14)...Br(1) <sup>(ix)</sup>	0.93	2.912	3.57(1)	128.7	
	N(1)-H(1)...O(2) <sup>(intra)</sup>	0.86	2.12	2.58(2)	113.6	
		∠C(3)-N(1)-C(11)-C(12)				83.0(2)
		∠C(13)-C(12)-C(11)-N(1)				-175(1)

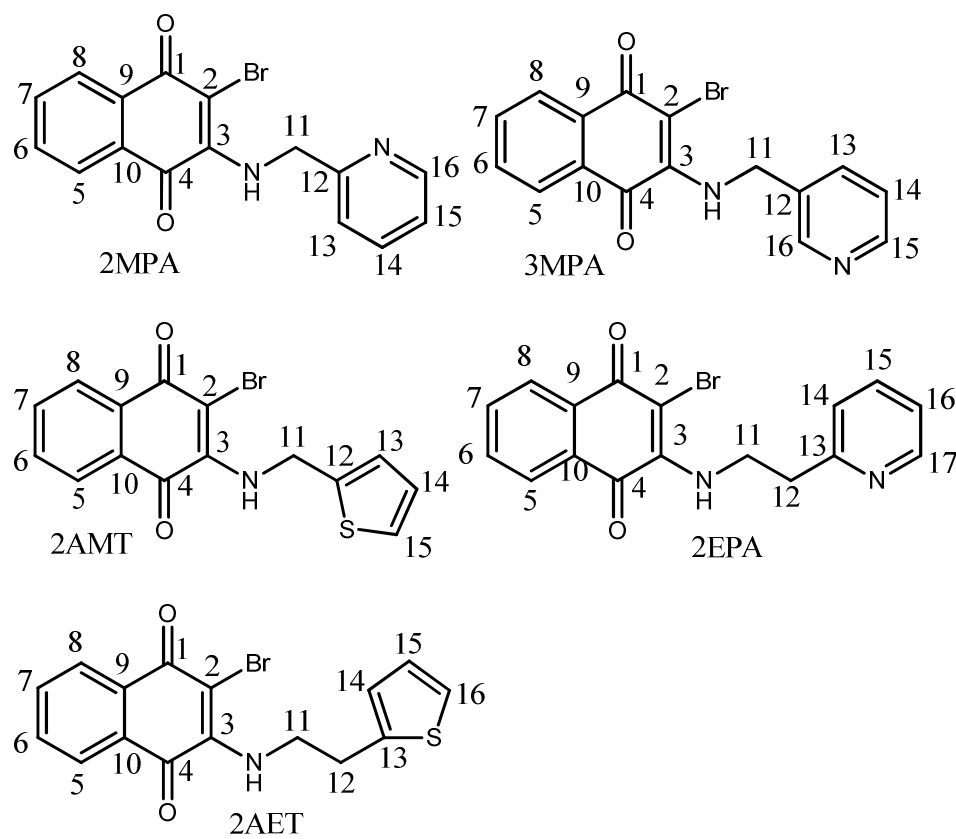
i) -x, -y, 1-z; ii) -1.5+x, 1/2-y, -1/2+z; iii) x, -1+y, z; iv) 1-x, -y, 2-z; v) -1+x, -1+y, z; vi) -x, 1-y, -z;  
vii) 1/2-x, -1/2+y, 1/2-z; viii) 1/2-x, -1/2-y, -z; ix) x, 1-y, -1/2+z; x) x, 2-y, -1/2+z

**Table 3** Molecular interaction of aminonaphthoquinone ligands

Com	Type of interaction	Figure	Number of similar neighbouring molecules	Angle between naphthoquinone ring plane and pyridine or thiophene ring plane(°)
2MPA	C-H...O, Br... $\pi$	Fig.S9	5	9
3MPA	N-H...O, C-H...O, C-H...Br, $\pi$ ... $\pi$ stacking	Fig.S10	5	85
2AMT	N-H...O, C-H...O	Fig.S11	4	89
2EPA	N-H...O, C-H...O, C-H...N	Fig.S12	4	22.2
2AET	N-H...O, C-H... $\pi$ , C-H...Br	Fig.S13	6	9

**Table 4** Experimental UV-visible absorption spectra of chemosensors 2MPA and 2EPA

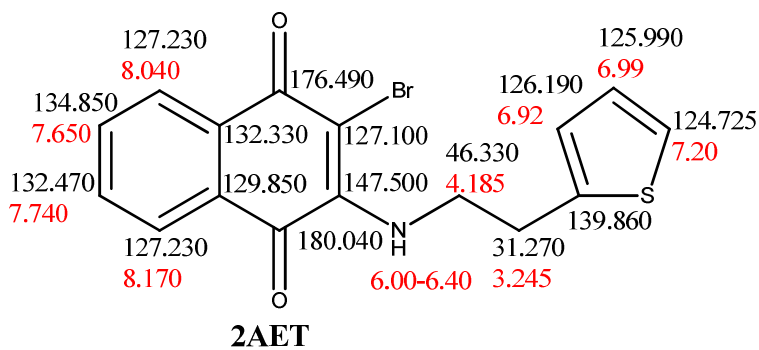
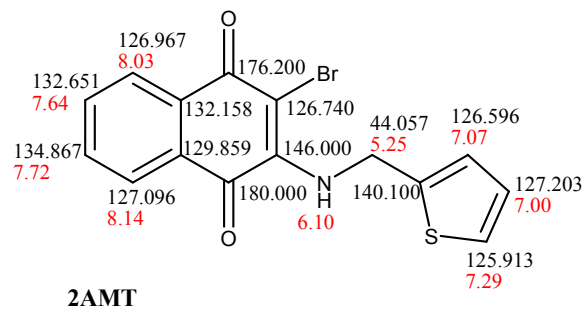
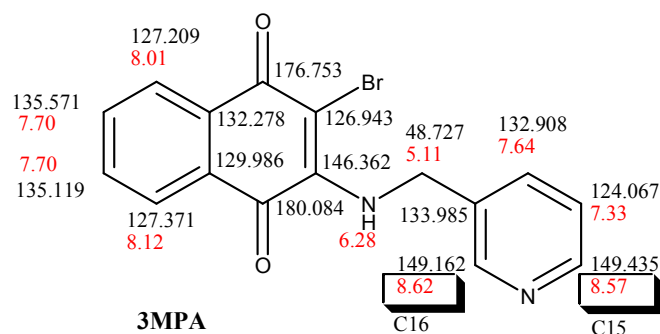
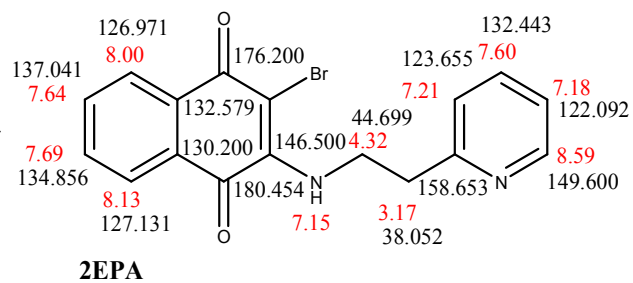
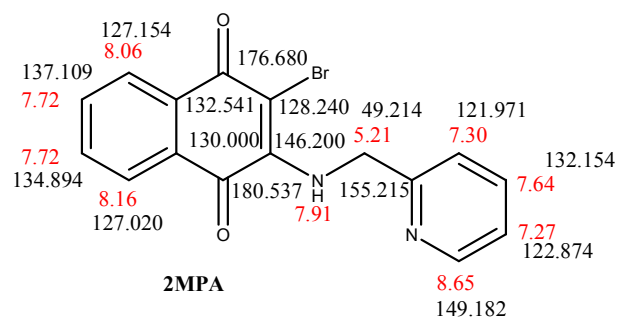
Solvent systems	$\lambda_{\max}$ (nm) for 2MPA	$\lambda_{\max}$ (nm) for 2EPA
Methanol	455, 284	468, 284
Methanol+ TEA	437, 287	468, 280
Methanol+ Water	467, 272	477, 282
Methanol+ TEA+ water	458, 362, 282	475, 282
TEA	449, 331, 307	465, 334, 287



Scheme 1 Molecular Structures of aminonaphthoquinones under investigation

Journal Name

ARTICLE

Scheme <sup>2</sup>H and <sup>13</sup>C chemical shift (ppm) of aminonaphthoquinone ligands

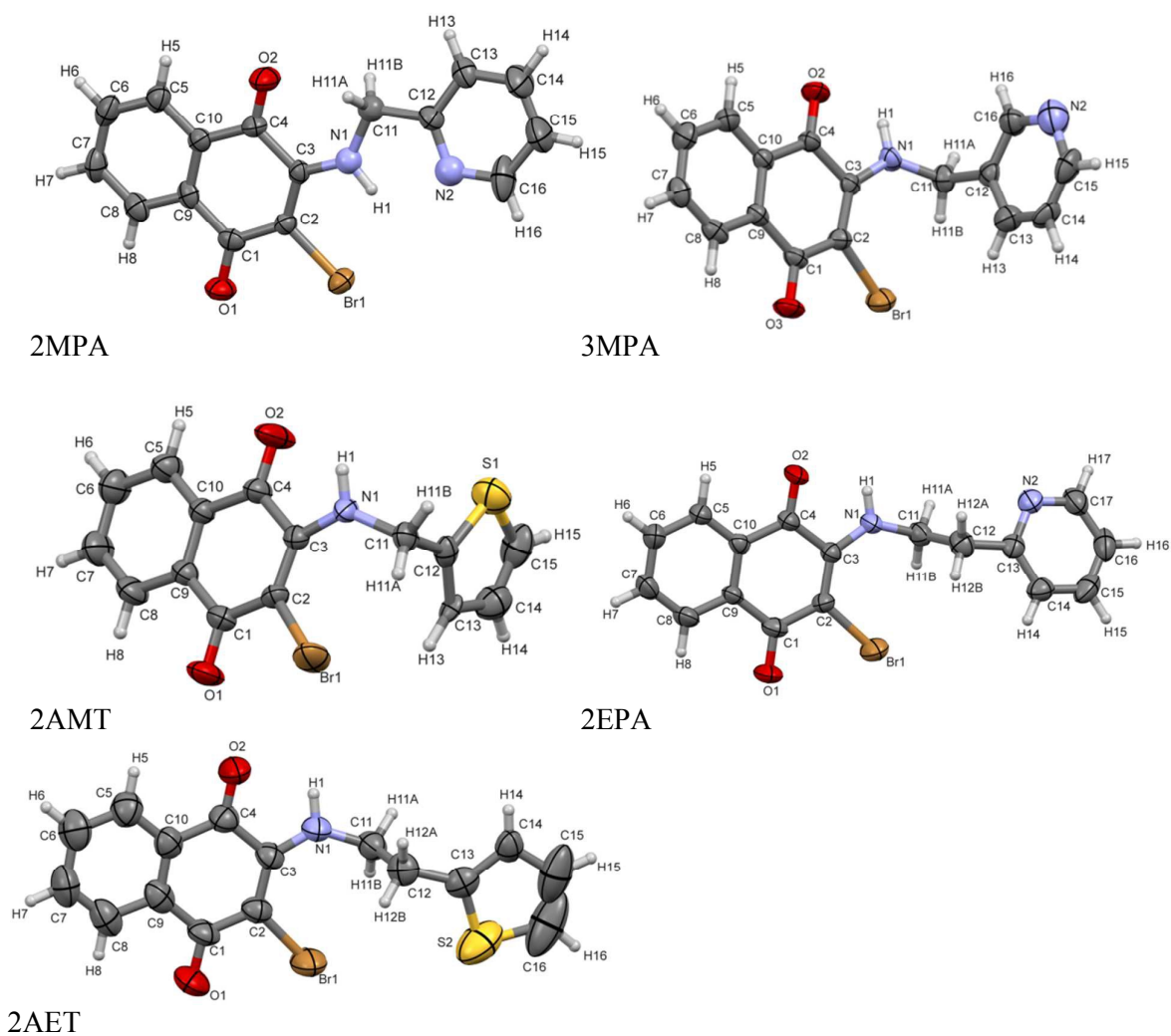


Fig.1 ORTEP plots of 2MPA, 3MPA, 2AMT, 2EPA and 2AET. The ellipsoid was drawn with 50% of probability

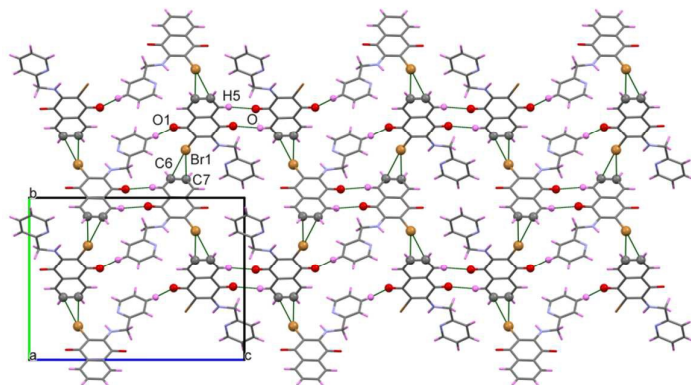


Fig.2 Molecular packing of 2MPA down a-axis

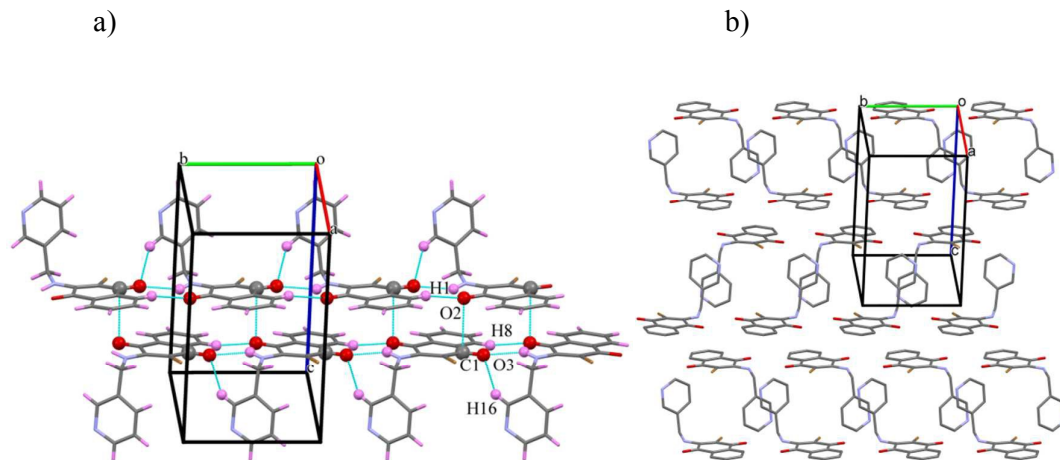


Fig.3a) Polymeric chains of 3MPA molecules formed by C(8)-H(8)⋯O(2) and N(1)-H(1)⋯O(1) interaction,. b) Stacked polymeric chains of 3MPA

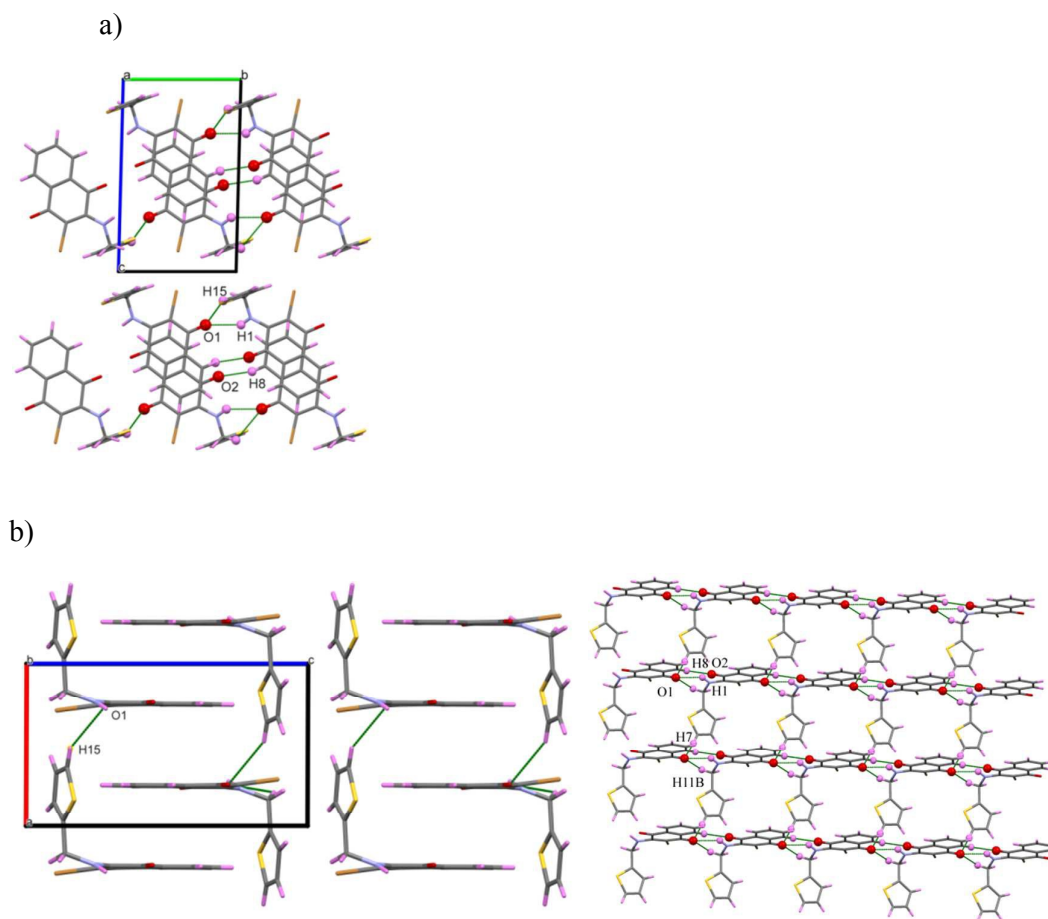


Fig.4a) Molecular packing of 2AMT molecules down a-axis, b) Molecular packing of 2AMT molecules down b-axis, c) Polymeric chains formed by hydrogen bonding separated by thiophene rings

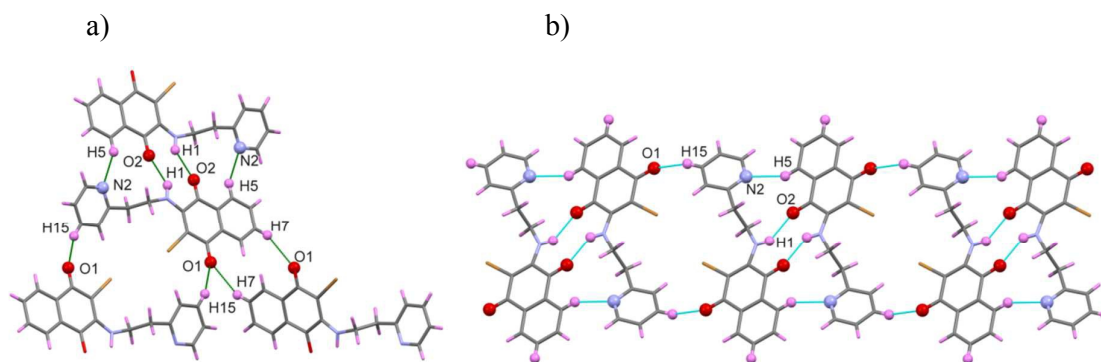


Fig.5a) Neighboring molecules of EPA. b) Dimeric chains of 2EPA formed by C-H...O interaction

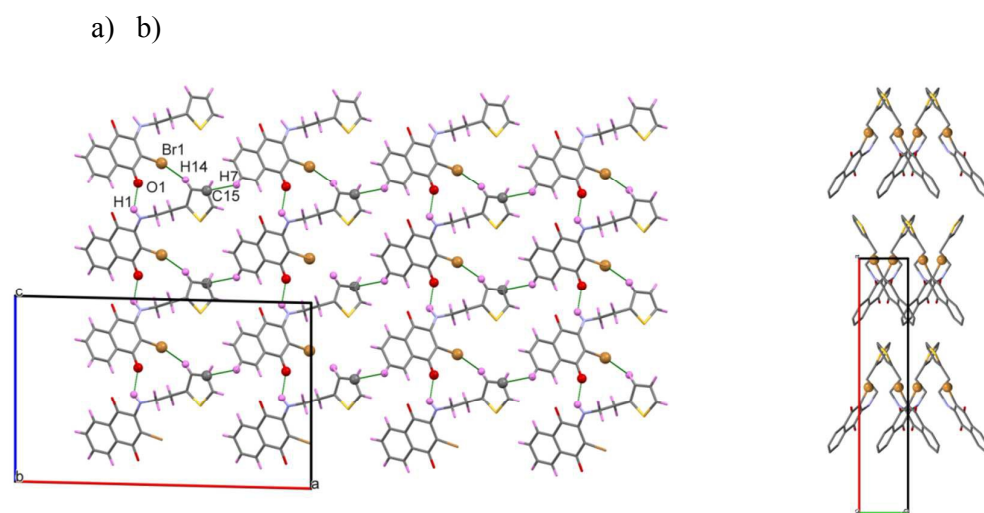
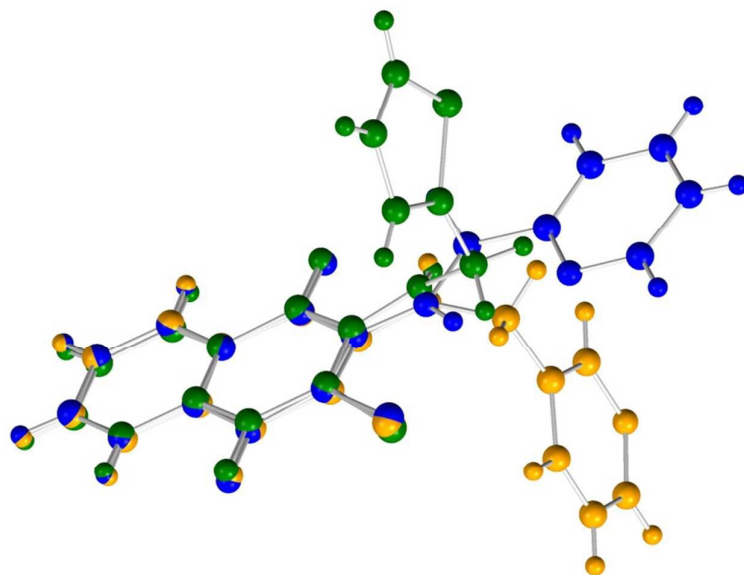


Fig.6 a) Molecular packing of 2AET molecules down b-axis and b) down c-axis

a) 2MPA(blue), 3MPA(yellow), 2AMT(green)



a) 2EPA(green), 2AET(Thiophene)

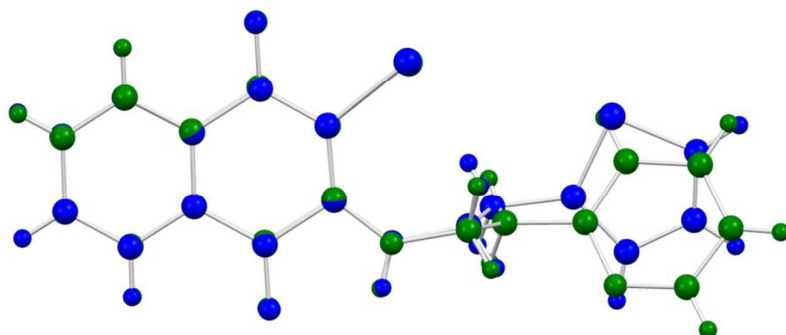
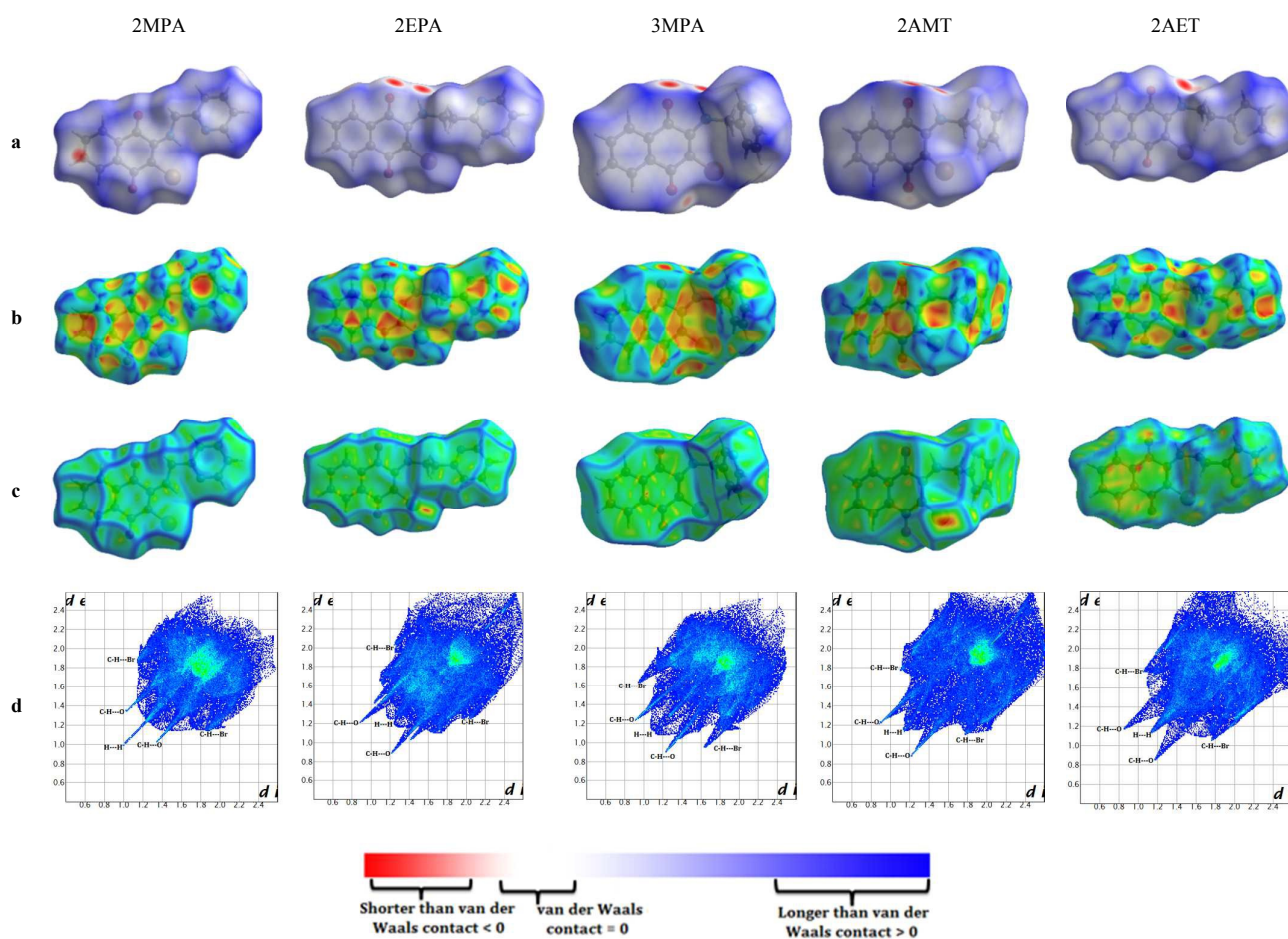


Fig.7 Overlay structures of a) 2MPA, 3MPA and 2AMT, b) 2EPA and 2AET



**Fig. 8** Hirshfeld surfaces mapped with (a)  $d_{\text{norm}}$  (b) shape index, (c) curvedness and (d) 2D fingerprint plots with  $d_i$  and  $d_c$  ranging from 0.6 to 2.4 Å for 2MPA, 2EPA, 3MPA, 2AMT and 2AET.

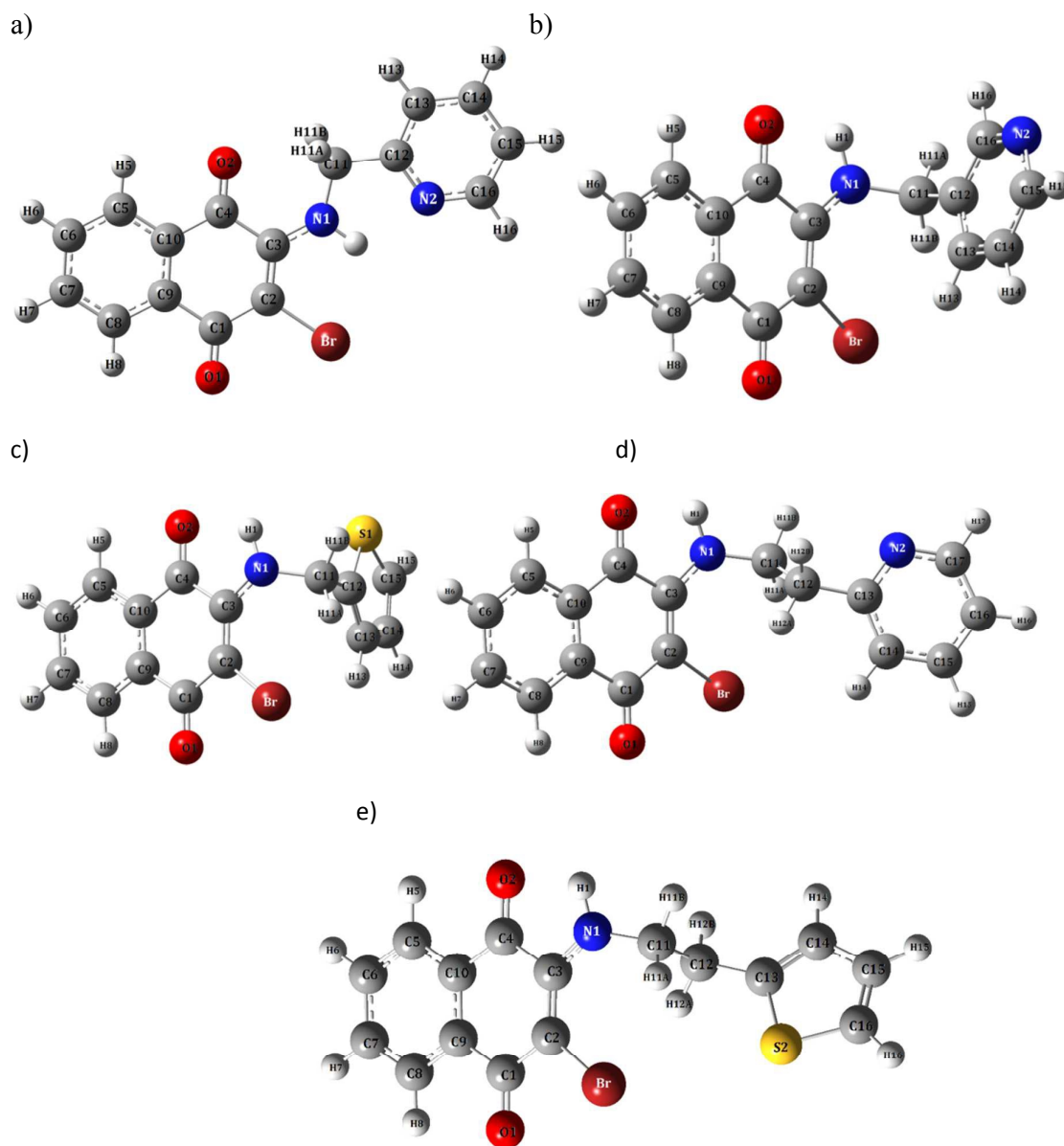


Fig.9 Optimized structures of (a) 2MPA, (b) 3MPA (c) 2AMT (d) 2EPA (e) AET. Atomic labelling scheme is shown.

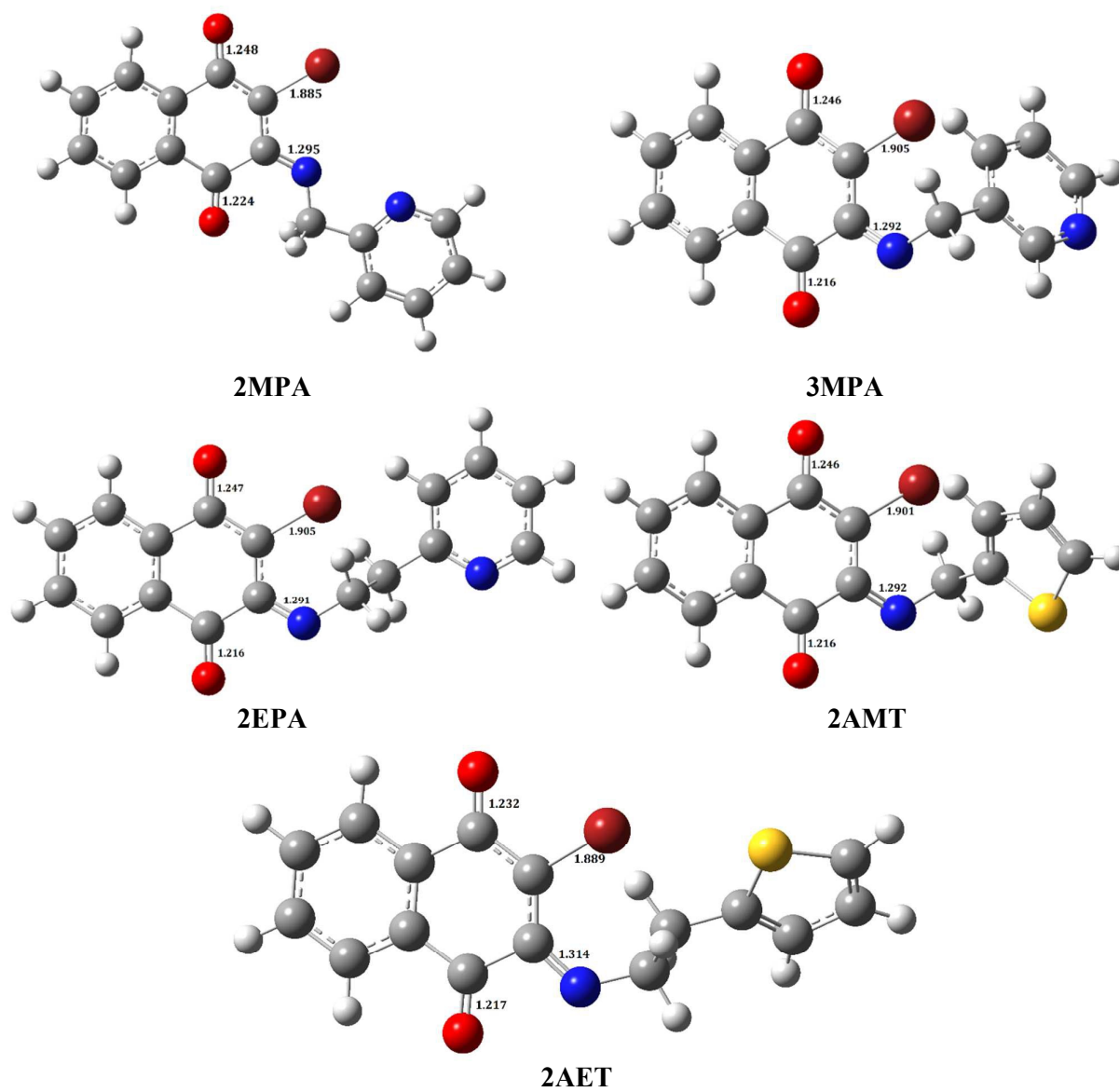
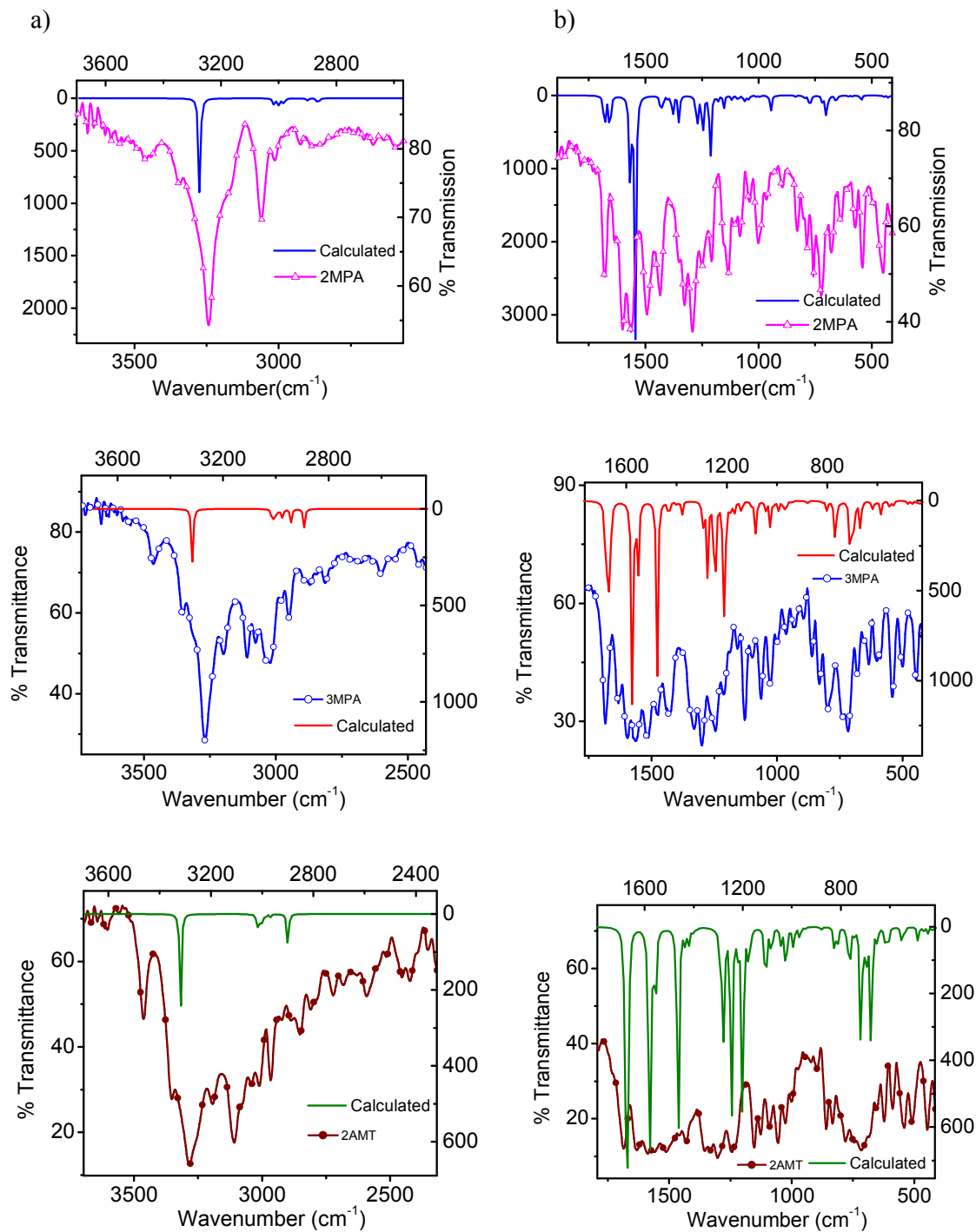


Fig.10 Optimized structures of anionic form (a) 2MPA, (b) 3MPA (c) 2AMT (d) 2EPA (e) 2AET



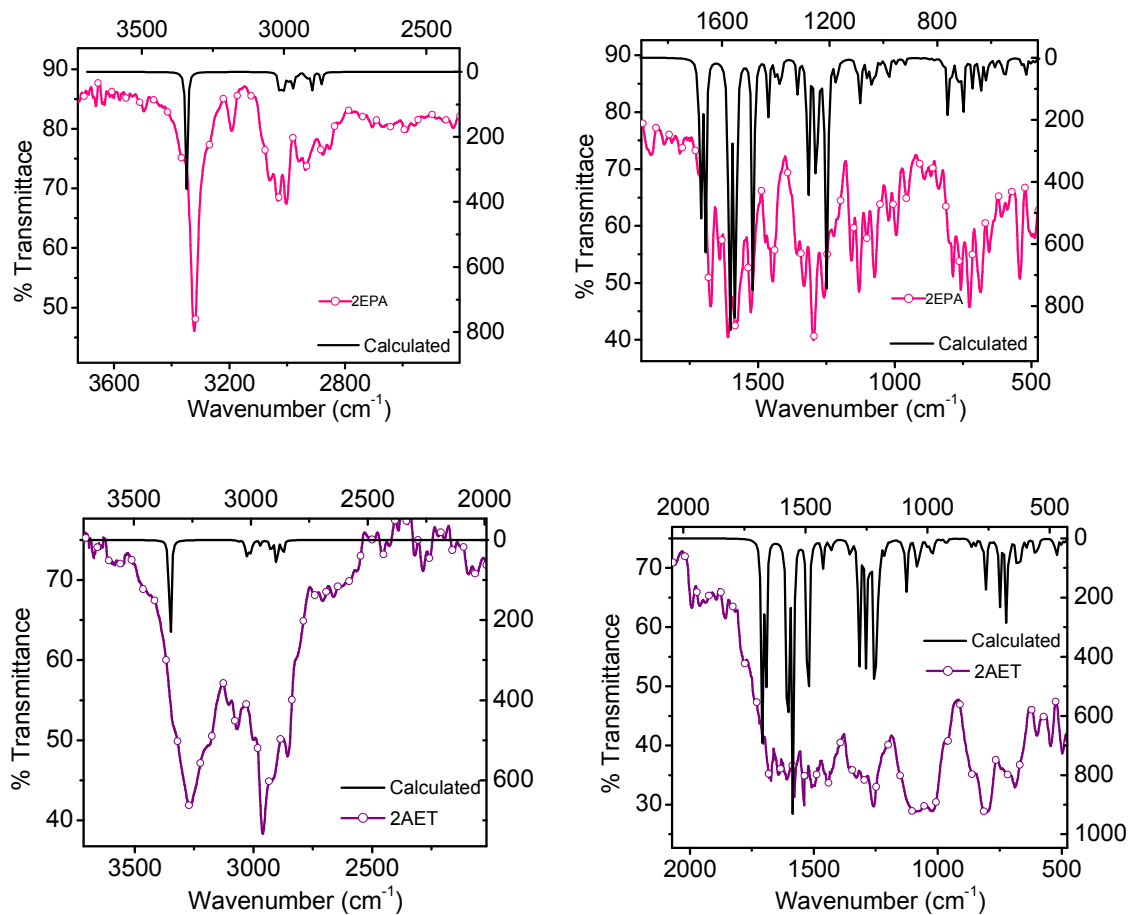


Fig.11 Observed and optimized FT-IR spectra of 2MPA, 3MPA, 2AMT, 2EPA and 2AET. The spectra is shown in two regions for peaks a)-NH, -CH and b) -C=O, -C-N, -C-Br.

Journal Name

ARTICLE

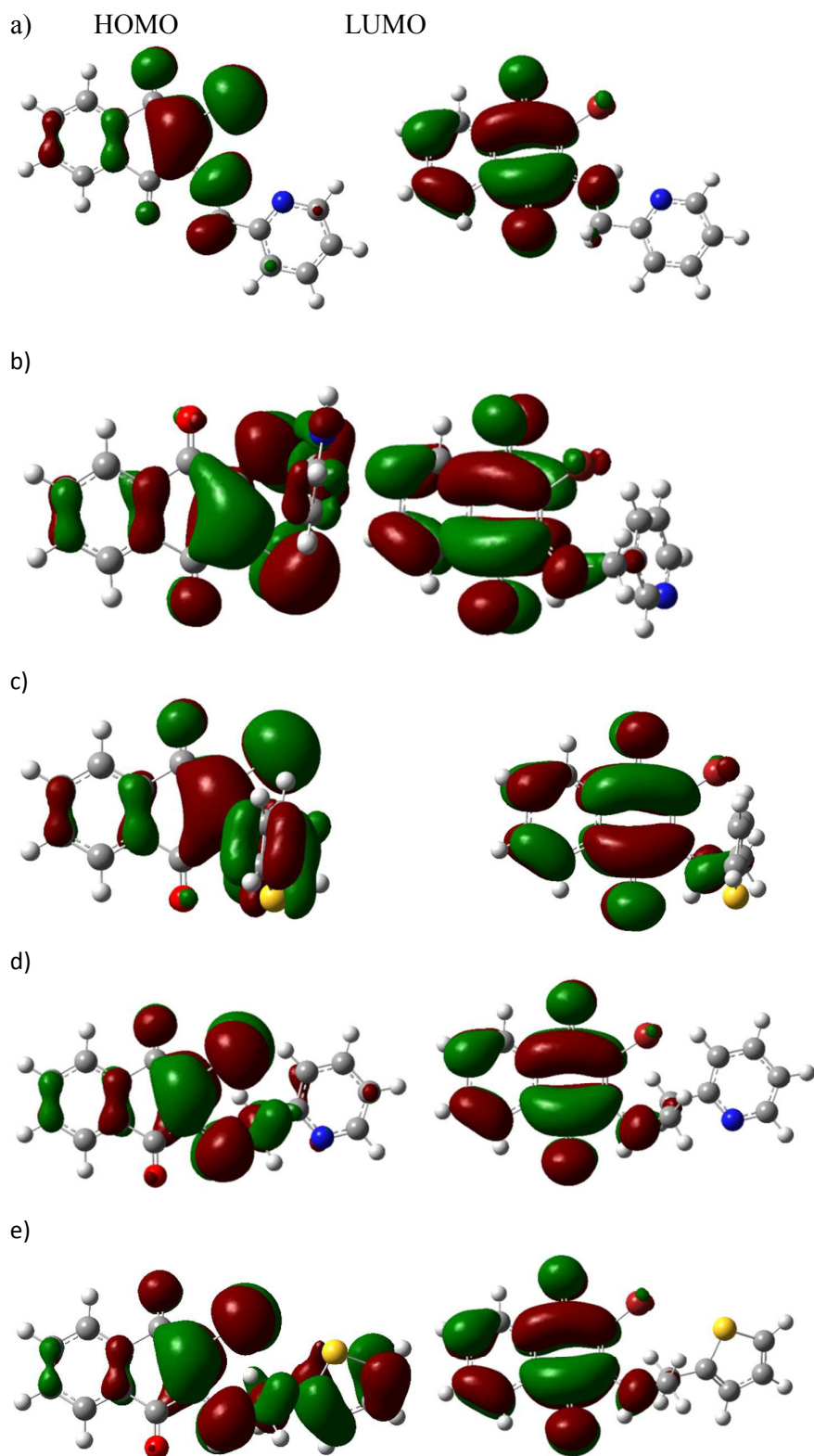
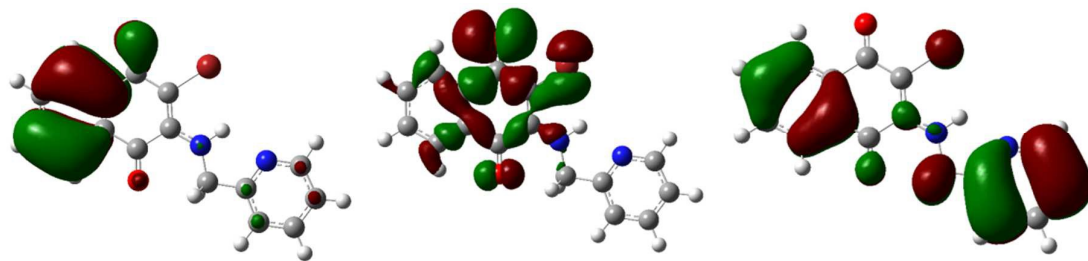


Fig.12 HOMO and LUMO in a) 2MPA, (b) 3MPA (c) 2EPA (d) 2AMT (e) 2AET

Journal Name

ARTICLE

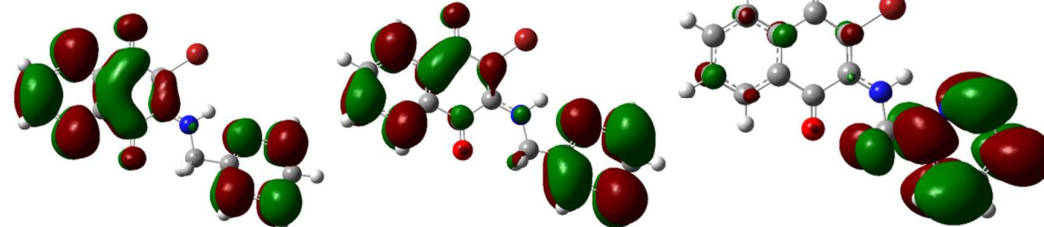
a)



HOMO-1

HOMO-2

HOMO-3

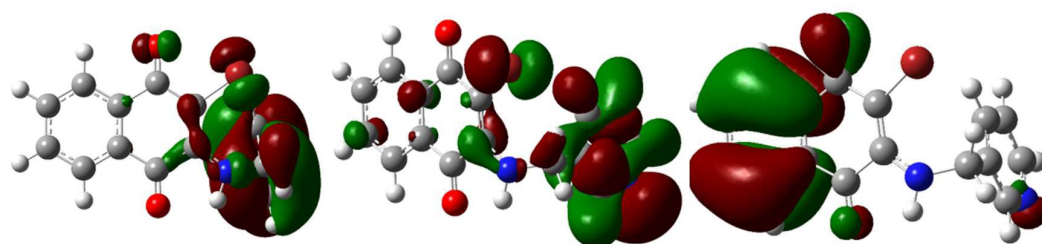


LUMO+1

LUMO+2

LUMO+3

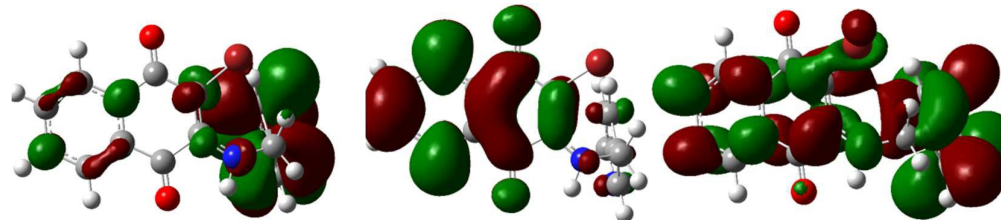
b)



HOMO-1

HOMO-2

HOMO-3



LUMO-1

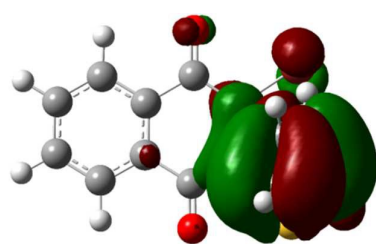
LUMO-2

LUMO-3

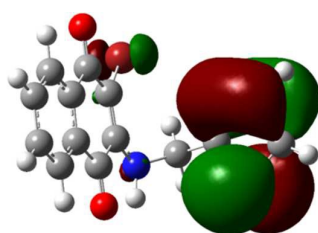
Journal Name

ARTICLE

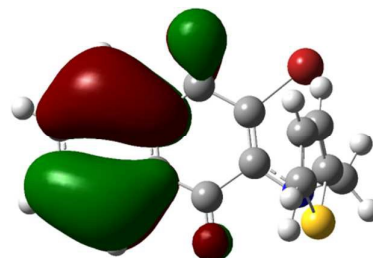
c)



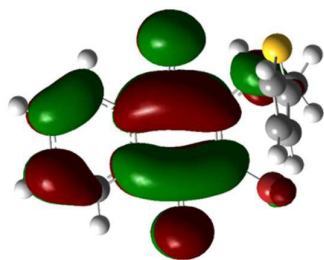
HOMO-1



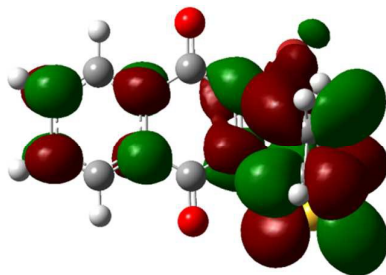
HOMO-2



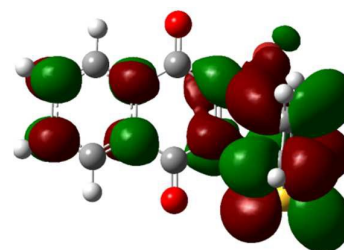
HOMO-3



LUMO-1

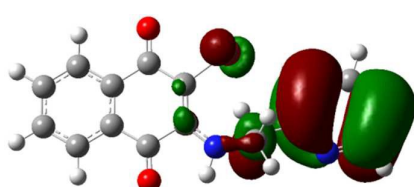


LUMO-2

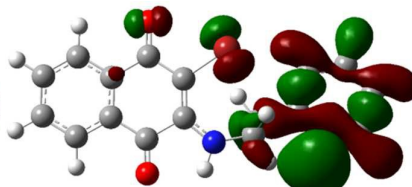


LUMO-3

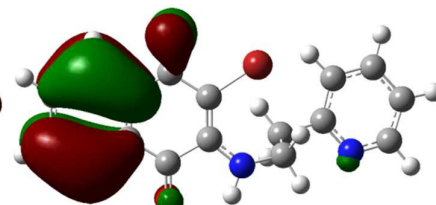
d)



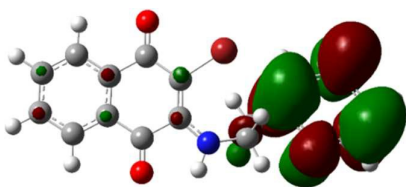
HOMO-1



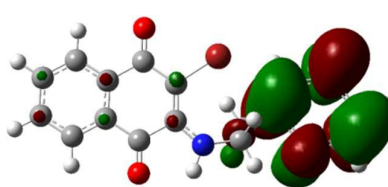
HOMO-2



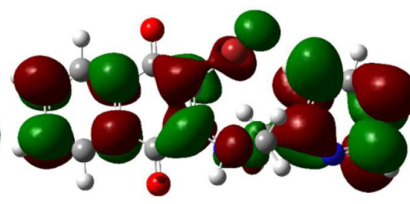
HOMO-3



LUMO-1



LUMO-2



LUMO-3

e)

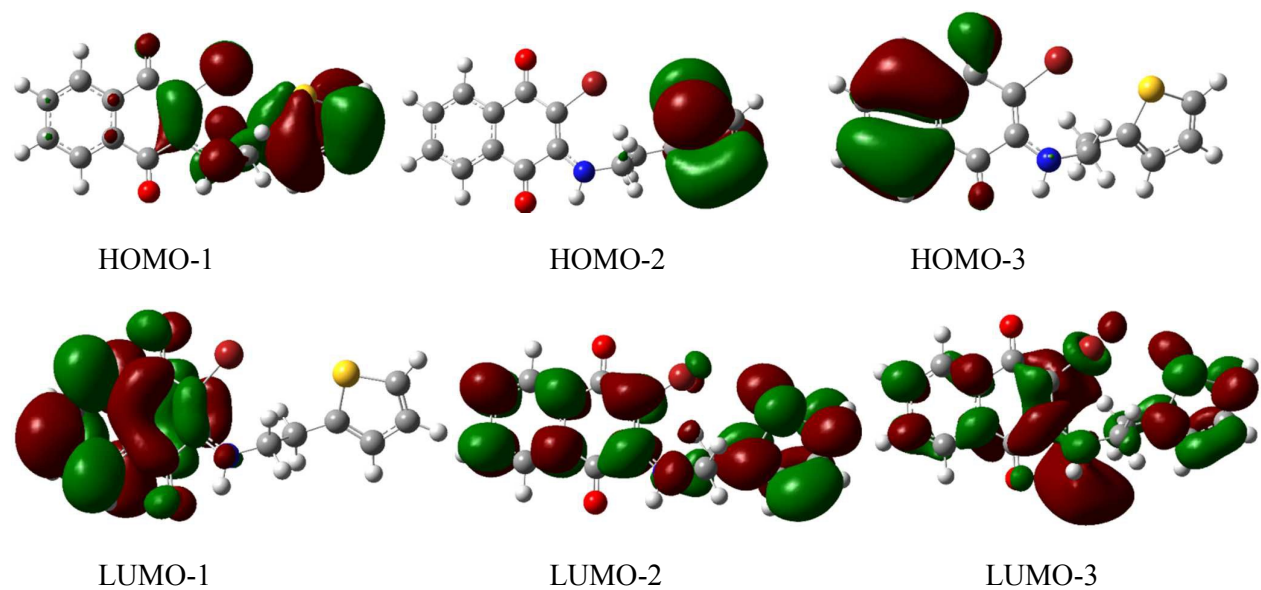


Fig.13 MOs namely, HOMO-1, HOMO-2 and HOMO-3 and LUMO+1, LUMO+2 and LUMO+3 in a) 2MPA, (b) 3MPA, (c) 2AMT, (d) 2EPA, (e) 2AET are also depicted. These enable one to assign the transition in the electronic spectra derived from the TD-DFT theory

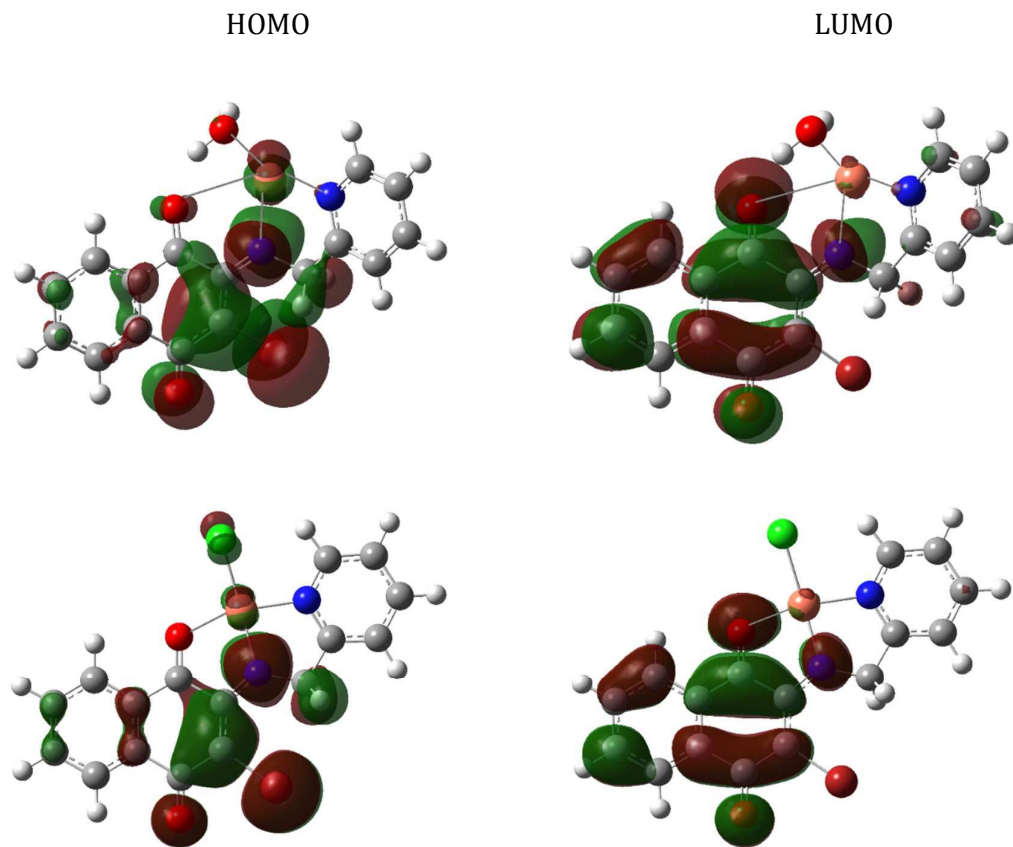


Fig. 14 HOMO and LUMO in 2MPA-Cu<sup>2+</sup> complexes.

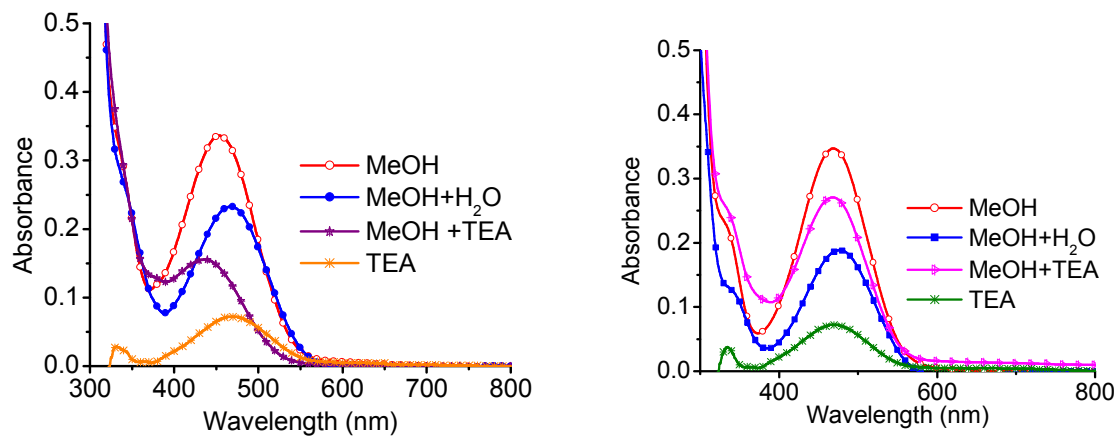


Fig.15 UV-visible spectra of a) 2MPA and b)3MPA in various solvents

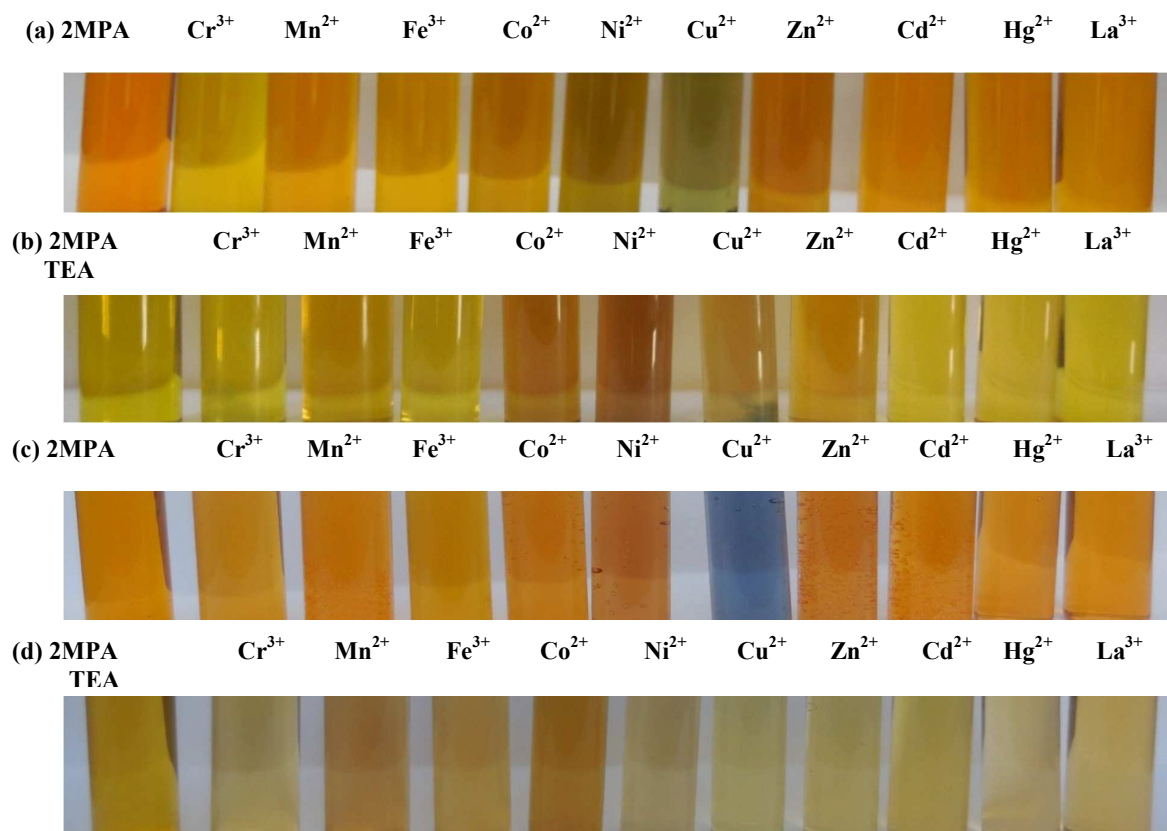


Fig. 16 a) Color change in Chemosensor 2MPA ( $10^{-4}$  M) with metal ions ( $10^{-4}$  M) in methanol, b) Chemosensor 2MPA ( $10^{-4}$  M) with metal ions ( $10^{-4}$  M) in methanol and triethylamine, c) Chemosensor 2MPA with metal ions ( $10^{-4}$  M) in methanol and water, d) Chemosensor 2MPA ( $10^{-4}$  M) with metal ions ( $10^{-4}$  M) in methanol-water-triethylamine

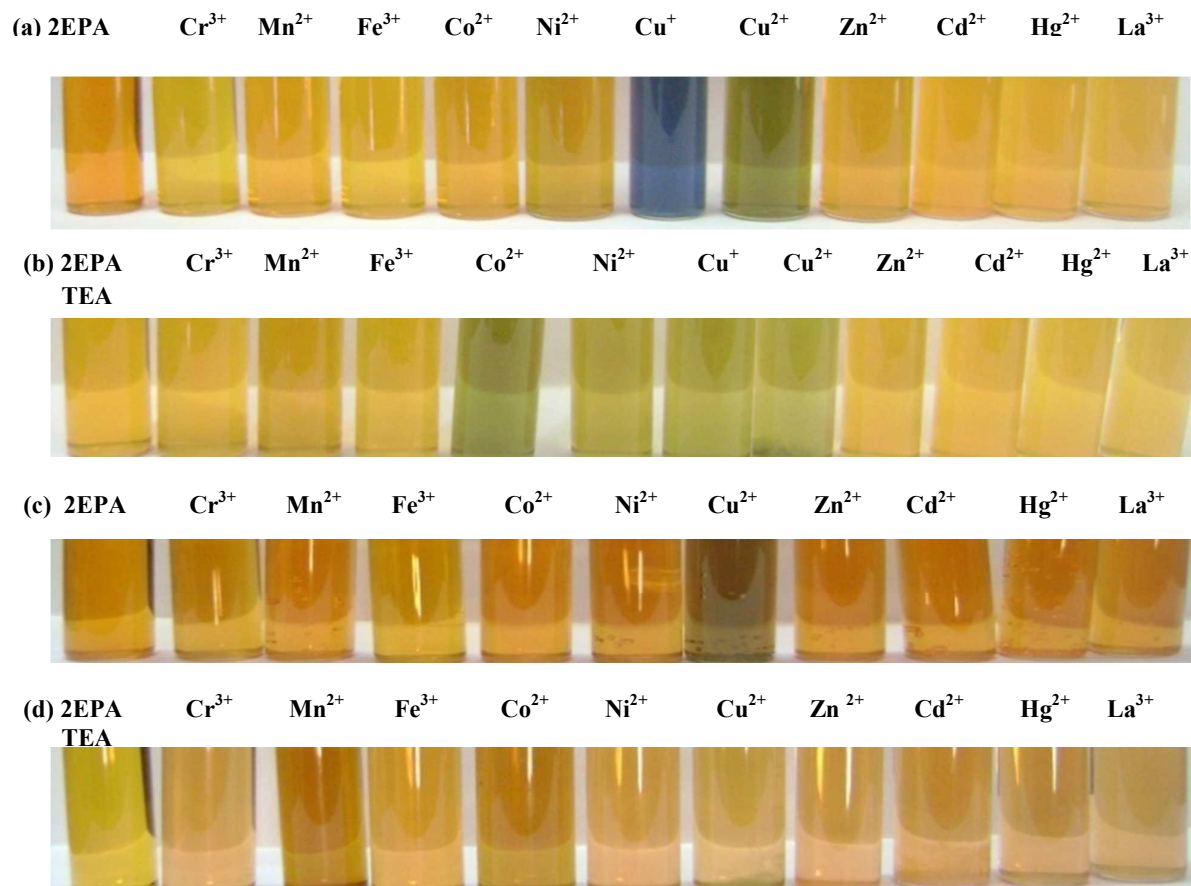


Fig. 17 Color change in Chemosensor 2EPA ( $10^{-4}$  M) with metal ions ( $10^{-4}$  M) in methanol, b) Chemosensor 2EPA ( $10^{-4}$  M) with metal ions ( $10^{-4}$  M) in methanol and triethylamine, c) Chemosensor 2EPA with metal ions ( $10^{-4}$  M) in methanol and water, d) Chemosensor 2EPA ( $10^{-4}$  M) with metal ions ( $10^{-4}$  M) in methanol, water and triethylamine

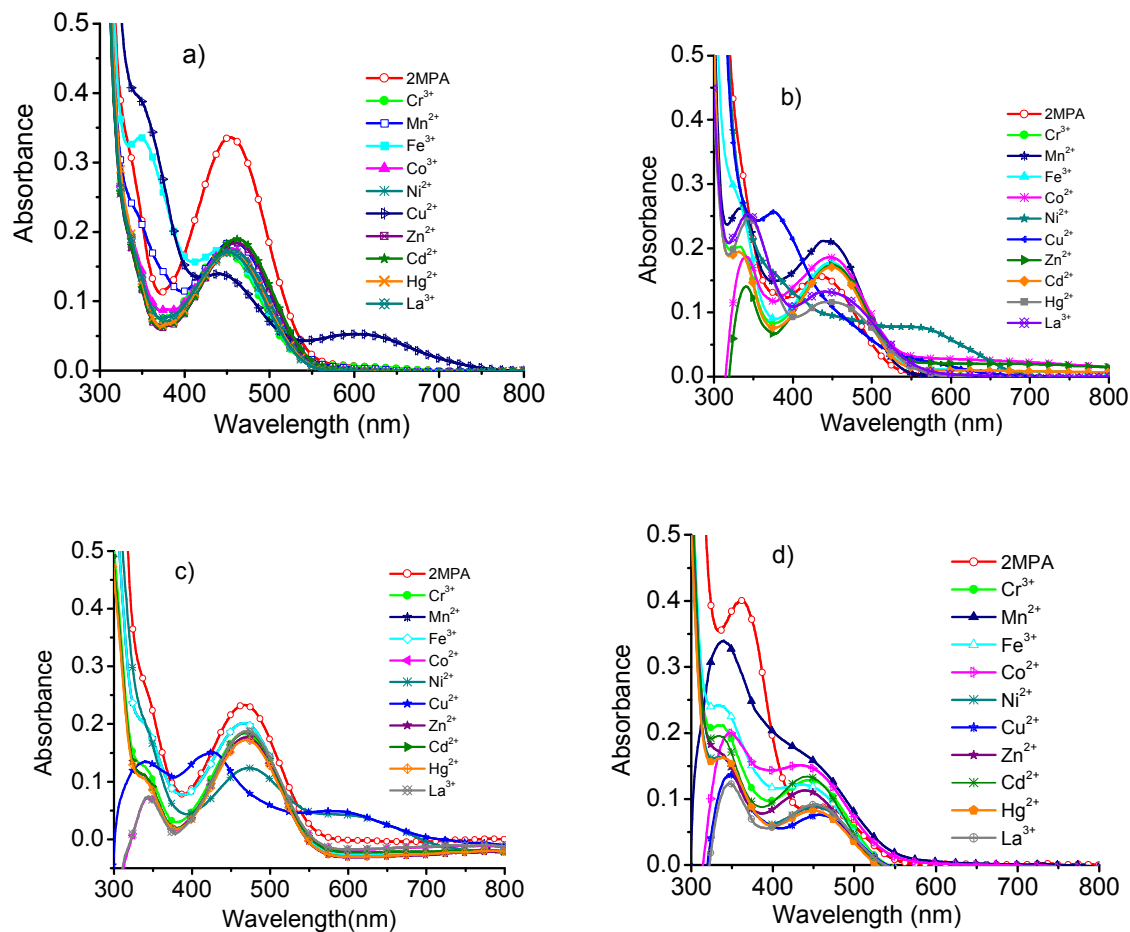


Fig.18 UV-Visible spectra of a) 2MPA (10<sup>-4</sup> M) with metal ions (10<sup>-4</sup> M) in methanol, b) In methanol and triethylamine, c) 2MPA in methanol and with metal ions (10<sup>-4</sup> M) in water, d) 2MPA in methanol and with metal ions (10<sup>-4</sup> M) in water and triethylamine.

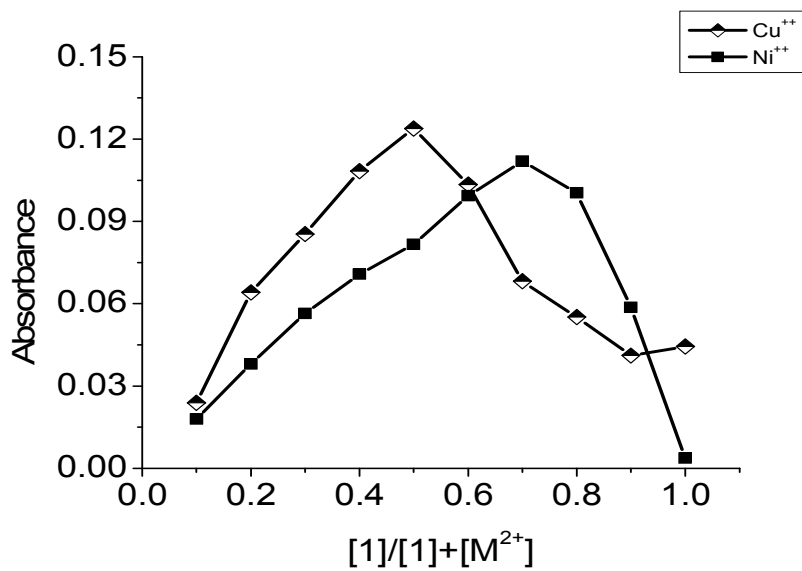
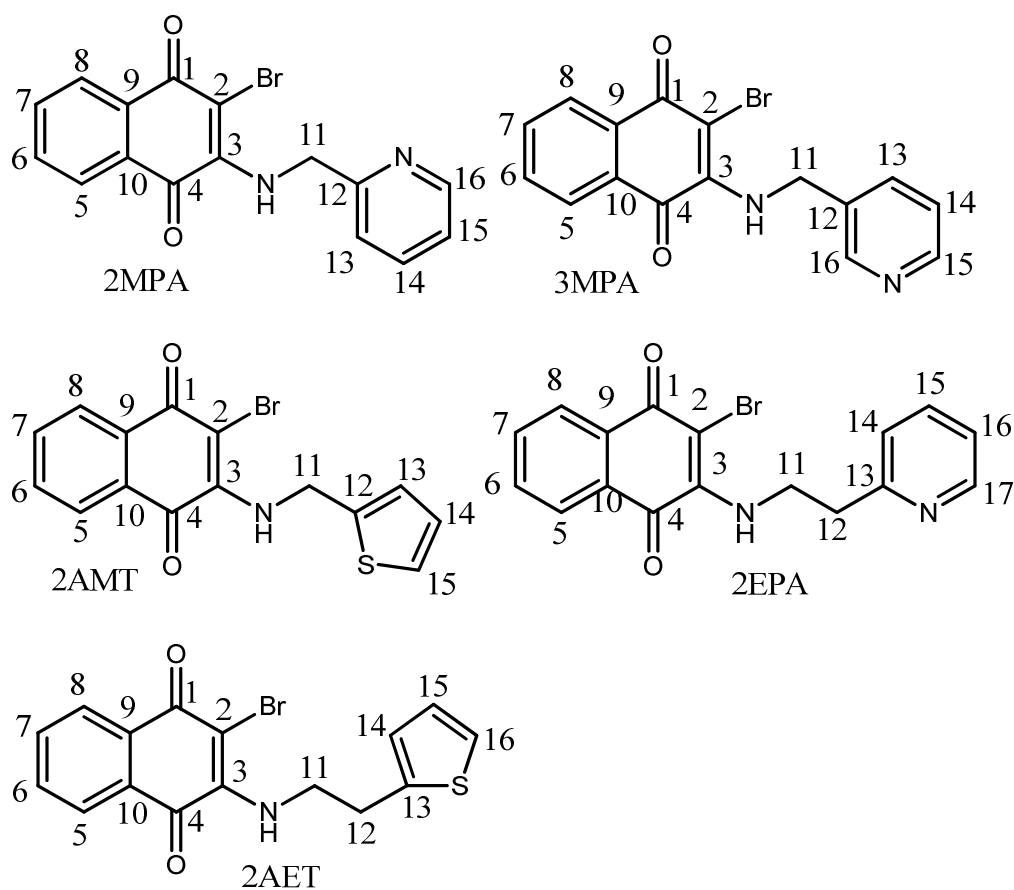
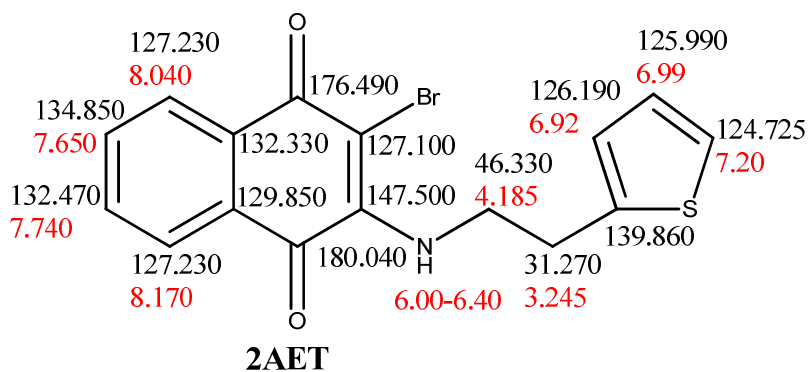
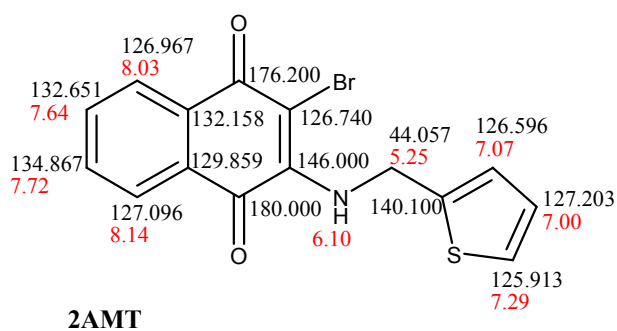
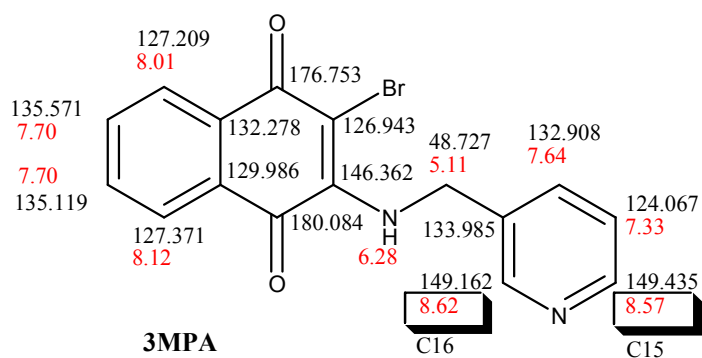
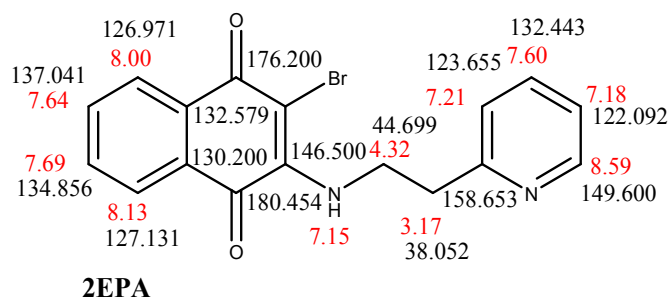
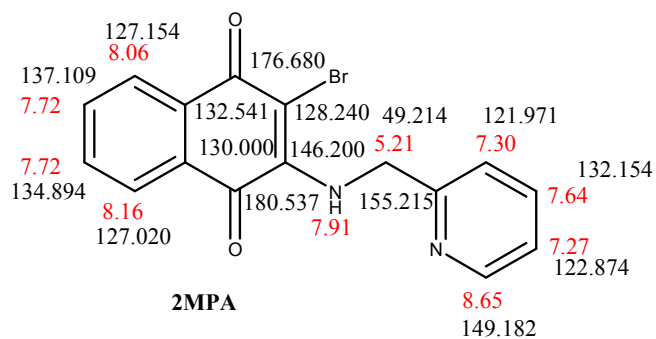
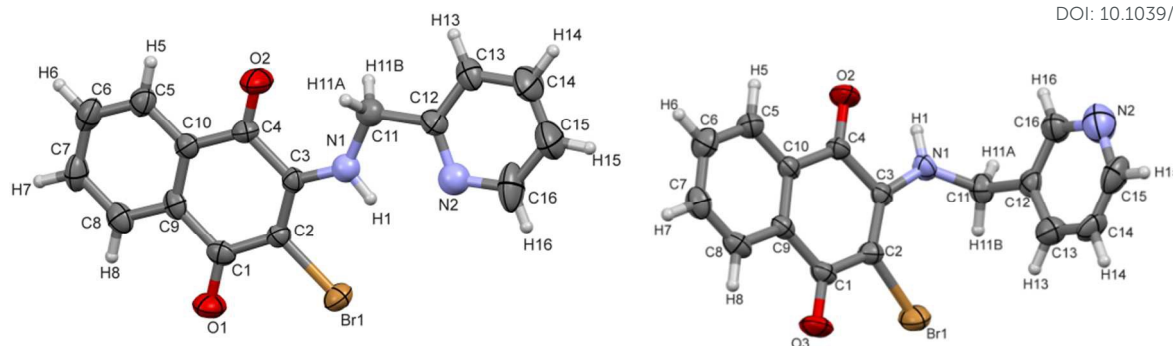


Fig. 19 Job plot obtained for  $Cu^{2+}$  and  $Ni^{2+}$  in methanol for 2MPA.



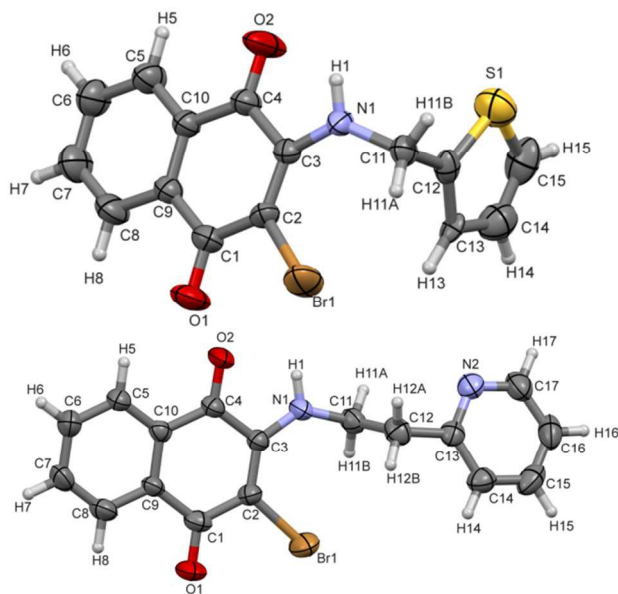
Scheme 1 Molecular Structures of aminonaphthoquinones under investigation

Scheme 2<sup>1</sup>H and <sup>13</sup>C chemical shift (ppm) of aminonaphthoquinone ligands



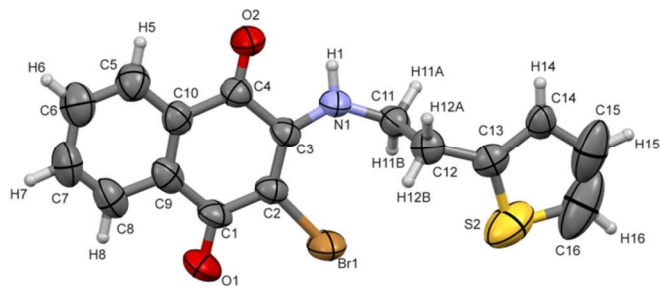
2MPA

3MPA



2AMT

2EPA



2AET

Fig.1 ORTEP plots of 2MPA, 3MPA, 2AMT, 2EPA and 2AET. The ellipsoid was drawn with 50% of probability

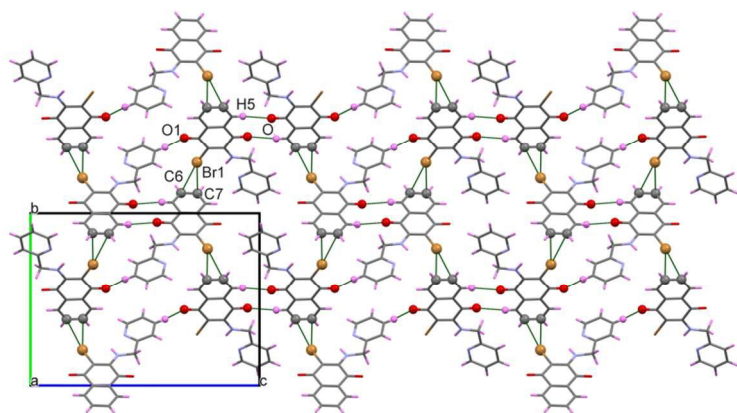


Fig.2 Molecular packing of 2MPA down a-axis

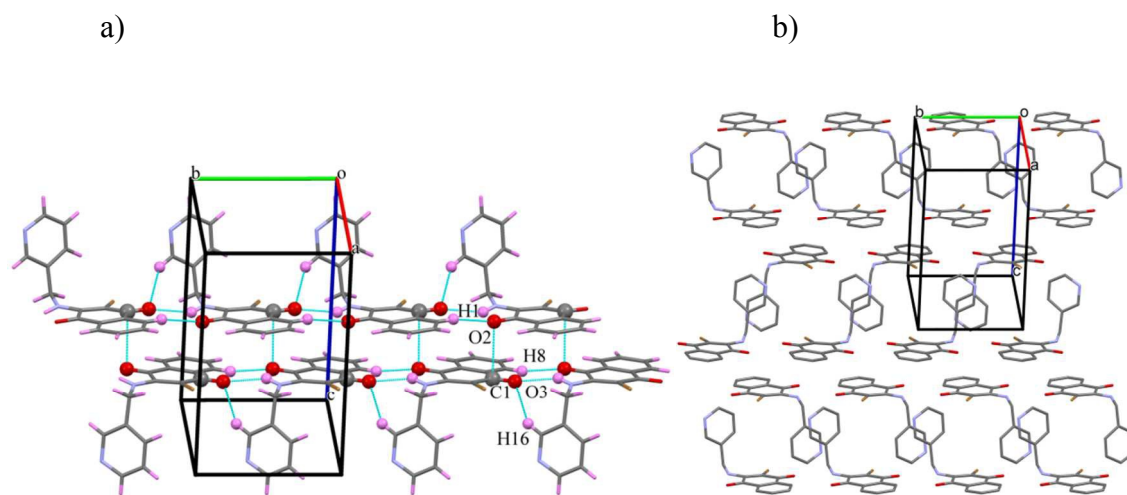


Fig.3a) Polymeric chains of 3MPA molecules formed by C(8)-H(8)⋯O(2) and N(1)-H(1)⋯O(1) interaction., b) Stacked polymeric chains of 3MPA

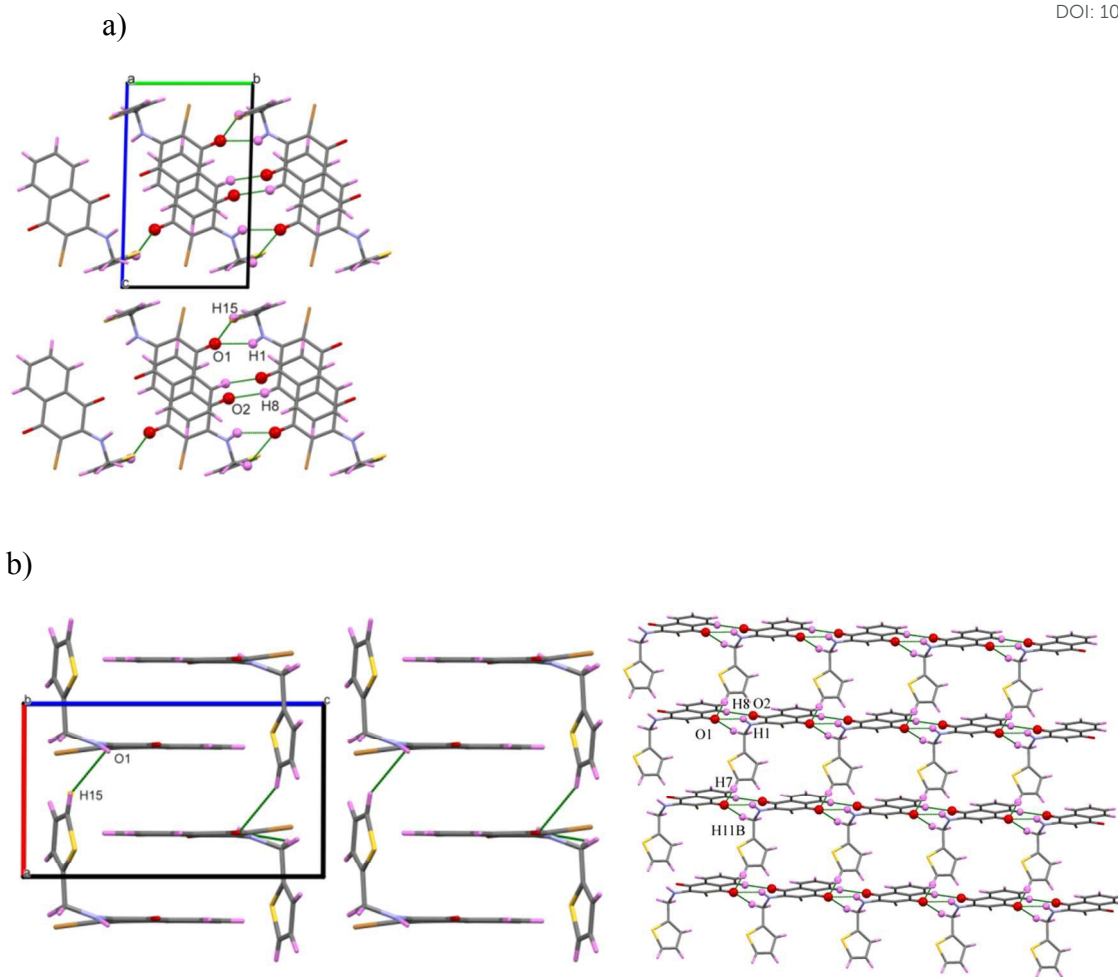


Fig.4a) Molecular packing of 2AMT molecules down a-axis, b) Molecular packing of 2AMT molecules down b-axis, c) Polymeric chains formed by hydrogen bonding separated by thiophene rings

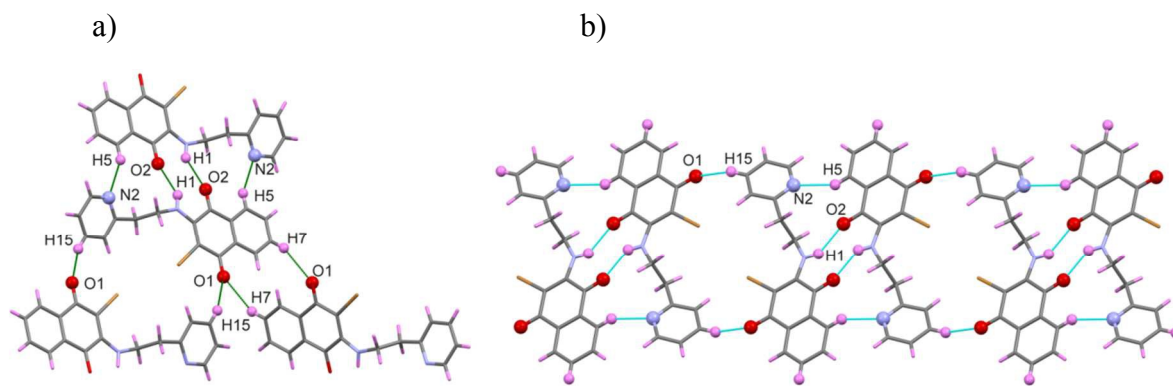


Fig.5a) Neighboring molecules of EPA. b) Dimeric chains of 2EPA formed by C-H...O interaction

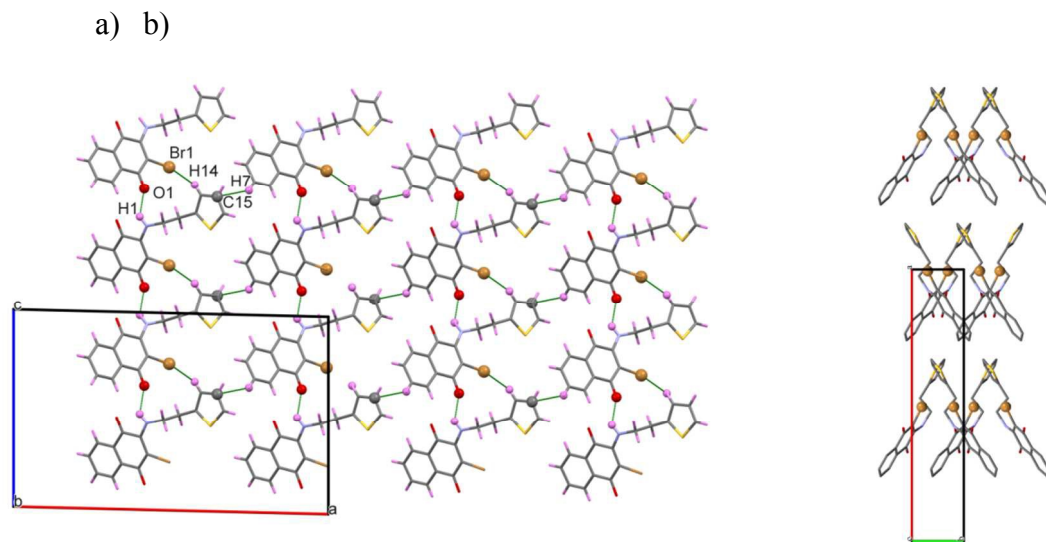
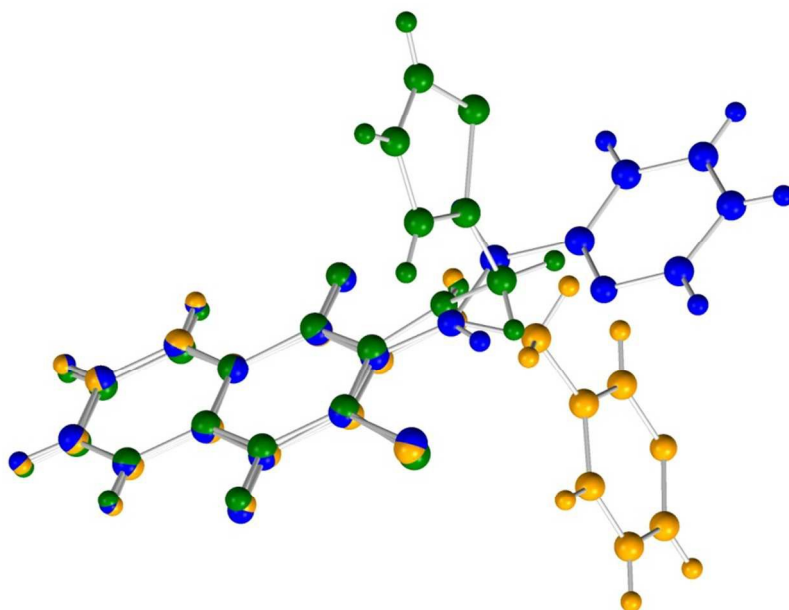


Fig.6 a) Molecular packing of 2AET molecules down b-axis and b) down c-axis

a) 2MPA(blue), 3MPA(yellow), 2AMT(green)



a) 2EPA(green), 2AET(Thiophene)

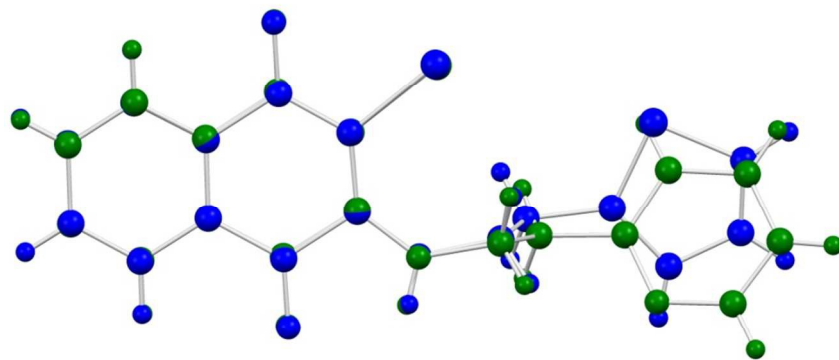
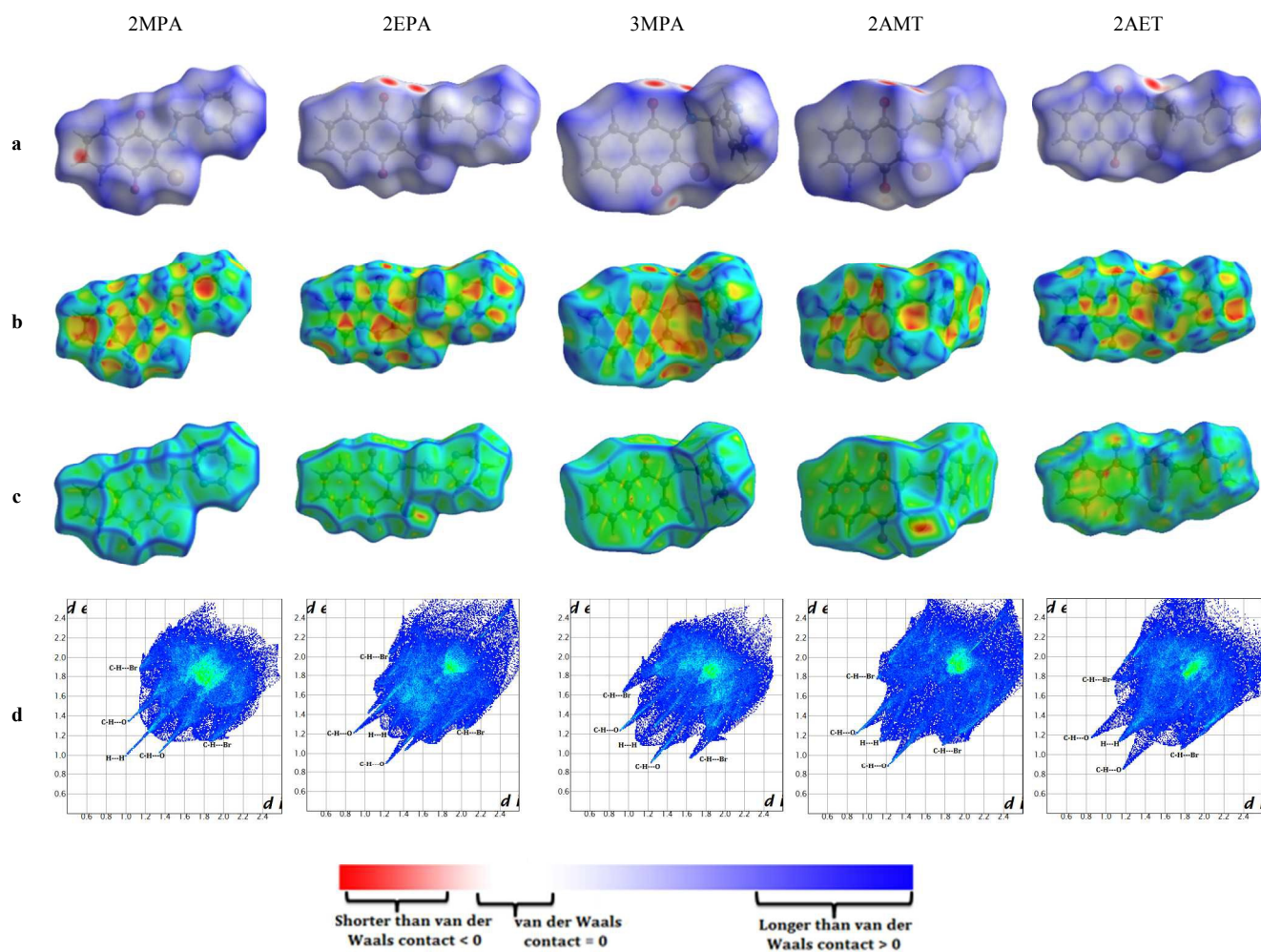


Fig.7 Overlay structures of a) 2MPA, 3MPA and 2AMT, b)2EPA and 2AET



**Fig. 8** Hirshfeld surfaces mapped with (a)  $d_{\text{norm}}$  (b) shape index, (c) curvedness and (d) 2D finger print plots with  $d_i$  and  $d_e$  ranging from 0.6 to 2.4 Å for 2MPA, 2EPA, 3MPA, 2AMT and 2AET.

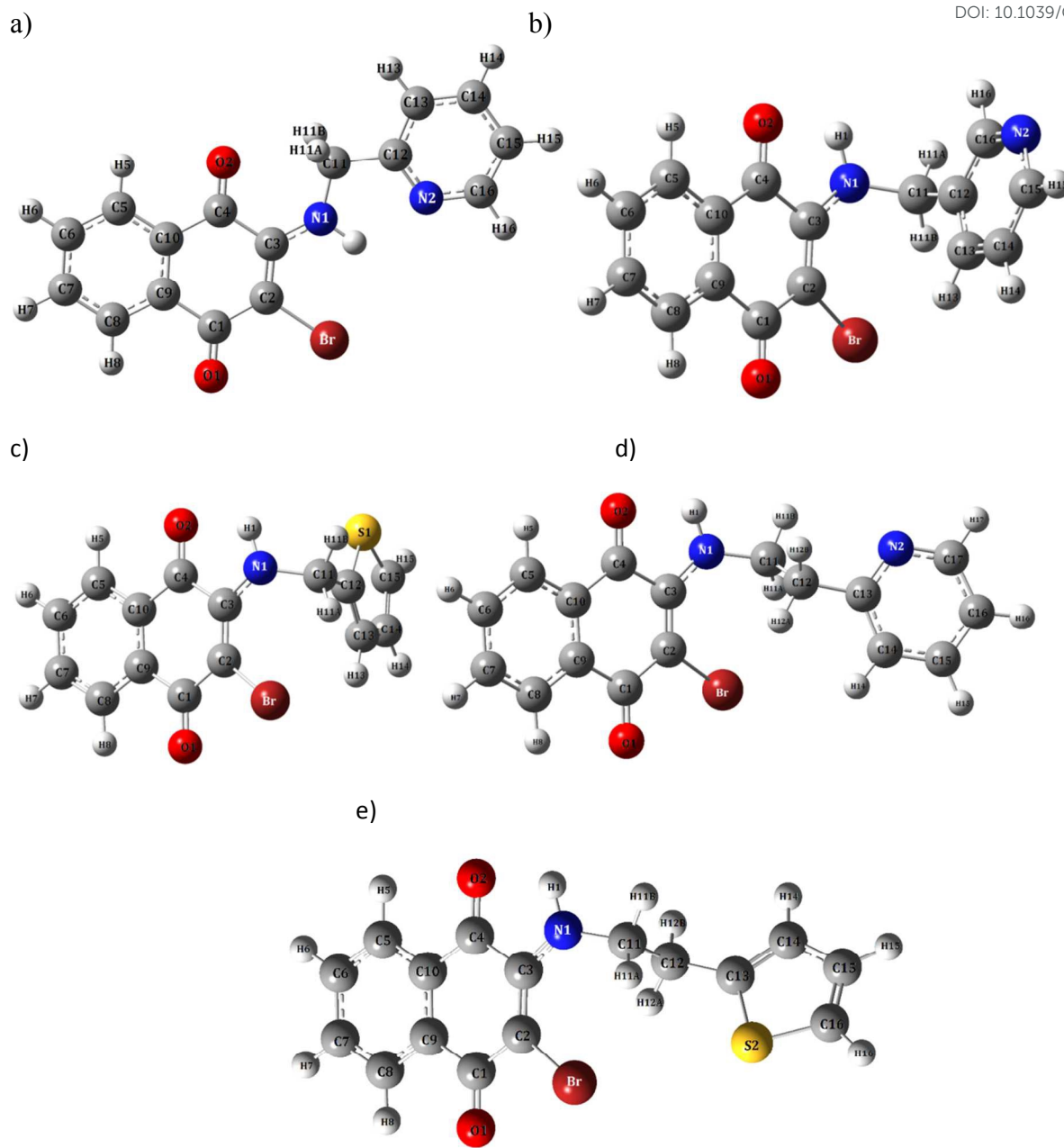


Fig.9 Optimized structures of (a) 2MPA, (b) 3MPA (c) 2AMT (d) 2EPA (e) AET. Atomic labelling scheme is shown.

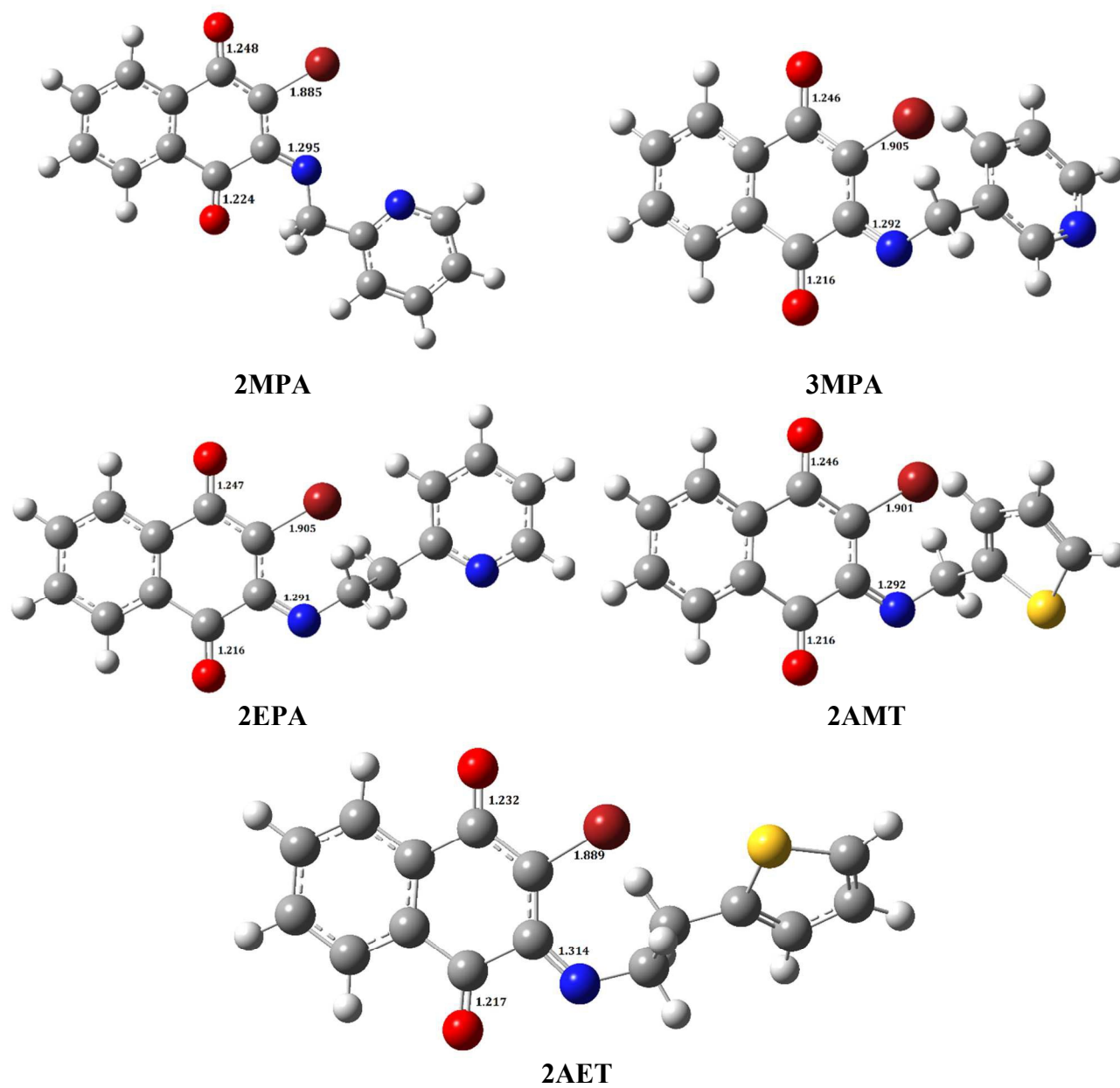
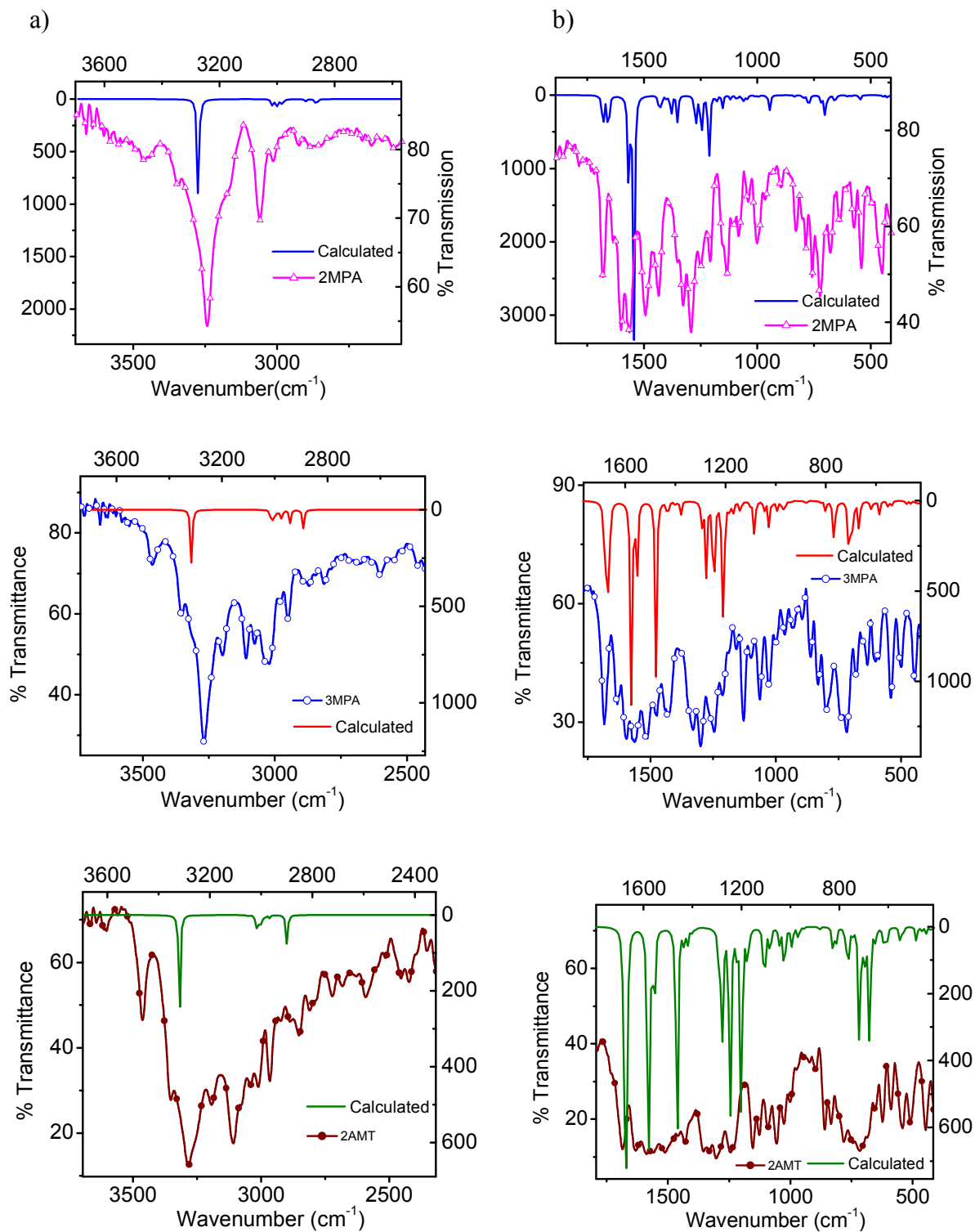


Fig.10 Optimized structures of anionic form (a) 2MPA, (b) 3MPA (c) 2AMT (d) 2EPA (e) 2AET



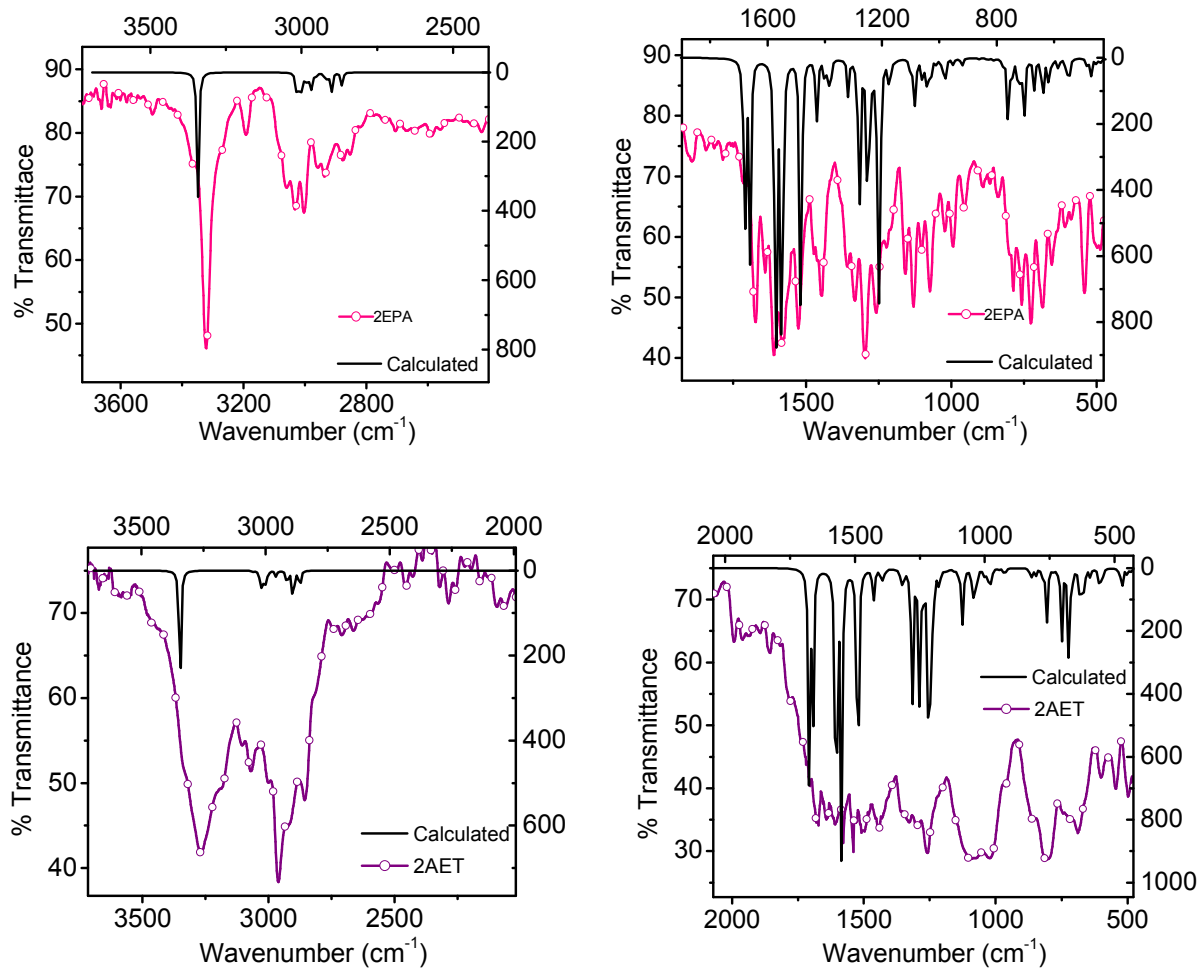


Fig.11 Observed and optimized FT-IR spectra of 2MPA, 3MPA, 2AMT, 2EPA and 2AET. The spectra is shown in two regions for peaks a)-NH, -CH and b)-C=O, -C-N, -C-Br.

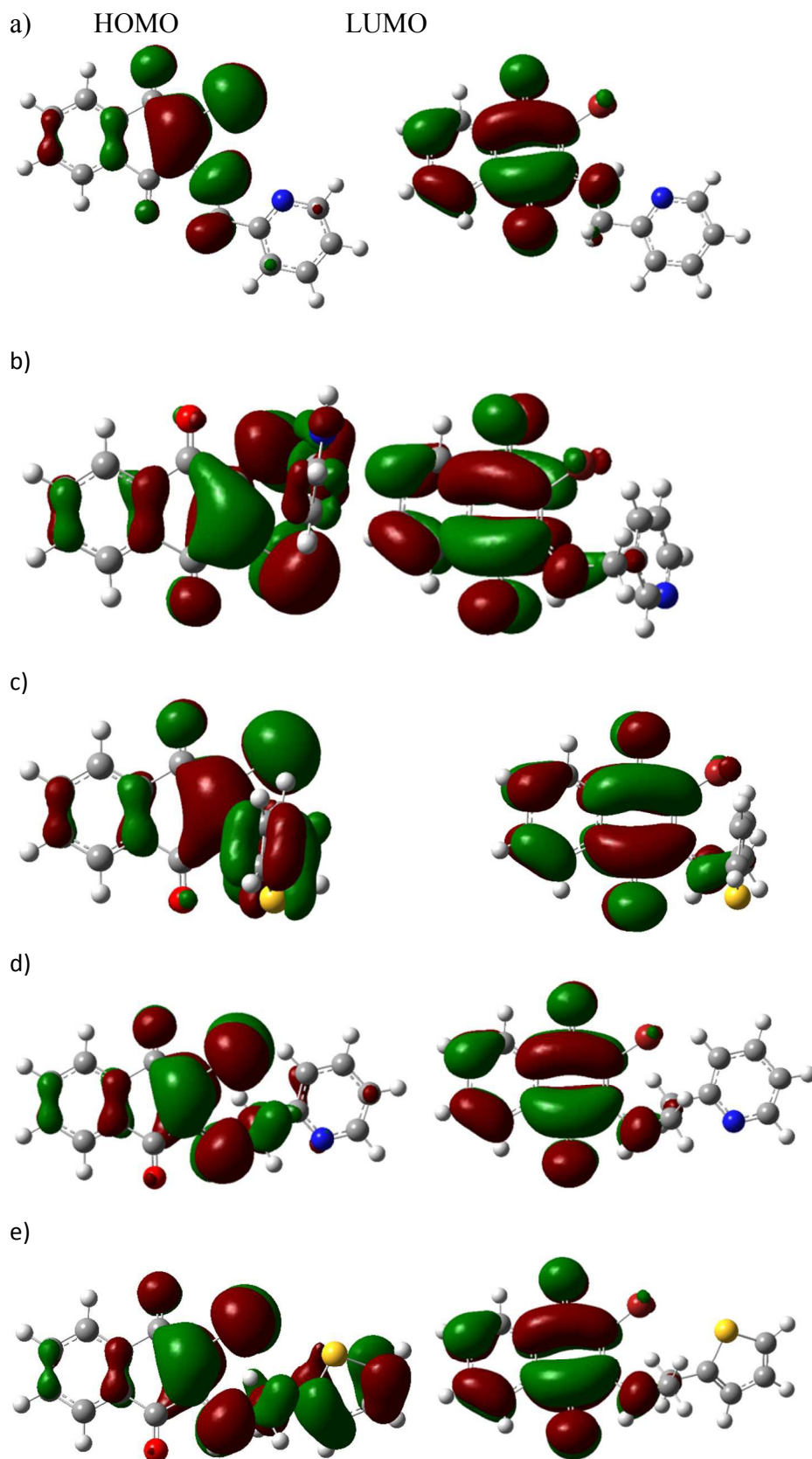
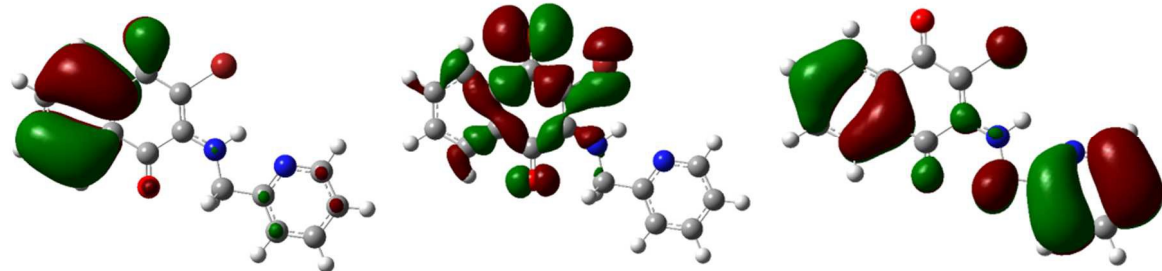


Fig.12 HOMO and LUMO in a) 2MPA, (b) 3MPA (c) 2EPA (d) 2AMT (e) 2AET

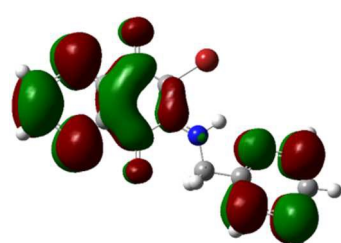
a)



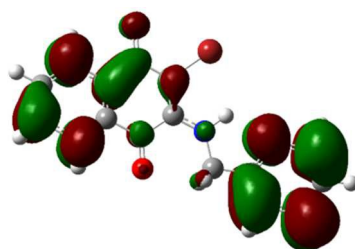
HOMO-1

HOMO-2

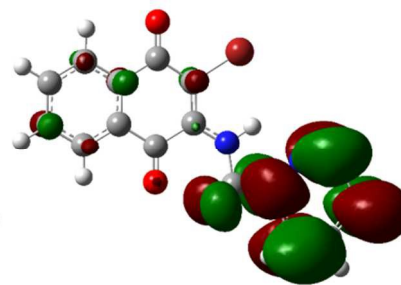
HOMO-3



LUMO+1

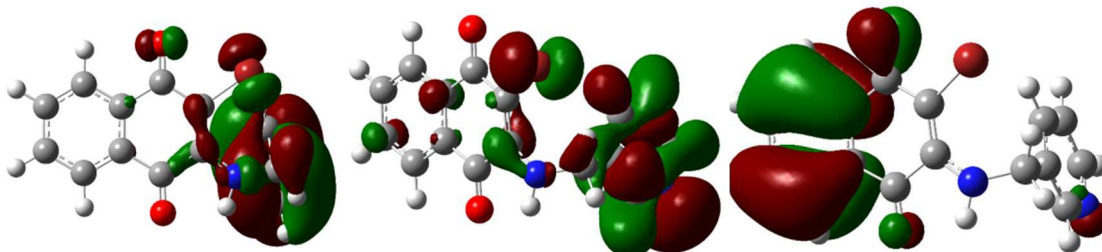


LUMO+2



LUMO+3

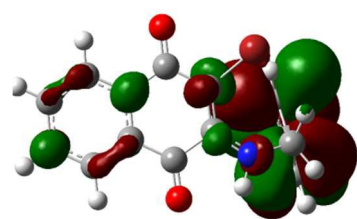
b)



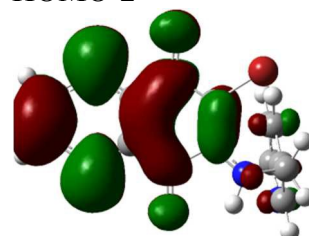
HOMO-1

HOMO-2

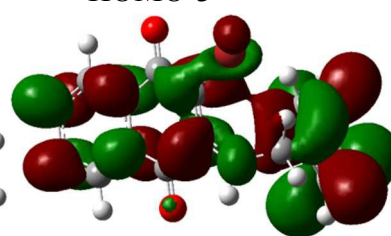
HOMO-3



LUMO-1

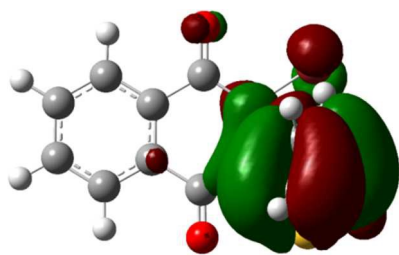


LUMO-2

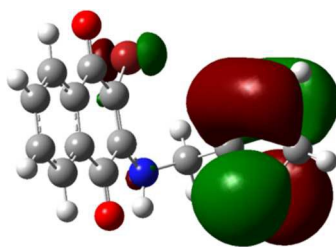


LUMO-3

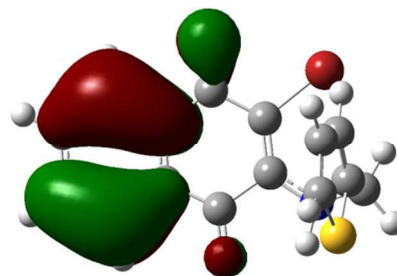
c)



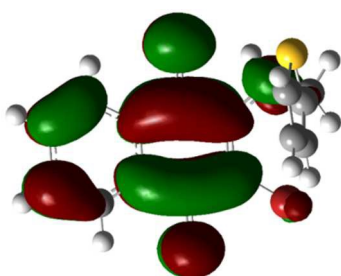
HOMO-1



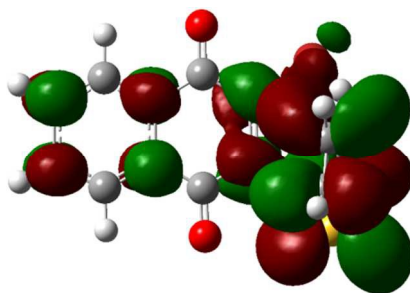
HOMO-2



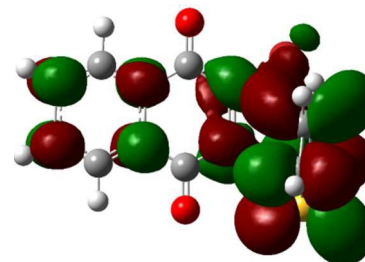
HOMO-3



LUMO-1

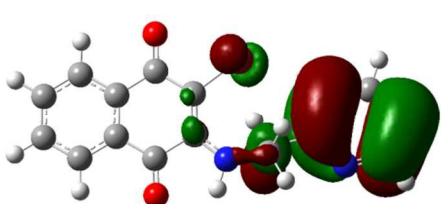


LUMO-2

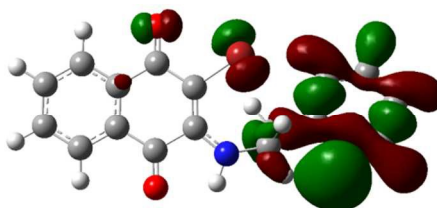


LUMO-3

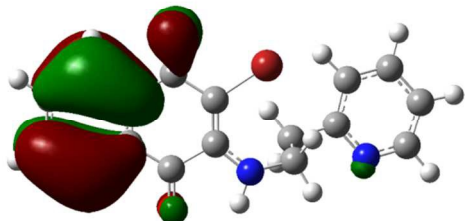
d)



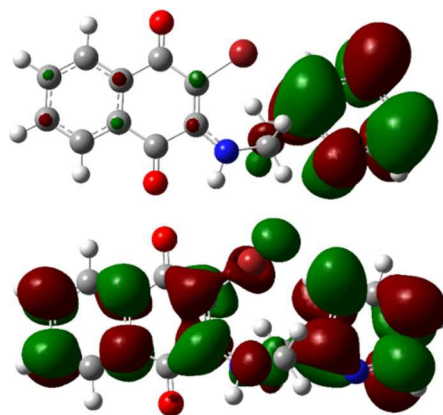
HOMO-1



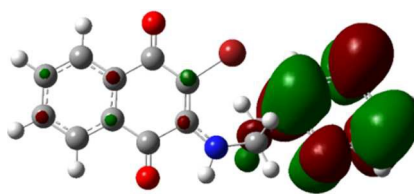
HOMO-2



HOMO-3



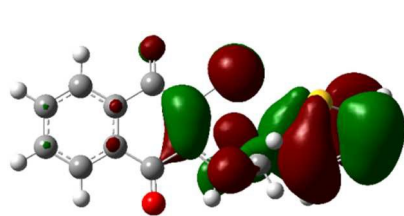
LUMO-1



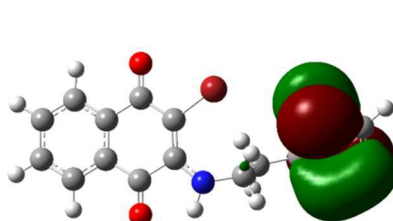
LUMO-2

LUMO-3

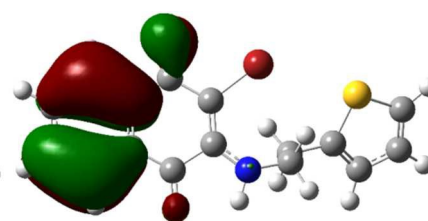
e)



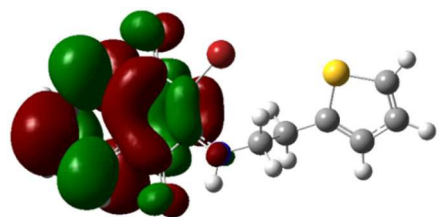
HOMO-1



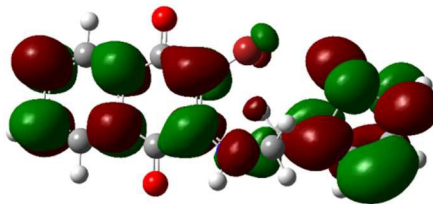
HOMO-2



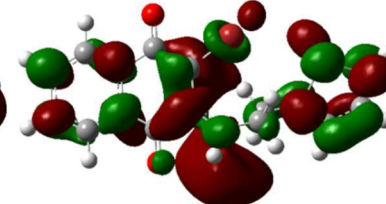
HOMO-3



LUMO-1



LUMO-2



LUMO-3

Fig.13 MOs namely, HOMO-1, HOMO-2 and HOMO-3 and LUMO+1, LUMO+2 and LUMO+3 in a) 2MPA, (b) 3MPA, (c) 2AMT, (d) 2EPA, (e) 2AET are also depicted. These enable one to assign the transition in the electronic spectra derived from the TD-DFT theory

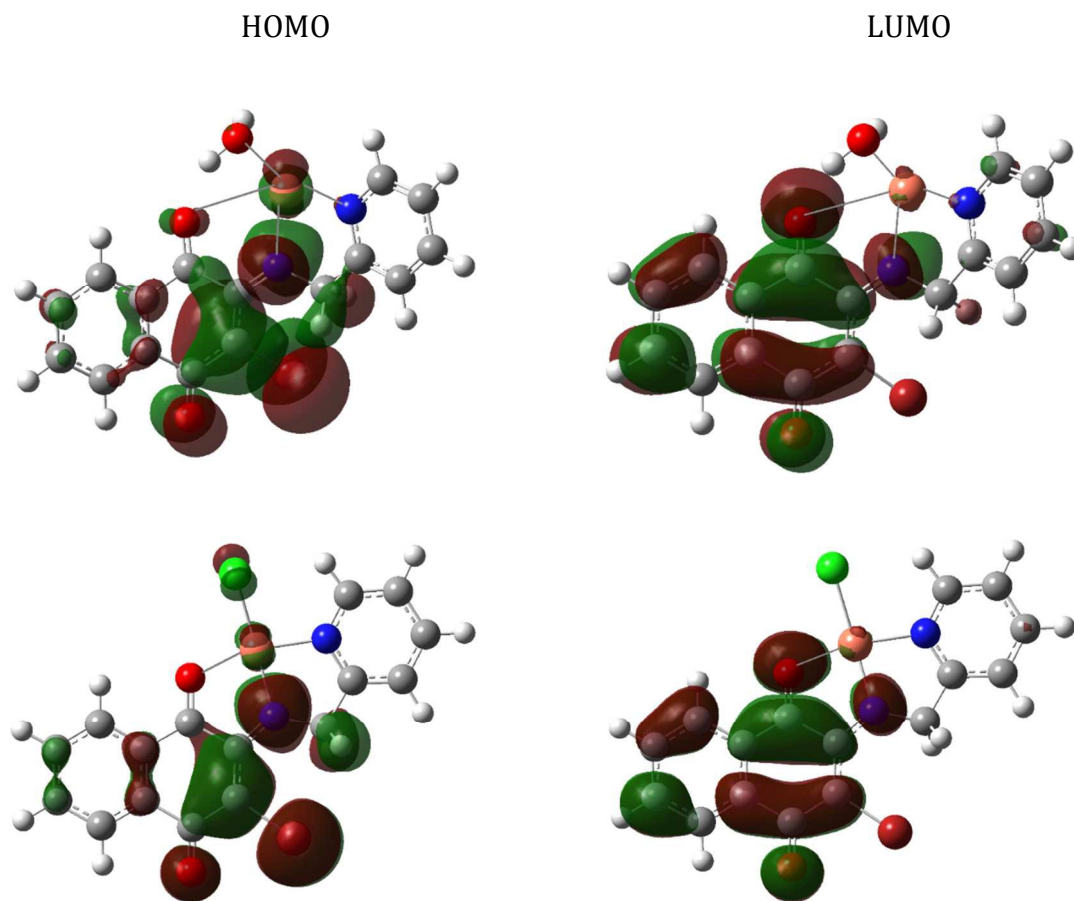


Fig. 14 HOMO and LUMO in 2MPA-Cu<sup>2+</sup> complexes.

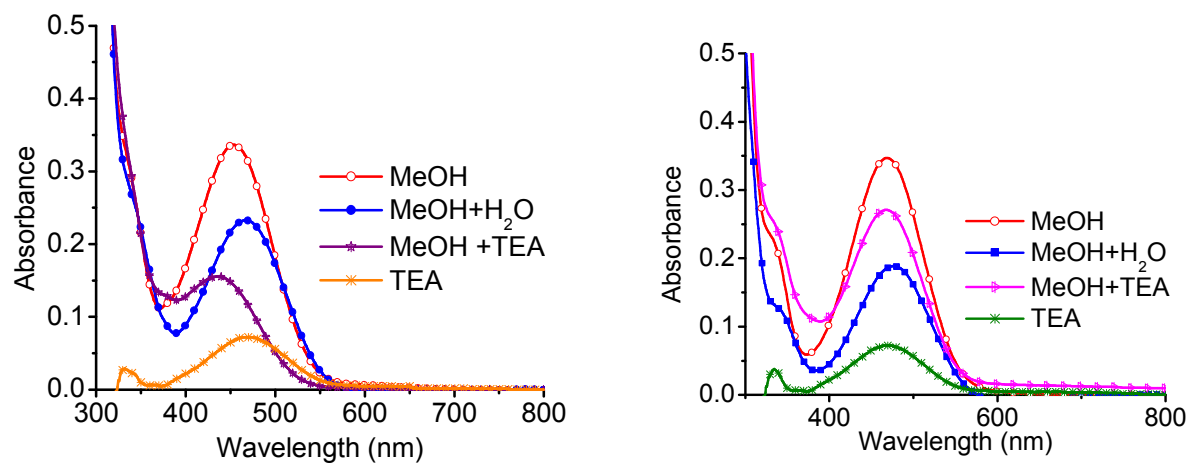


Fig.15 UV-visible spectra of a) 2MPA and b)3MPA in various solvents

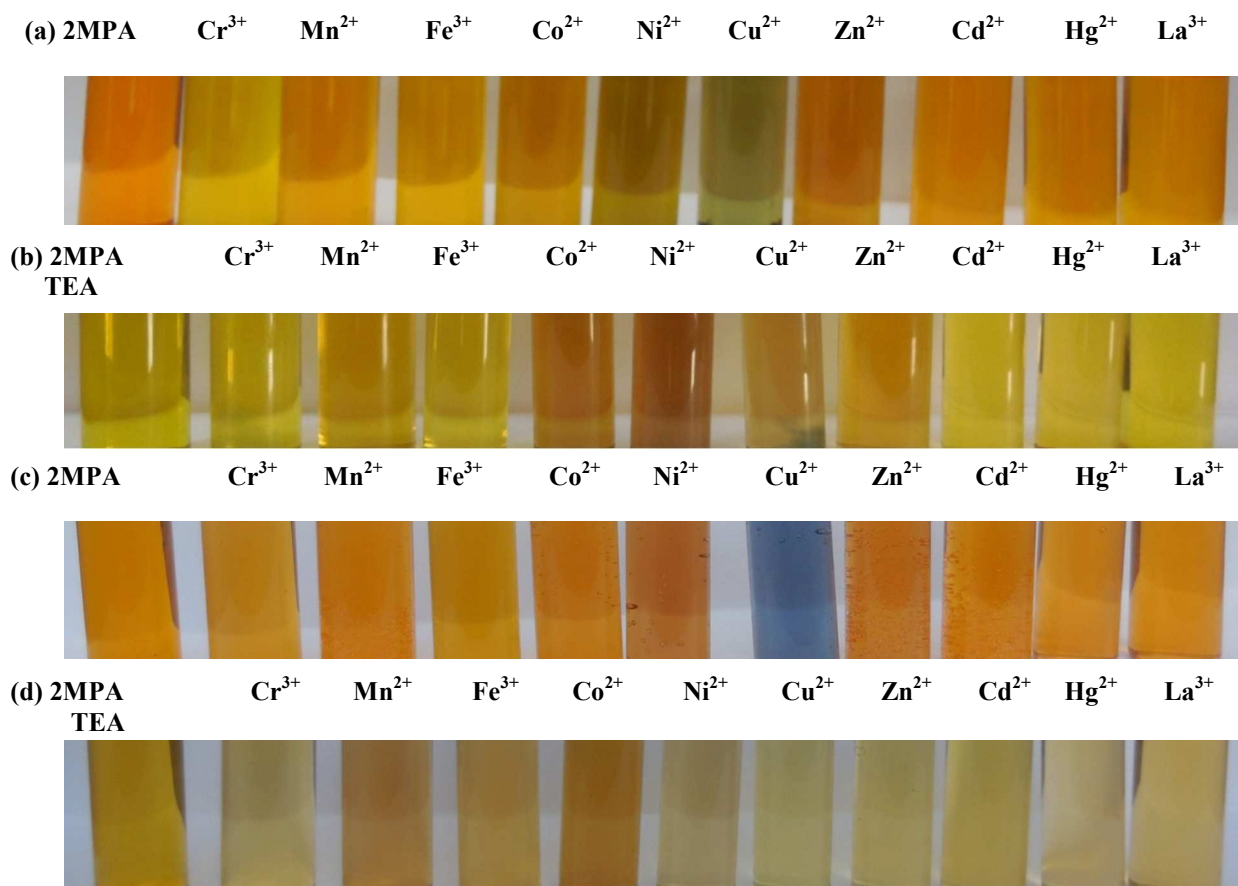


Fig. 16 a) Color change in Chemosensor 2MPA ( $10^{-4}$  M) with metal ions ( $10^{-4}$  M) in methanol, b) Chemosensor 2MPA ( $10^{-4}$  M) with metal ions ( $10^{-4}$  M) in methanol and triethylamine, c) Chemosensor 2MPA with metal ions ( $10^{-4}$  M) in methanol and water, d) Chemosensor 2MPA ( $10^{-4}$  M) with metal ions ( $10^{-4}$  M) in methanol-water-triethylamine

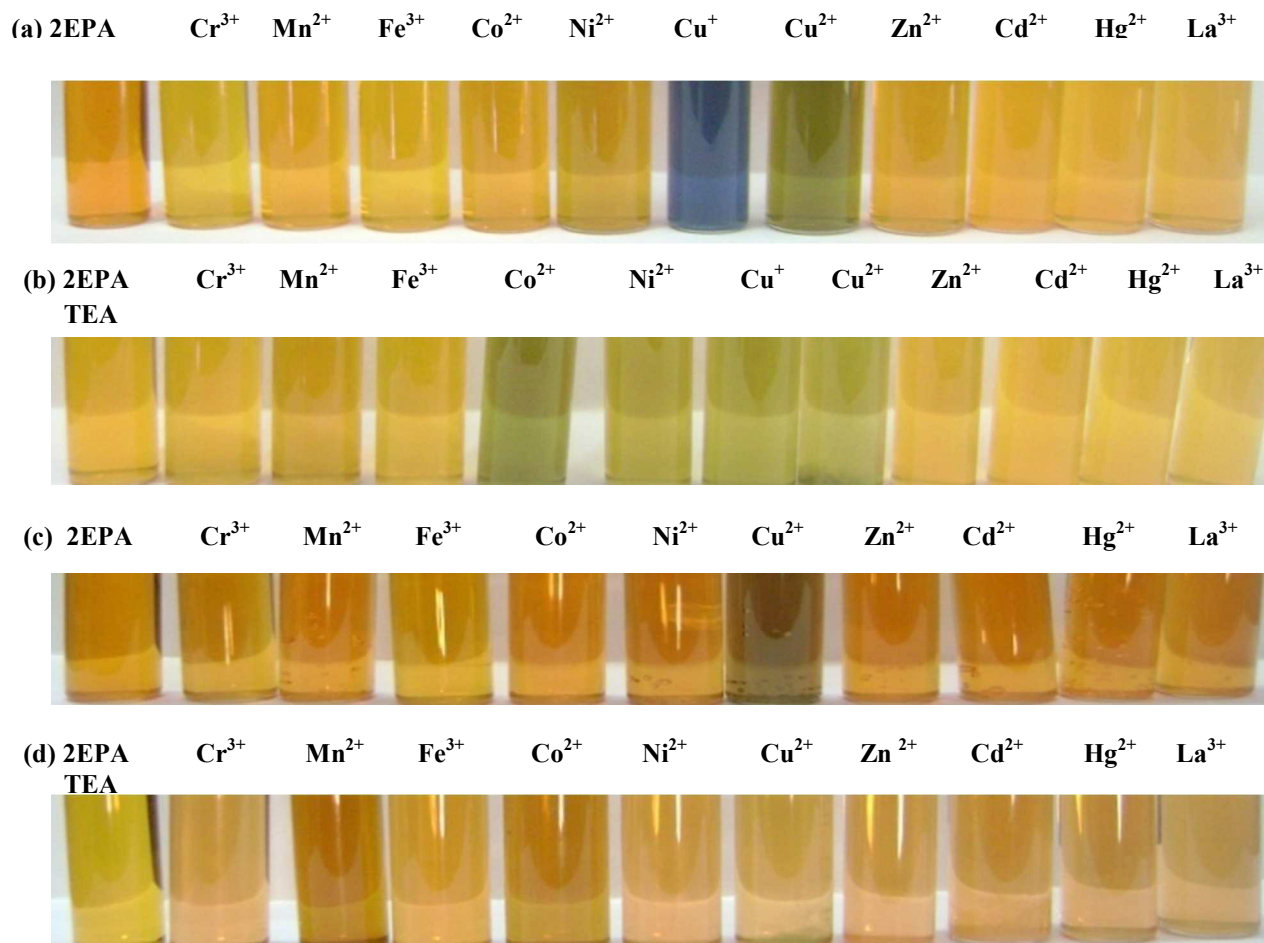


Fig. 17 Color change in Chemosensor 2EPA ( $10^{-4}$  M) with metal ions ( $10^{-4}$  M) in methanol, b) Chemosensor 2EPA ( $10^{-4}$  M) with metal ions ( $10^{-4}$  M) in methanol and triethylamine, c) Chemosensor 2EPA with metal ions ( $10^{-4}$  M) in methanol and water, d) Chemosensor 2EPA ( $10^{-4}$  M) with metal ions ( $10^{-4}$  M) in methanol, water and triethylamine

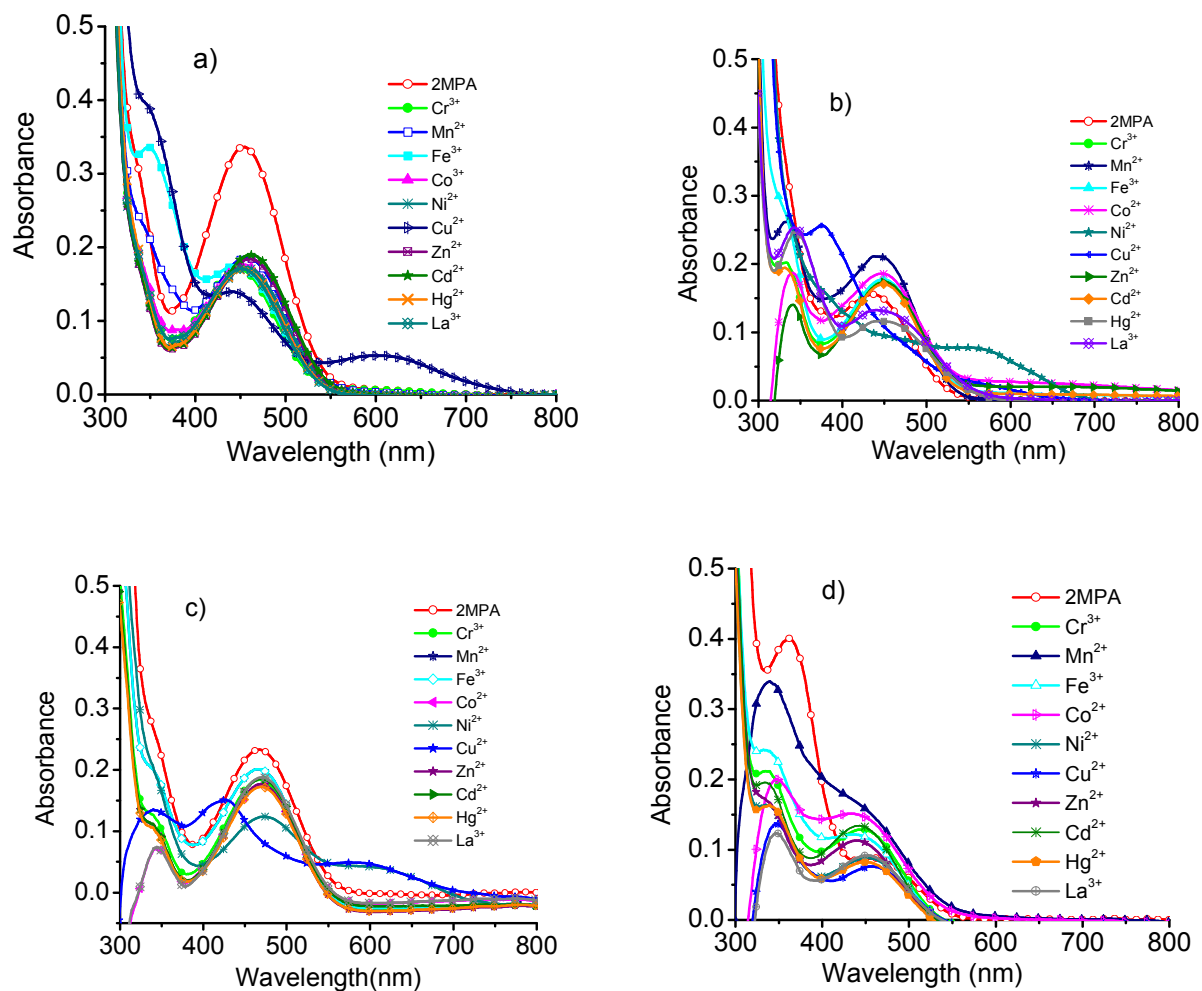


Fig.18 UV-Visible spectra of a) 2MPA ( $10^{-4}$  M) with metal ions ( $10^{-4}$  M) in methanol, b) In methanol and triethylamine, c) 2MPA in methanol and with metal ions ( $10^{-4}$  M) in water, d) 2MPA in methanol and with metal ions ( $10^{-4}$  M) in water and triethylamine.

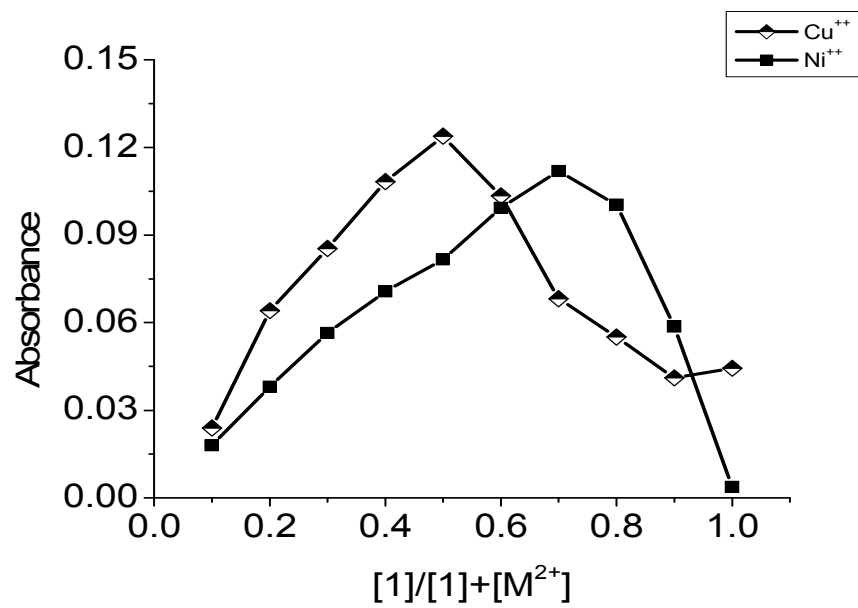
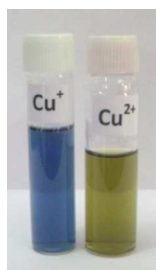
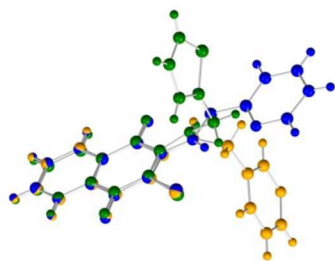
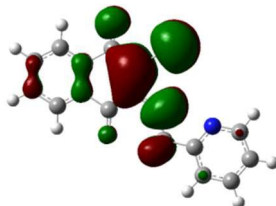


Fig. 19 Job plot obtained for  $Cu^{2+}$  and  $Ni^{2+}$  in methanol for 2MPA.

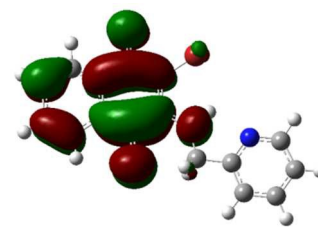
## Bromine substituted aminonaphthoquinones, chemosensors for metal ions

Chemosensors for Cu<sup>2+</sup>

Overlay diagram 2MPA, 3MPA, 2AET



HOMO 2MPA



LUMO 2MPA